Naval Research Laboratory

Washington, DC 20375-5000

NRL Memorandum Report 6622

X-Ray Laser Program Final Report for FY89

Radiation Hydrodynamics Branch and Pulsed Power Physics Branch
Plasma Physics Division

May 24, 1990

UNCLASSIFIED

SECURITY CLASSIFICATION OF THIS PAGE

REPORT DOCUMENTATION PAGE

Form Approved OMB No. 0704-0188

1a REPORT SECURITY CLASSIFICATION: UNCLASSIFIED	1b RESTRICTIVE MARKINGS
2a SECURITY CLASSIFICATION AUTHORITY	3 DISTRIBUTION / AVAILABILITY OF REPORT: Approved for public release; distribution unlimited.
2b DECLASSIFICATION / DOWNGRADING SCHEDULE	
4 PERFORMING ORGANIZATION REPORT NUMBER(S): NRL Memorandum Report 6622	5 MONITORING ORGANIZATION REPORT NUMBER(S)
6a NAME OF PERFORMING ORGANIZATION: Naval Research Laboratory; 6b OFFICE SYMBOL (If applicable): 4720 and 4770	7a NAME OF MONITORING ORGANIZATION
6c ADDRESS (City, State, and ZIP Code): Washington, D.C. 20375-5000	7b ADDRESS (City, State, and ZIP Code)
8a NAME OF FUNDING / SPONSORING ORGANIZATION: Strategic Defense Initiative; 8b OFFICE SYMBOL (If applicable): IST	9 PROCUREMENT INSTRUMENT IDENTIFICATION NUMBER
8c ADDRESS (City, State, and ZIP Code): Washington, D.C. 20301-7100	10 SOURCE OF FUNDING NUMBERS: PROGRAM ELEMENT NO 63220C; PROJECT NO; TASK NO; WORK UNIT ACCESSION NO 017L7

11 TITLE (Include Security Classification): X-Ray Laser Program Final Report for FY 1989

12 PERSONAL AUTHOR(S): Listed in individual chapters

13a TYPE OF REPORT	13b TIME COVERED	14 DATE OF REPORT (Year, Month, Day)	15 PAGE COUNT
Interim	FROM 10/1/88 TO 9/30/89	1990 May 24	85

16 SUPPLEMENTARY NOTATION: This work was supported by the Strategic Defense Initiative Organization under Job Order Title, Ultra Short Wavelength Laser Research, MIPR No. DGAM60091.

17 COSATI CODES			18 SUBJECT TERMS (Continue on reverse if necessary and identify by block number)
FIELD	GROUP	SUB-GROUP	X-Ray laser; Recombination Pumping; Pulsed power; Auger laser; Resonant photoexcitation; Spectroscopy

19 ABSTRACT (Continue on reverse if necessary and identify by block number)

This report details the progress achieved by the Radiation Hydrodynamics and Pulsed Power Physics Branches in X-Ray Laser experiments and modeling during FY 1989. Significant experimental accomplishments in photopumping of neon by both neon and sodium to produce inversions via either the Auger effect or resonant photopumping are described in the first section. Subsequent sections present in detail modeling of neon-neon photopumping, recombination lasers and development of a new diagnostic for neonlike x-ray laser plasmas.

20 DISTRIBUTION / AVAILABILITY OF ABSTRACT	21 ABSTRACT SECURITY CLASSIFICATION
☒ UNCLASSIFIED/UNLIMITED ☐ SAME AS RPT ☐ DTIC USERS	UNCLASSIFIED
22a NAME OF RESPONSIBLE INDIVIDUAL: Dr. John Apruzese	22b TELEPHONE (Include Area Code): (202) 767-2939; 22c OFFICE SYMBOL: Code 4720

DD Form 1473, JUN 86 — Previous editions are obsolete. — SECURITY CLASSIFICATION OF THIS PAGE

S/N 0102-LF-014-6603

TABLE OF CONTENTS

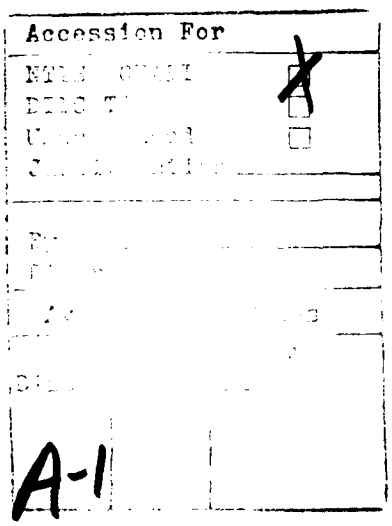

EXECUTIVE PROGRAM SUMMARY

This report, divided into 4 sections, is a detailed description of the X-Ray Laser research conducted by the Pulsed Power Physics and Radiation Hydrodynamics Branches of the Plasma Physics Division during Fiscal Year 1989. The individual authors of each section are listed at the beginning of the section.

A major thrust of this research has been the utilization of pulsed-power driven plasmas as a source of x-ray photons to create population inversions leading to gain at soft x-ray wavelengths. To this end, two approaches have been pursued in the experiments conducted by the Pulsed Power Sciences Branch (Section I). The first method uses the strong alpha resonance line of heliumlike sodium at 11 Å to resonantly pump the $1s^2$-1s4p $^1P_1$ transition of heliumlike neon whose wavelength lies within a Doppler width of the sodium line. Under proper conditions, the resulting over-population of the heliumlike neon n=4 levels would lead to inversions in the 4-3 singlet transitions near 230 Å, and possibly also the 4-2 and 3-2 transitions at approximately 58 and 82 Å, respectively. At a sodium-neon separation of 3 cm, for instance, sodium helium alpha powers of about 100 GW would be required for a gain demonstration. It is obviously important to maximize the power output of the sodium pump line. On Gamble-II, 25-30 GW has been consistently produced at the relatively modest current of 1 MA, using a NaF capillary source. This is a very encouraging result in terms of the outlook for gain demonstration on a larger machine. Two reasons underlie this optimism. First, half of the energy is absorbed by the useless fluorine ions. A pure sodium source could well double this power to 50 GW even at 1 MA. Second, K-shell power outputs are expected to scale as (current)$^\alpha$ where $\alpha \sim 2$-4. The availability of machines with 3-4 MA current (for instance Double Eagle at Physics International Corp.) or even 10 MA (Saturn at Sandia National Laboratory) points to the ultimate achievement of pump line powers of several hundred GW, suitable for significant gain in neon. Indeed, at the beginning of FY 90, the NaF capillary source was adapted to and fired on the Double-Eagle generator and preliminary results indicate that powers in excess of 100 GW were produced on several shots. Full details will be given in next year's report.

Proper preparation of the neon lasant plasma is as important as is achievement of high pump power from sodium. In this regard, significant results have been achieved, also discussed in Section I. In a series of experiments wherein one of the Gamble-II return current posts was replaced with a neon gas-puff plasma fluorescence of the neon by photopumping with the central NaF plasma was demonstrated.

Since the neon lasant plasma needs to be cooler (50-100 eV) than the sodium pump plasma, considerably less current than required for the sodium is appropriate. Neon implosions are being studied on a test stand providing currents of 120-140 kA. A technique to measure the Ne IX ground state population based on observed Ne VIII transitions is being employed. One of the potential heliumlike laser lines (3-2 transition at ~ 78 Å) has been detected at a current of 150 kA. When this study is completed, the conditions for correct preparation of a Ne IX lasant plasma using pulsed power will be determined so that optimal Na/Ne gain experiments may be carried out.

Another important facet of the experimental and theoretical photopumped x-ray laser program also involves the use of a neon lasant plasma. However, that is the only similarity to the Na/Ne scheme described above. In the Ne/Ne scheme, the lasant consists of a static fill "gasbag" containing 100-Torr of room-temperature neon. The photon pump source is a separate neon Z pinch located on the axis of the Gamble-II generator, which generates ~ 160 GW of K-shell line pump power. In this Auger laser scheme the K-shell neon Z pinch photons of energy $h\nu \geq 900$ eV, photoionize inner K-shell electrons from the neutral neon, leading to Auger decay from Ne II to Ne III. Given the branching ratios of Auger decay to various levels of Ne III, a natural laser is set up with the possibility of gain at 514 Å in Ne III. About 2% of the time K_α fluorescence of Ne II at 849 Å occurs instead of Auger decay to Ne III. Initial experiments on Gamble II have detected this K_α radiation but at levels an order of magnitude smaller than the expected optically thin power. Modeling suggests that self-absorption of this line may be responsible, but this should not affect the gain which should be achievable of Gamble-II. Details of the experiments and calculations are given in sections I and II, respectively.

Sections III and IV are detailed reports of calculations of laser schemes which may be the subject of future experiments. In Section III, the question of how to cool a plasma to promote recombination lasing is considered in detail. The two methods which have been both considered and demonstrated at other laboratories are hydrodynamic expansion and radiative cooling. The relative merits of radiative and hydrodynamic cooling in a freely expanding plasma have been examined. The specific lasing scheme studied is recombination in helium-like silicon, but the general results apply to other elements and ionization stages which are capable of generating gain the the soft x-ray region. It is found that the higher radiative cooling rates obtained by mixing the silicon lasant with a high atomic number coolant are more than offset by the reduced expansion cooling brought on by the higher mass density associated with the high Z elements. Specific results are presented for hydrogen, carbon, aluminum, and selenium coolants mixed with silicon lasant. These results do not apply for magnetically confined lasant plasmas where high Z radiators might be valuable.

Nine different neonlike ions with atomic numbers ranging from 28 to 42 have exhibited lasing in various 3p-3s transitions in experiments carried out at various laboratories (including the NRL work of Lee, McLean, and Elton). The temperature of the lasing plasma is critical in determining the state of ionization and the relative importance of collisional excitation and recombination pumping. In Section IV a potentially useful new temperature diagnostic for these plasmas is demonstrated: the absolute intensity of 3p-3s sodiumlike lines. Due to their large collisional couplings and high optical depths, their brightness temperature approaches the actual kinetic temperature of the plasma in temperature and density regimes of importance for achieving gain in neonlike ions.

Section I

NRL EXPERIMENTAL PULSED POWER X-RAY LASER PROGRAM

F. C. Young, S. J. Stephanakis, V. E. Scherrer[+], D. D. Hinshelwood[+], P. J. Goodrich[+], D. Mosher, and B. L. Welch[*]

Pulsed Power Physics Branch

+ JAYCOR, Vienna, Virginia

* University of Maryland, College Park, Md.

X-RAY LASER PROGRAM FINAL REPORT for FY 1989

I. Introduction

Two approaches to developing a laboratory soft x-ray laser using a pulsed power driver were investigated at NRL in FY89. In these experiments, intense incoherent K-line x-rays from a pulse-power driven z-pinch implosion are used as an x-ray pump. One approach involves pumping neutral Ne atoms with K-shell radiation from a nearby Ne implosion. Auger decay following this photopumping leads to population inversion and lasing. The other approach utilizes line-coincidence photopumping of heliumlike Ne ions by x-rays from heliumlike Na ions produced in a nearby z-pinch implosion.

II. Neon-Neon Photopumping

Photopumping of Ne with x-rays from a pulsed power driver followed by Auger decay to produce lasing is a particularly attractive scheme.[1] The use of Auger decay to produce lasing has been demonstrated in Xe (1089 Å) and in Kr (907 Å).[2] A Ne z-pinch implosion on the Gamble II pulsed-power generator at NRL is an attractive pump source for this scheme because more than 6 kJ of Ne K-shell radiation have been produced in a 40-ns pulse.[3] A gas bag of neutral Ne can provide a uniform lasant of known density for photopumping. Finally, quasi-cw lasing may be possible because the lower lasing level in this scheme is not a ground state but an excited state which rapidly depopulates.[4]

A simplified energy level diagram with decay rates for this lasing scheme is shown in Fig. 1. Neutral neon (Ne I) is ionized into the n=2 level of Ne II by x-rays with energies greater than 870 eV. Auger decay of this level to Ne III leads to lasing at 514 Å. The n=2 level of Ne II also decays by the emission of an 849-eV K-α x-ray. In the present experiments we have concentrated on measuring the K-α emission of Ne II in order to confirm the production of Ne II by photopumping. No measurements of radiation from Ne III have been attempted.

The geometry for the photopumping experiment is illustrated in Fig. 2. An annular Ne gas puff is imploded with a megampere-level peak-current pulse from the Gamble II generator to produce a 4-cm long Ne plasma. This plasma radiates about 6 kJ of K-shell radiation into 4π sr. Located about 5 cm from

Manuscript approved January 31, 1990.

the Ne plasma is a cylinder of Ne gas confined behind a 1.8-μm Kimfol ($C_{16}H_{14}O_3$) window. Calculations indicate that for a 100-Torr Ne fill, a few Joules of K-α x-rays from Ne II should be emitted into 4π. This radiation, transmitted through a 1.8-μm Kimfol window on the end of the gas bag, is recorded with an x-ray diode filtered to preferentially detect Ne K-α x-rays.

The absorption of the pump radiation by neutral neon and the transmission of x-rays through 1.8-μm Kimfol are shown in Fig. 3. The Ne pump source consists primarily of 0.92 keV (He-α) and 1.02 keV (Ly-α) line radiations[5] which are strongly absorbed by the neutral Ne because their energies are just above the Ne K-edge. About 50% of this radiation is transmitted through the Kimfol window, of which about 60% is absorbed in the 1.8-cm diameter cylinder of Ne gas. Neutral Ne is relatively transparent to its K-α radiation because the K-α x-ray energy is just below the Ne K-edge. About 40% of the emitted Ne K-α radiation is transmitted through the Kimfol filter on the end of the gas bag.

Measurements of the x-ray emission from a Ne implosion are presented in Figs. 4 and 5. An annular Ne gas puff with an initial diameter of 1.75 cm was imploded with a 1.2-MA current pulse to produce 6 kJ of Ne K-shell radiation. This radiation is emitted in a 160-GW, 35-ns FWHM pulse as measured by an x-ray diode (XRD) with a 13-μm Al filter. XRD measurements in Fig. 5 indicate that this pump source consists primarily of 1 to 2 keV x-rays. The energy in the Ne He-α line (0.92 keV) is only 10 to 20% of the K-shell emission and the hard x-ray emission (3 to 4 keV) is even less. Most of the energy is contained in the Ly-α (1.02 keV) and higher-order lines in the hydrogenlike series.

X-ray emission from the Ne gas bag was recorded with an XRD designed for optimum sensitivity near 849 eV. The sensitivity of this XRD is shown in Fig. 6. A Ni filter is used because it transmits Ne K-α x-rays and attenuates the 1 to 2 keV pump radiation. A Co cathode is used to increase the detector response just above the 784-eV L-edge of Co. From 784 to 860 eV the XRD sensitivity is large and relatively constant. Measurements with this XRD for two different shots are compared in Fig. 7. The signal with a 100-Torr Ne gas fill is only slightly larger than the signal recorded with no gas. This signal is much smaller than expected, and the fluctuations in both signals are indicative of the noise level of this detector. An estimate of the power expected in the Ne K-α line emission is given in Fig. 8. The power in the K-α line (P_α) is a fraction of the pump power (P_p). Contributions to this fraction

are identified in Fig. 8. This fraction is 2.7×10^{-4} for a 100-Torr Ne gas fill. For 160 GW in the pump, a power of 40 MW is expected in the Ne K-α line. This result is an order of magnitude larger than the measured signal!

This extremely small K-α emission may be due to increased opacity of the Ne plasma due to collisional ionization. Calculations of the ionization of Ne under conditions similar to this experiment have been carried out by J. Apruzese. Results for fractional populations of Ne I, Ne II, and Ne III without and with collisional ionization are compared in Fig. 9. With collisional ionization, the Ne II population increases by more than two orders of magnitude to nearly 30%, while the Ne III population remains small (~ 5%) and is nearly unchanged. This ionization is generated by electrons which are produced in the photoionization of Ne I. For example, ionization by the Ly-α line produces 150-eV photoelectrons which have enough energy to cause several collisional ionizations of Ne I. The large Ne II population is sufficient to produce at least an order-of-magnitude reduction in the opacity of the Ne plasma and to account for the unexpectedly small K-α emission. This collisional ionization of Ne II is not detrimental to the lasing by Ne III.

In conclusion, a Ne gas bag with a 100-Torr fill has been fielded successfully adjacent to an imploding Ne gas puff. The imploded Ne plasma has produced 6 kJ (160 GW) of Ne K-shell radiation to pump the neutral Ne in the gas bag. Ne II K-α radiation from the gas bag was much less than expected, probably due to self absorption. Measurements using lower Ne density in the gas bag are needed to confirm the self-absorption explanation. Spectral measurements of x-rays from the gas bag should be carried out to confirm that this emission is really Ne II K-α x-rays. Finally, emission from the neon gas bag in the region of the lasing radiation (~ 500 Å) needs to be diagnosed.

III. Sodium-Neon Photopumping

Effort to develop a pulsed-power driven Na/Ne photopumped soft x-ray laser was initiated a few years ago, and the first experiments to demonstrate the fluorescence of Ne by Na were carried out in FY88 and published in FY89.[6] This publication was awarded an Alan Berman Research Publication Award at NRL in FY89. Since much of this work has been published recently, only the highlights will presented here. I will concentrate on continuing efforts to quantify the Ne lasant plasma conditions and to increase the Na pump power.

A simplified energy level diagram for the Na-Ne photopumped system is given in Fig. 10. Line-coincident radiation (11 Å) from the n=2-1 transition in heliumlike Na pumps the n=4-1 transition in heliumlike Ne. The n=4 level is overpopulated relative to the n=3 and possibly n=2 levels of heliumlike Ne leading to lasing at 230 Å, 82 Å, and 58 Å. Fluorescence experiments are based on relative measurements of x-rays from the n=4-1 (He-γ) and n=3-1 (He-β) transitions under different experimental conditions. No measurements of the potential lasing transitions have been carried out. Optimum conditions for photopumping are that the intensity of the 11-Å heliumlike Na radiation be maximized (i.e., $T_e \sim 300$ eV, $n_i \sim 10^{20}$ cm^{-3}) and that the Ne plasma be primarily in the heliumlike ground state at sufficiently low density to avoid radiation trapping (i.e., $T_e \sim 50$-100 eV, $n_i \sim 10^{18}$ cm^{-3}). Because the densities and temperatures of these two plasmas are so different, two separate, but closely spaced, plasmas are required.

The development of a sodium fluoride (NaF) plasma source to produce the Na pump through a z-pinch implosion was a major accomplishment in this program. A detailed description of this capillary-discharge source was published in FY89.[7] Implosion of the plasma from this source was used to produce the Na pump for fluorescence experiments carried out on the Gamble II generator.

Another breakthrough was the simultaneous creation of side-by-side Na and Ne plasmas under conditions appropriate for fluorescence experiments. The arrangement of these two plasmas on the Gamble II generator is shown in Fig. 11. The NaF plasma was injected on the axis of the generator and imploded by the total generator current. The Ne plasma was located 5 cm from the Na plasma and replaced one of the return-current rods. Only a fraction of the generator current was carried by the Ne plasma so that a softer implosion, with correspondingly lower temperature and density, was produced.

Experiments which confirm the photopumping of Ne by Na were carried out using this geometry in FY89. The experiments are described in Ref. 8, and the results are highlighted in Fig. 12. In this figure, the ratio of the intensities of the He-γ and He-β lines from the Ne plasma are compared for different experimental conditions. This ratio is 0.64 when the sodium pump is not present, as indicated by the "neon only" region in Fig. 12. This ratio corresponds to the average of the measured ratios for three different shots where the Na pump was replaced by a short circuit. The γ/β ratio is enhanced when the Na pump is coincident with or slightly later than the Ne implosion.

There is a time interval associated with producing the Ne plasma due to "zippering" of the Ne implosion. Because the Ne diverges as the gas emerges from the nozzle, the Ne implodes first at the nozzle and later further from the nozzle. This explains why the γ/β ratio is enhanced up to 30 ns after the Ne first implodes. No enhancement is observed when the Na pump occurs before the Ne has imploded or when the Na is replaced by Mg. Finally, none of the spectral lines associated with Ne were observed when the Ne was replaced by Ar. Fluorescence was observed only when both the Na and Ne were present and their implosions were coincident in time.

Preparation of the Ne plasma for lasing experiments is being carried out on a test stand where Ne implosions are being studied under conditions similar to the Ne return-current geometry used on Gamble II. The test stand is used to make detailed measurements of the lasant plasma without involving operation of the much larger Gamble II generator. Implosion calculations (0-D) were carried out to determine the driving current and mass loading required to implode Ne to the temperature (50-100 eV) and density (10^{18} cm^{-3}) needed for lasing. The results in Fig. 13 indicate that currents of about 150 kA and mass loadings of about 5 μgm/cm should be adequate. A test stand with a low inductance current source which can produce 120-240 kA is being used to study Ne implosions. The test-stand arrangement is shown in Fig. 14. The Ne gas-puff hardware is the same as that used in the Gamble II experiments. The risetime of the current can be reduced from 0.8 μs to about 0.1 μs with a plasma opening switch (POS). X-rays from the Ne plasma are recorded with a variety of diagnostics as indicated in Fig. 14 and preliminary results of these studies have been reported.[9,10]

Implosions of Ne with and without the POS are compared in Fig. 15. The L-shell x-ray traces were recorded by an XRD with a 1.8-μm Kimfol filter. Without the POS, the implosion occurs about 0.5-μs after the current starts. With the POS, the upstream current is conducted by the POS for 0.4 μs; then the switch opens and the downstream current rises in about 0.1 μs to drive the implosion. This current waveform and implosion are similar to that produced in the return-current geometry on Gamble II.

Quantitative measurements of the ground-state population of heliumlike Ne (Ne IX) in the imploded plasma are important to optimize the lasant. Radiations from Ne VIII, rather than Ne IX, are used for such measurements because the excited states of Ne VIII are much closer in energy to the Ne IX

ground state than the excited states of Ne IX, as indicated in Fig. 16. The Ne IX ground-state population can be determined from measurements of excited-state populations of Ne VIII using equilibrium atomic-physics models provided the temperature and density are known. Grazing incidence spectra from Ne implosions driven by low current (80 kA) and high current (150 kA) are shown in Fig. 17. These spectra were recorded without the POS, and the currents correspond to values at the time of implosion. Spectral lines from Ne VIII and Ne VII are identified in these spectra. For the larger current, there is evidence of a spectral line from Ne IX. The presence of this line indicates that this plasma is too hot, and a lower current or larger linear mass density should produce a larger Ne IX ground-state population. Such measurements are being used to establish the current and linear mass density required to optimize the Ne IX ground-state population for implosions in which the POS is used.

Absolute spectral intensity measurements are required to determine excited state populations. Because absolute measurements in the spectral region are so difficult, we are using radiations corresponding to 3p-3s transitions in Ne VIII to determine excited-state populations of Ne VIII, as shown in Fig. 18. The 3 -2 transitions in this figure at 88 Å, 98 Å, and 103 Å correspond to the three most intense spectral lines observed in Fig. 17, but absolute measurements of these these lines are very difficult. The 3p-3s transitions at 2819 Å and 2858 Å have been observed in the present experiment, and an absolute measurement of the $3p_{3/2}$-$3p_{1/2}$ transition (2819 Å) is being carried out to determine excited-state populations of Ne VIII. This measurement is complicated by the presence of an intense continuum in this spectral region which is associated with the implosion. Spectral, spatial, and temporal resolution are required to make this measurement.

The power of the Na pump must be increased to obtain detectable lasing. Calculations[6] indicate that a pump power of at least 200 GW is needed for a 5-cm separation of the pumped Ne and the Na pump. To achieve higher power, a driving current of 3-4 MA from the Double Eagle generator at Physics international will be used to implode plasma from the NaF discharge source. A schematic of this source geometry on Double Eagle is shown in Fig. 19. To match the implosion to the increased driving current, the mass per unit length of the NaF plasma must be increased. Measurements on Gamble II have suggested that the mass can be increased by driving more current through the capillary.

The capillary current has been increased to about 200 kA by doubling the storage capacitance and doubling the voltage on the capacitors. This modified source was operated successfully at NRL. Spatial and temporal properties of the NaF plasma have been characterized by measurements of visible light from the emitted plasma. In FY90, this source will be fielded on Double Eagle in collaboration with personnel at Physics International.

In conclusion, the fluorescence of heliumlike Ne by 11-Å line radiation from a Na plasma has been demonstrated. Experiments are underway to determine the experimental conditions needed to optimize the heliumlike ground-state population of Ne in the Ne lasant plasma. Finally, the NaF capillary-discharge source has been successfully modified for implosion experiments with 3-MA driving currents in order to produce higher Na pump power. Experiments with this source on Double Eagle are scheduled for FY90.

REFERENCES

1. E.J. McGuire, Phys. Rev. Lett. 35, 844 (1975).
2. H.C. Kapteyn and R.W. Falcone, Phys. Rev. A 37, 2033 (1988).
3. S.J. Stephanakis, S.W. McDonald, P.F. Ottinger, J.R. Boller, V.E. Scherrer and F.C. Young, Bull. Am. Phys. Soc. 30, 1389 (1985).
4. J.P. Apruzese, A. Dasgupta, and P.C. Kepple, Conf. on Atomic Processes in Plasmas, Gaithersburg, MD (1989).
5. G. Mehlman, P.G. Burkhalter, S.J. Stephanakis, F.C. Young, and D.J. Nagel, J. Appl. Phys. 60, 3427 (1986).
6. S.J. Stephanakis, et al., IEEE Trans. Plasma Sci. 16, 472, (1988).
7. B.L. Welch, F.C. Young, R.J. Commisso, D.D. Hinshelwood, D. Mosher, and B.V. Weber, J. Appl. Phys. 65, 2664 (1989).
8. F.C. Young, et al., in Proceedings, International Conference on LASERS'88, R.C. Sze and F.J. Duarte, Eds. (STS Press, McLean, VA 1989) pp.98-105.
9. B.L. Welch, H.R. Griem, D.D. Hinshelwood, G. Mehlman, V.E. Scherrer, and F.C. Young, Bull. Am. Phys. Soc. 33, 2064 (1988).
10. B.L. Welch, F.C. Young, H.R. Griem, and S.J. Stephanakis, Conference Record - IEEE Inter. Conf. on Plasma Sci., IEEE Catalogue No. 89CH-2760-7, 1989, p. 167.

Auger Lasing Scheme for Ne

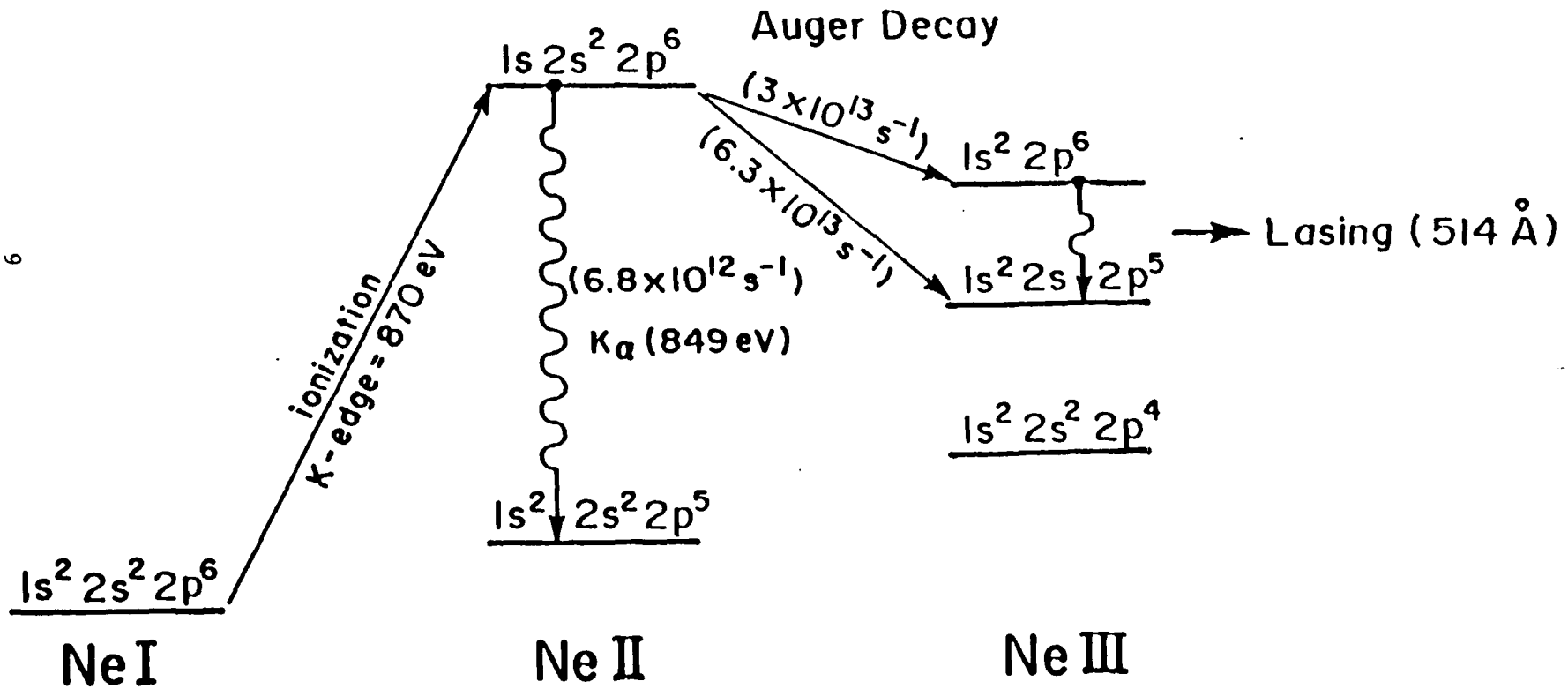

Figure 1.

NEON-NEON PHOTOPUMPING EXPERIMENT

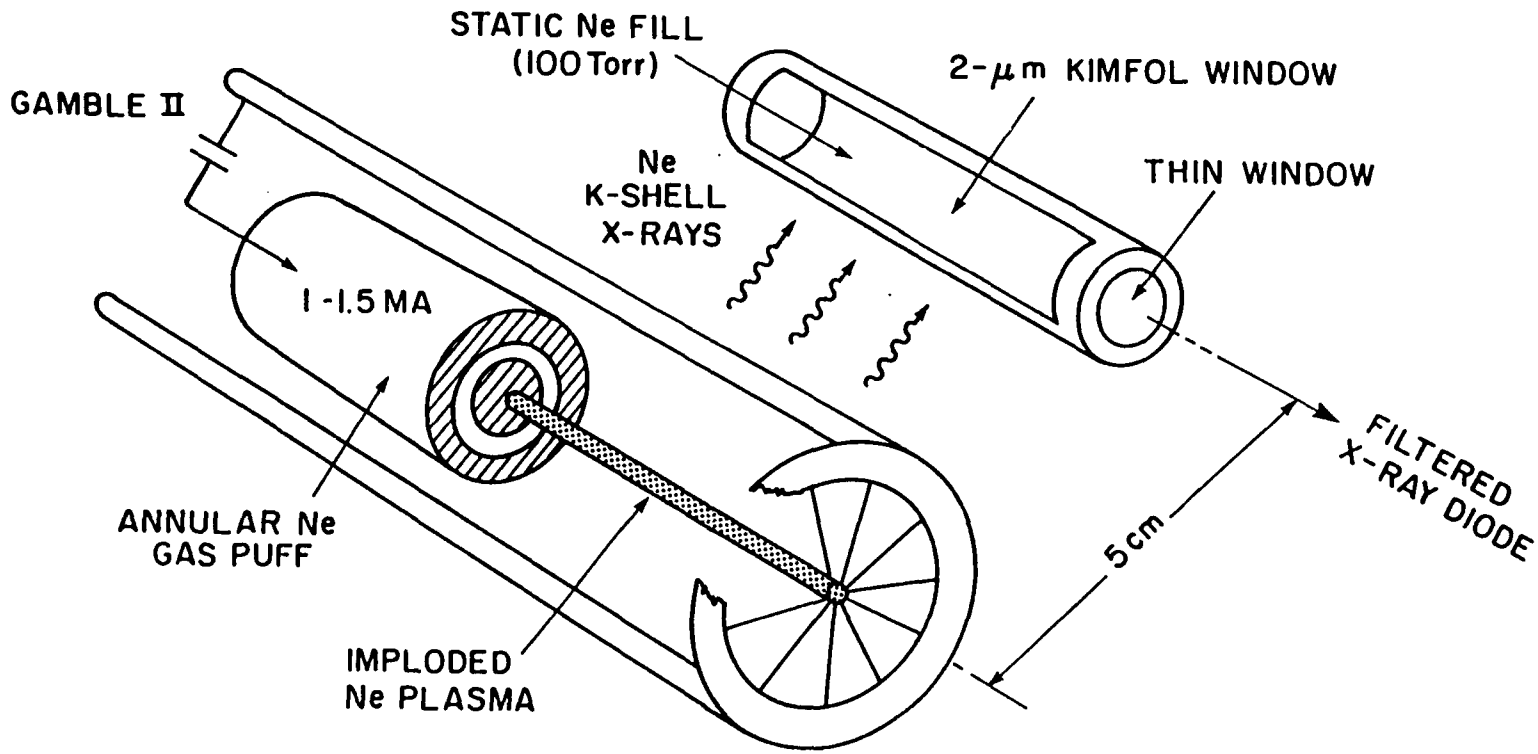

Figure 2.

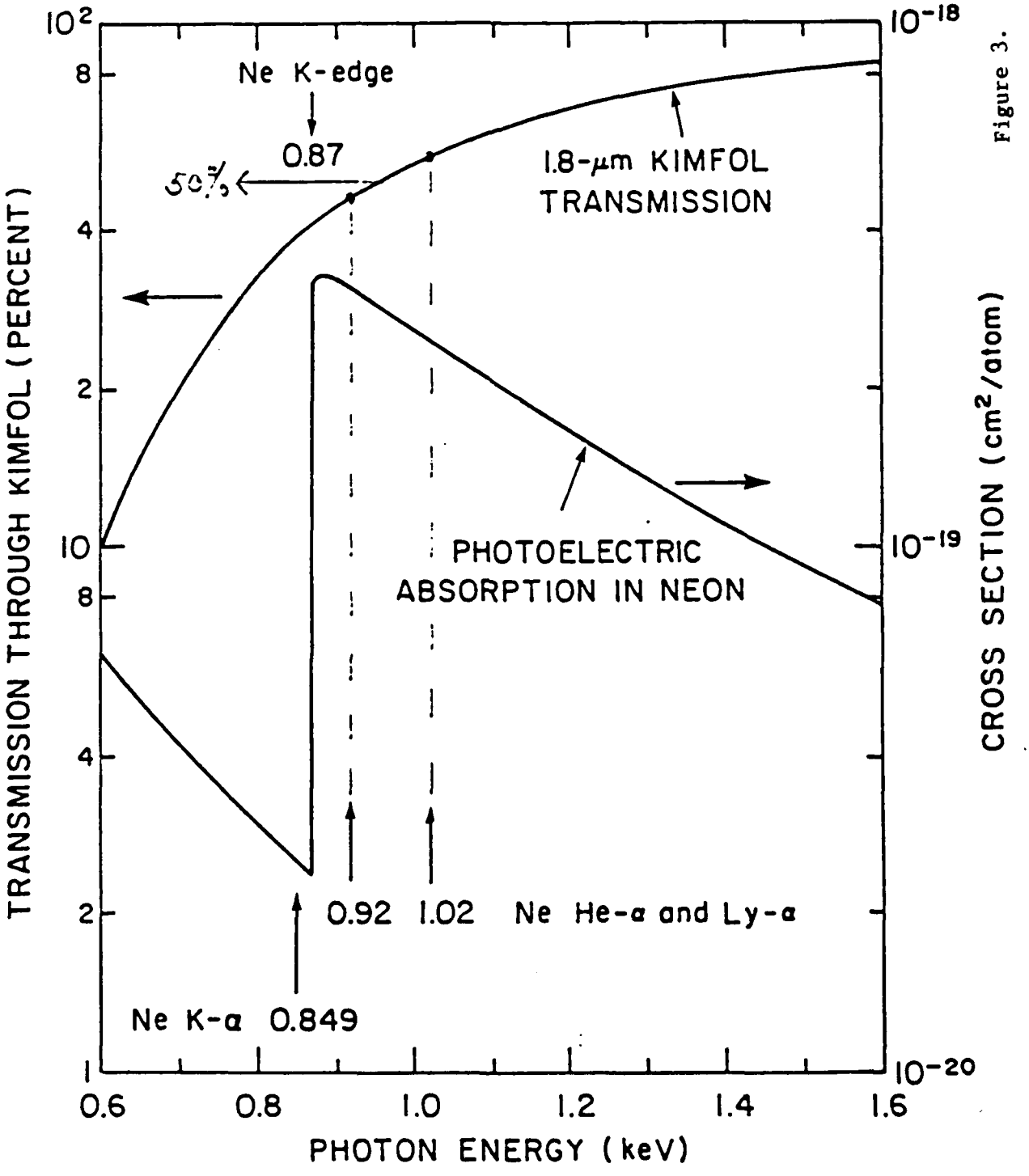
Ne K-edge
0.87
50%
1.8-μm KIMFOL
TRANSMISSION
PHOTOELECTRIC
ABSORPTION IN NEON
0.92
1.02
Ne He-α and Ly-α
Ne K-α 0.849
TRANSMISSION THROUGH KIMFOL (PERCENT)
CROSS SECTION (cm²/atom)
PHOTON ENERGY (keV)
10²
8
4
2
10
8
4
2
1
10⁻¹⁸
10⁻¹⁹
10⁻²⁰
0.6
0.8
1.0
1.2
1.4
1.6

Figure 3.

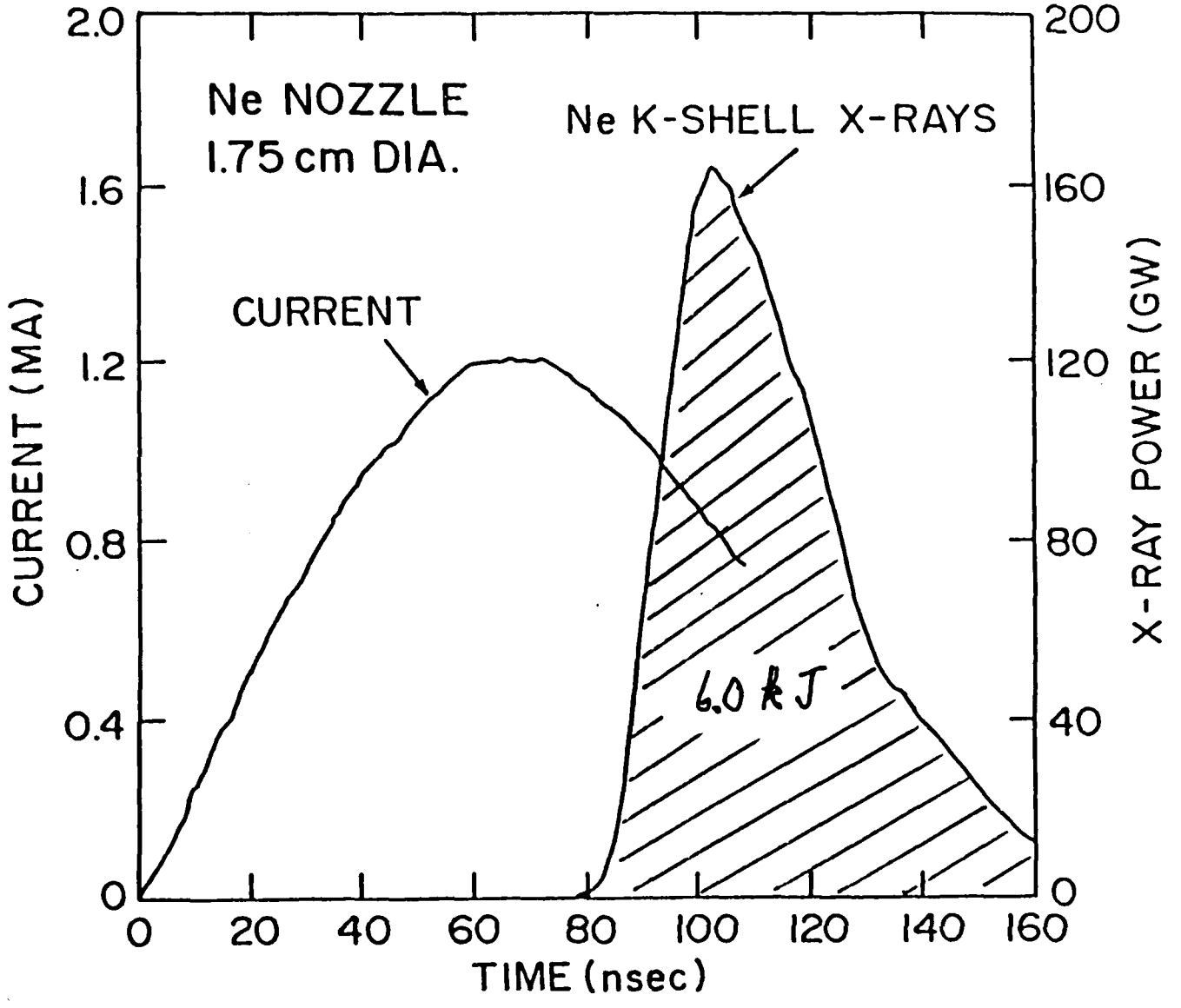
Ne NOZZLE
1.75 cm DIA.
Ne K-SHELL X-RAYS
CURRENT
6.0 kJ
CURRENT (MA)
X-RAY POWER (GW)
TIME (nsec)
2.0
1.6
1.2
0.8
0.4
0
200
160
120
80
40
0
0
20
40
60
80
100
120
140
160

Figure 4.

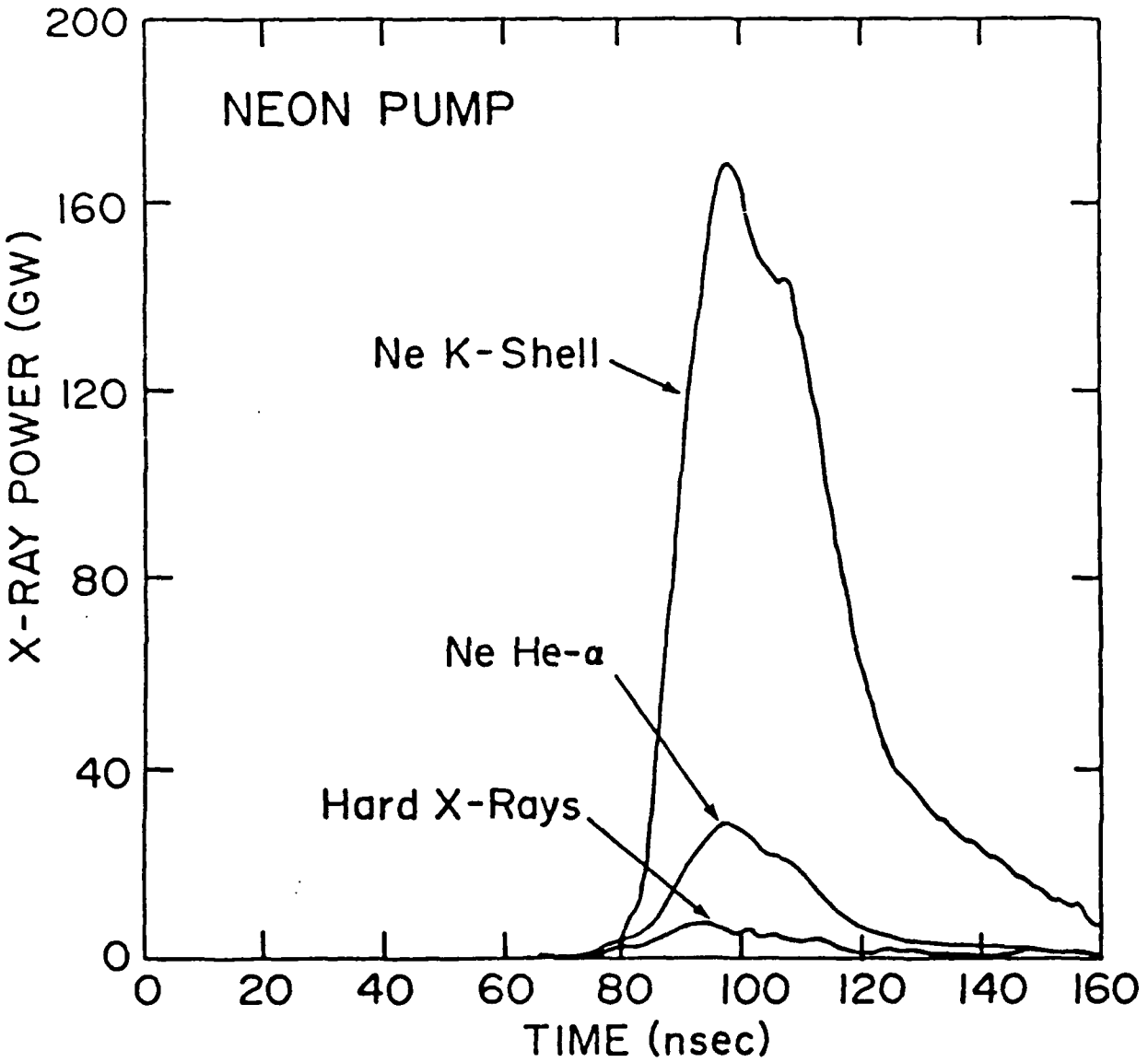
NEON PUMP
X-RAY POWER (GW)
200
160
120
80
40
0
Ne K-Shell
Ne He-α
Hard X-Rays
0
20
40
60
80
100
120
140
160
TIME (nsec)

Figure 5.

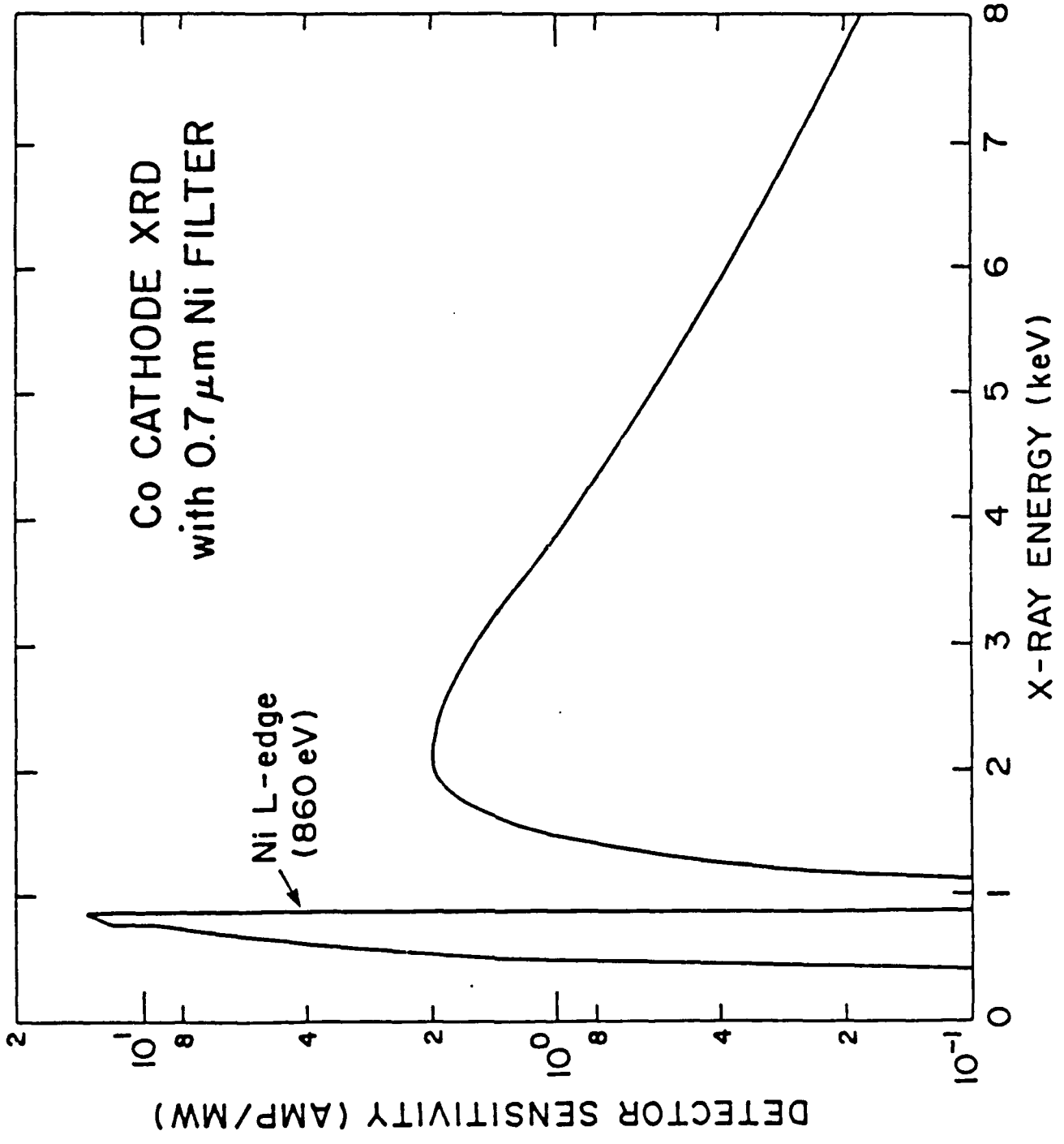
Co CATHODE XRD
with 0.7 μm Ni FILTER
Ni L-edge
(860 eV)
DETECTOR SENSITIVITY (AMP/MW)
X-RAY ENERGY (keV)
2
8
4
2
8
4
2
0
1
2
3
4
5
6
7
8

Figure 6.

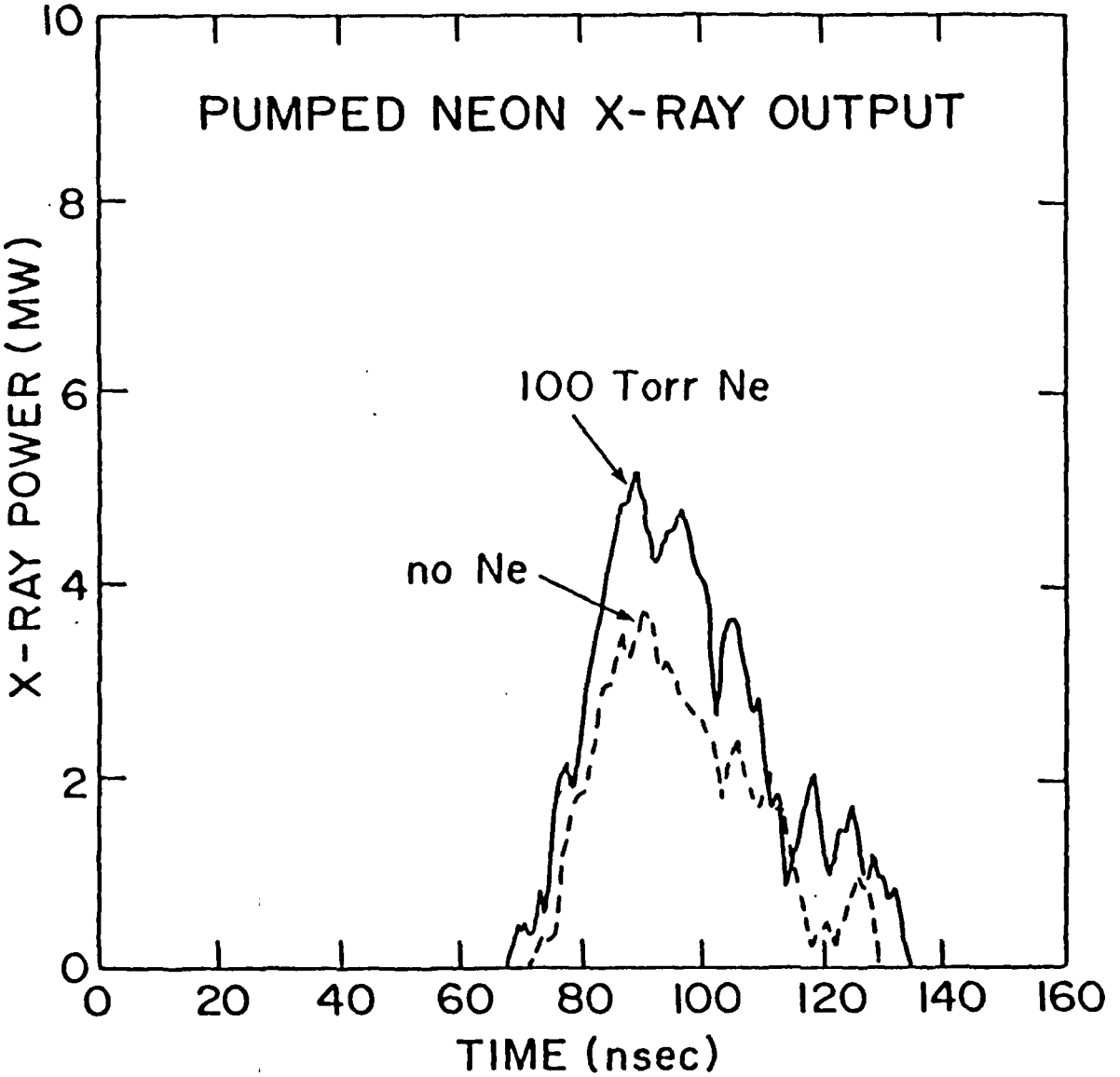
PUMPED NEON X-RAY OUTPUT
X-RAY POWER (MW)
TIME (nsec)
100 Torr Ne
no Ne
0
2
4
6
8
10
0
20
40
60
80
100
120
140
160

Figure 7.

CALCULATE NEON K_α LINE EMISSION

- Power of Ne K_α line; $P_\alpha = P_P * f_\Omega * T_P * f_A * B * T_S * T_K$

  where

  P_P = Pump Power (measured)

  f_Ω = solid angle fraction (17%)

  T_P = filter transmission of pump (49%)

  f_A = absorption fraction in cold Ne (57%)

  B = branching ratio for NeII K_α decay (1.85%)

  T_S = neon transmission of K_α x-rays (83%)

  T_K = filter transmission of K_α x-rays (38%)

- P_α is 5 to 10x larger than measured power.

Figure 8.

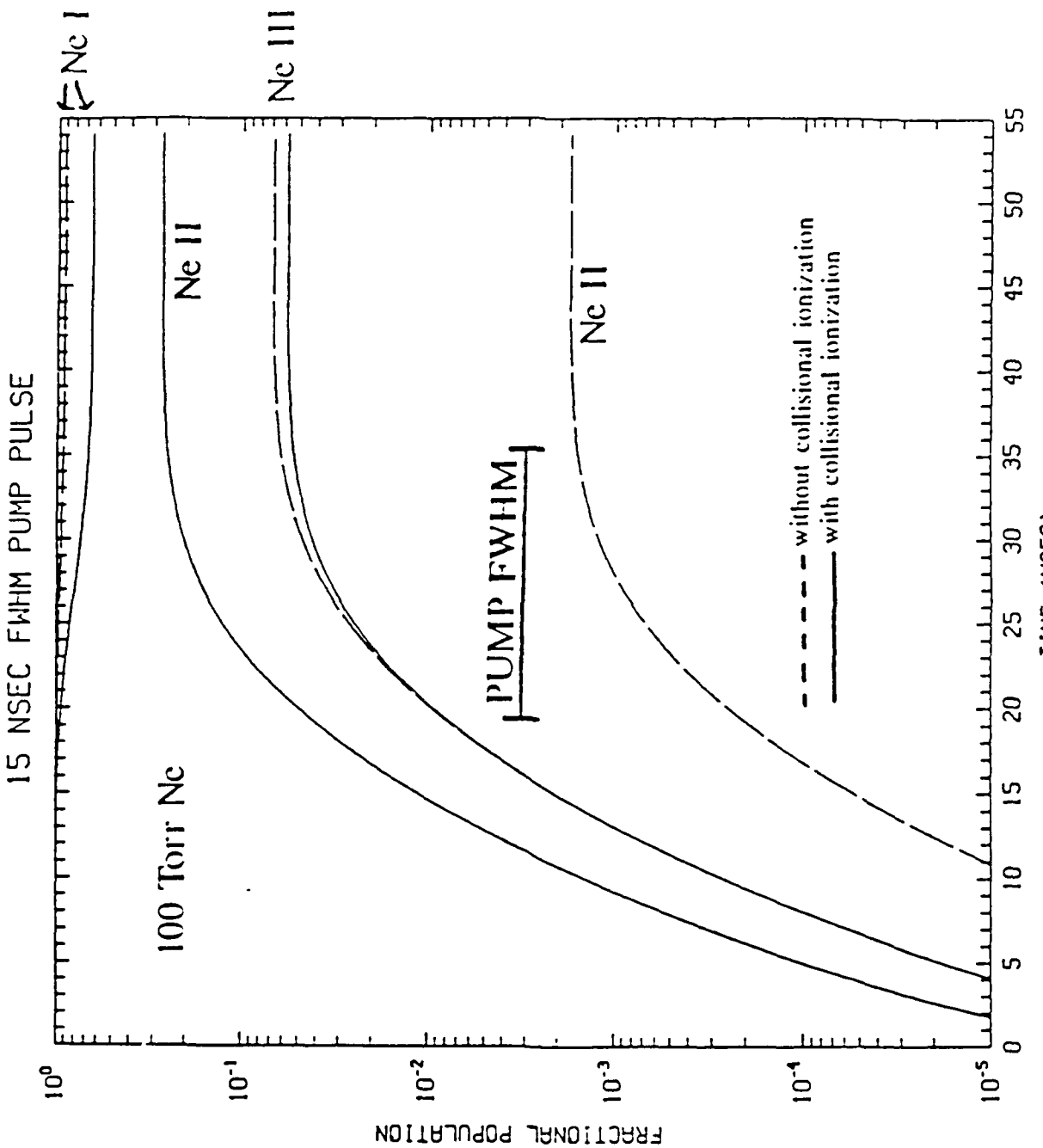
15 NSEC FWHM PUMP PULSE
100 Torr Ne
Ne I
Ne II
Ne III
Ne II
PUMP FWHM
without collisional ionization
with collisional ionization
FRACTIONAL POPULATION
TIME (NSEC)
10^0
10^-1
10^-2
10^-3
10^-4
10^-5
0
5
10
15
20
25
30
35
40
45
50
55

Figure 9.

SODIUM-NEON PHOTOPUMPED SYSTEM

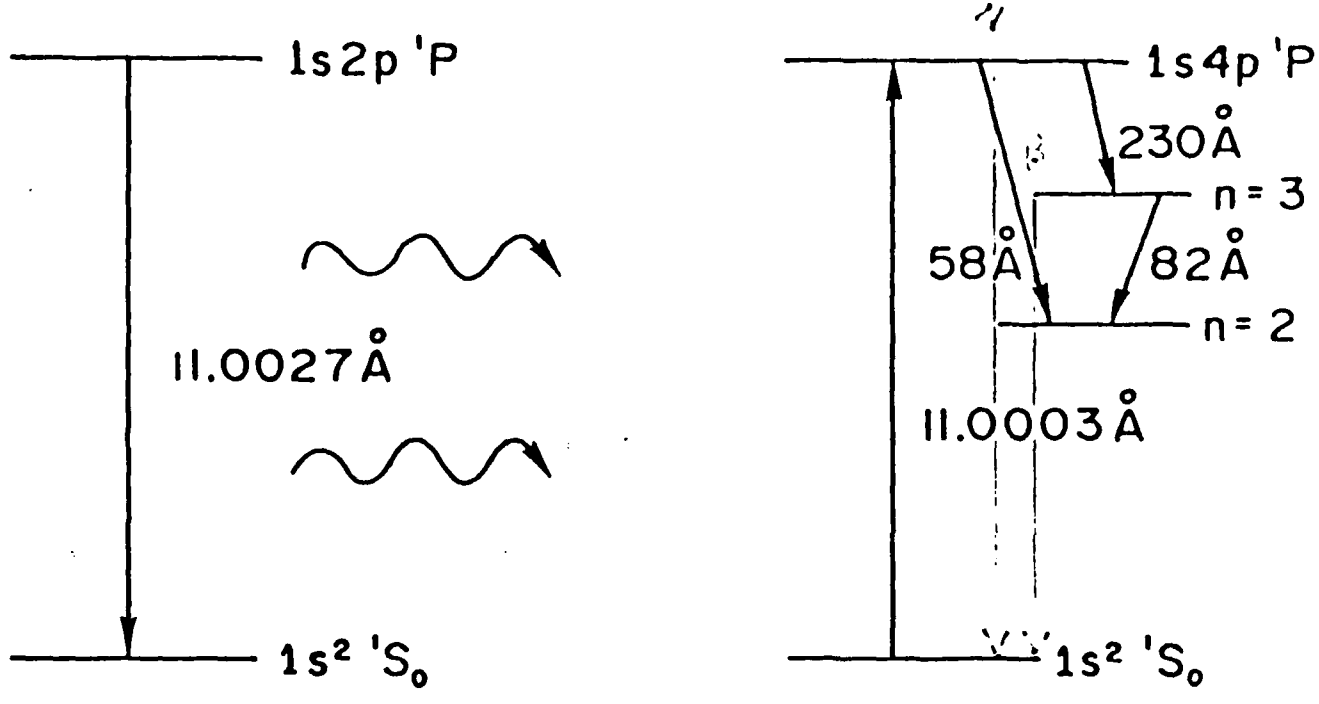

He-like Na
PUMP

~ 300 eV

~ 10^{20} ions/cm^3

He-like Ne
LASANT

50 - 100 eV

~ 10^{18} ions/cm^3

Figure 10.

FLUORESCENCE EXPERIMENT ON GAMBLE II

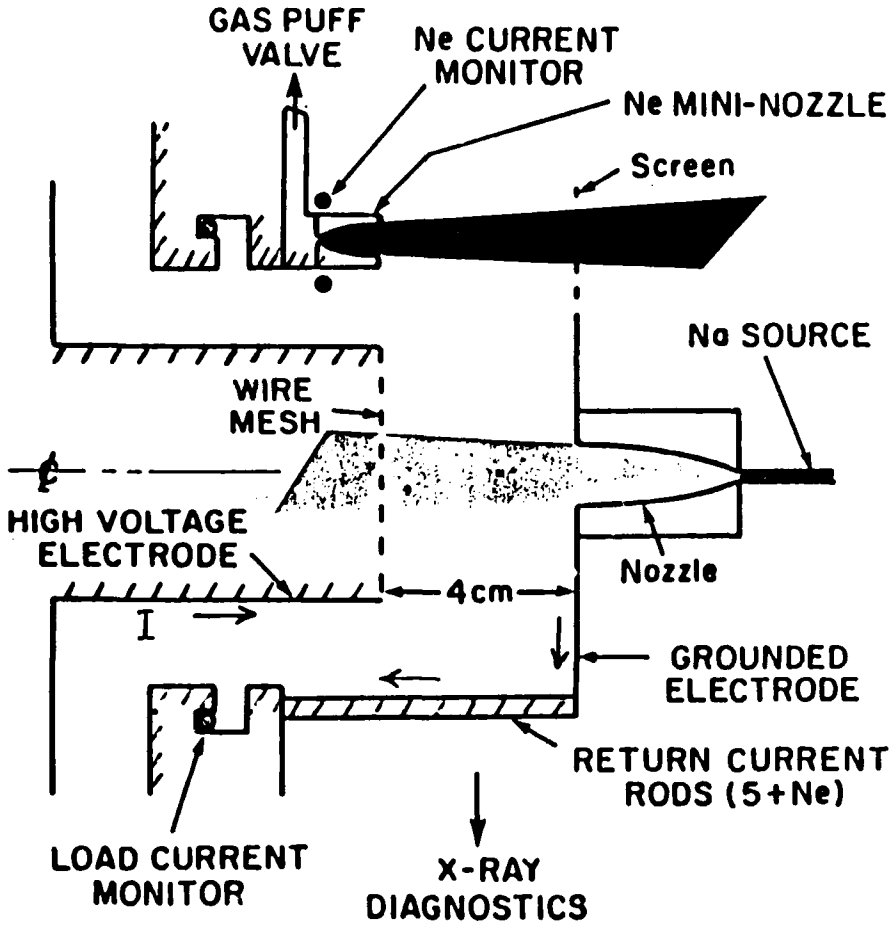

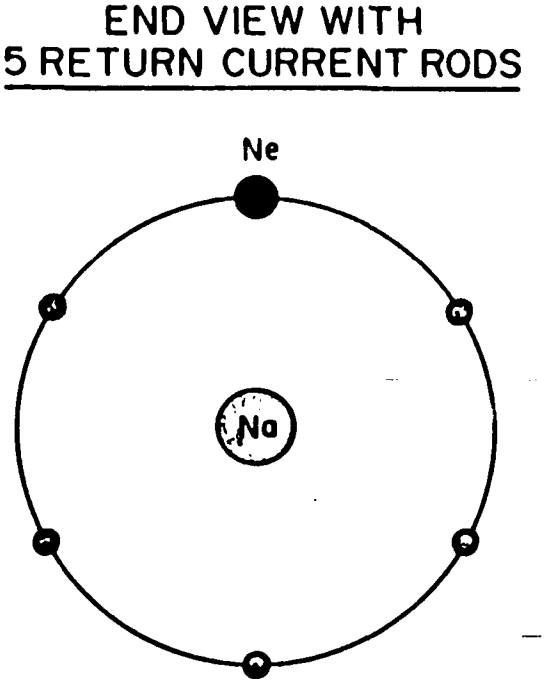

Figure 11.

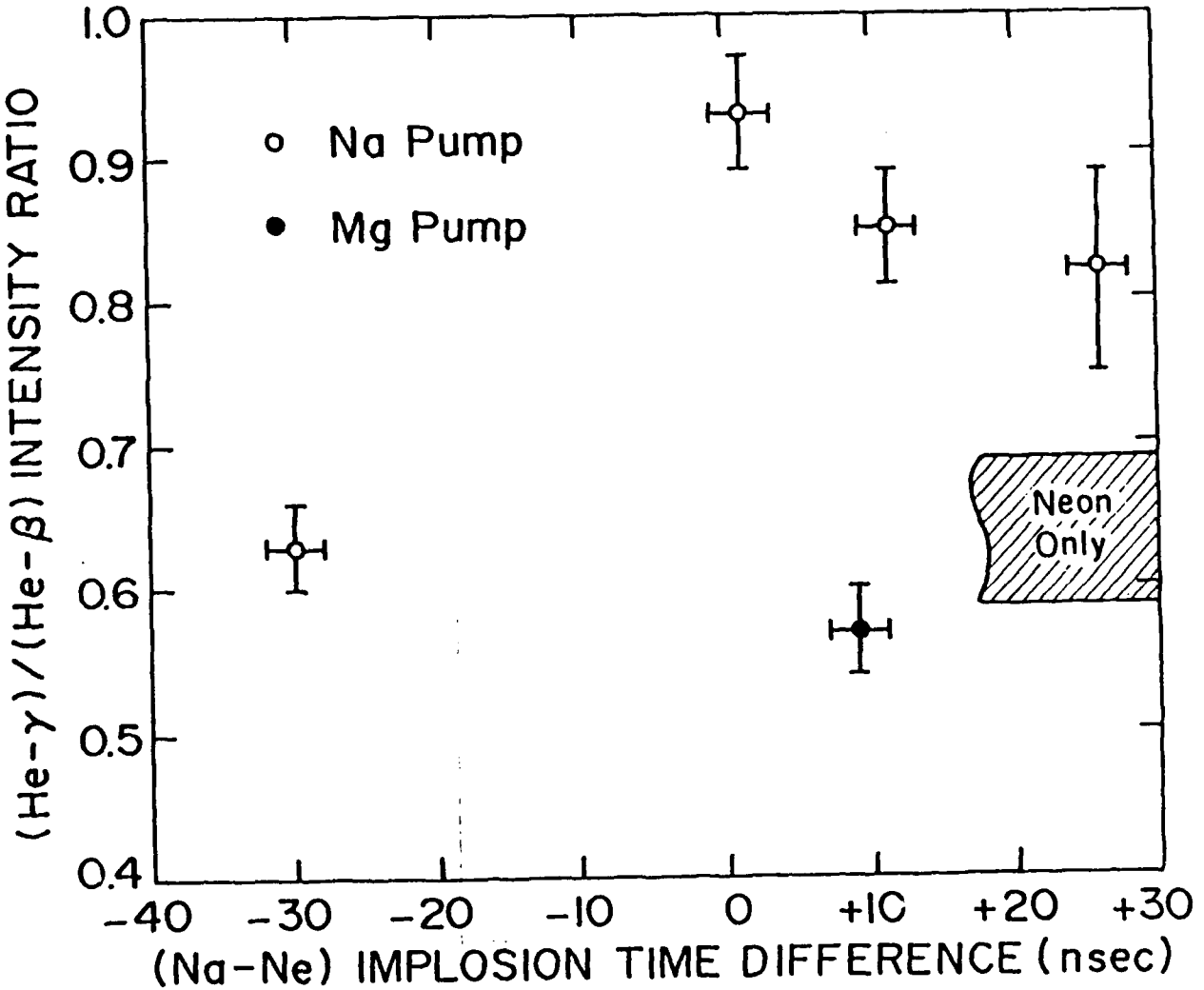
1.0
0.9
0.8
0.7
0.6
0.5
0.4
(He-γ)/(He-β) INTENSITY RATIO
o Na Pump
• Mg Pump
Neon
Only
-40
-30
-20
-10
0
+10
+20
+30
(Na-Ne) IMPLOSION TIME DIFFERENCE (nsec)

Figure 12.

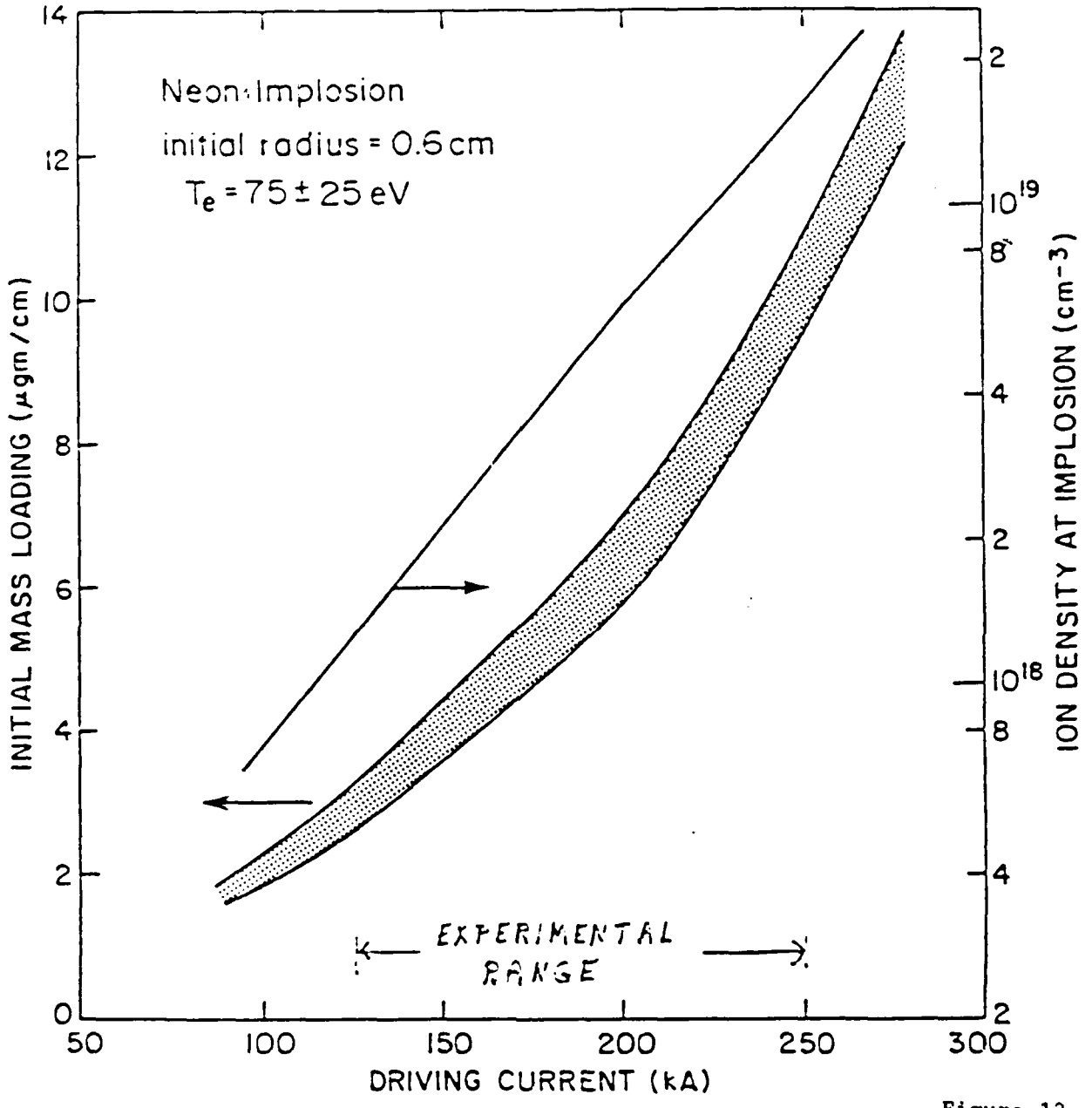
Neon Implosion
initial radius = 0.6 cm
$T_e = 75 \pm 25$ eV
INITIAL MASS LOADING (μgm/cm)
ION DENSITY AT IMPLOSION (cm^{-3})
DRIVING CURRENT (kA)
EXPERIMENTAL RANGE
0
2
4
6
8
10
12
14
50
100
150
200
250
300
10^{18}
10^{19}

Figure 13.

NEON LASANT PLASMA EXPERIMENT

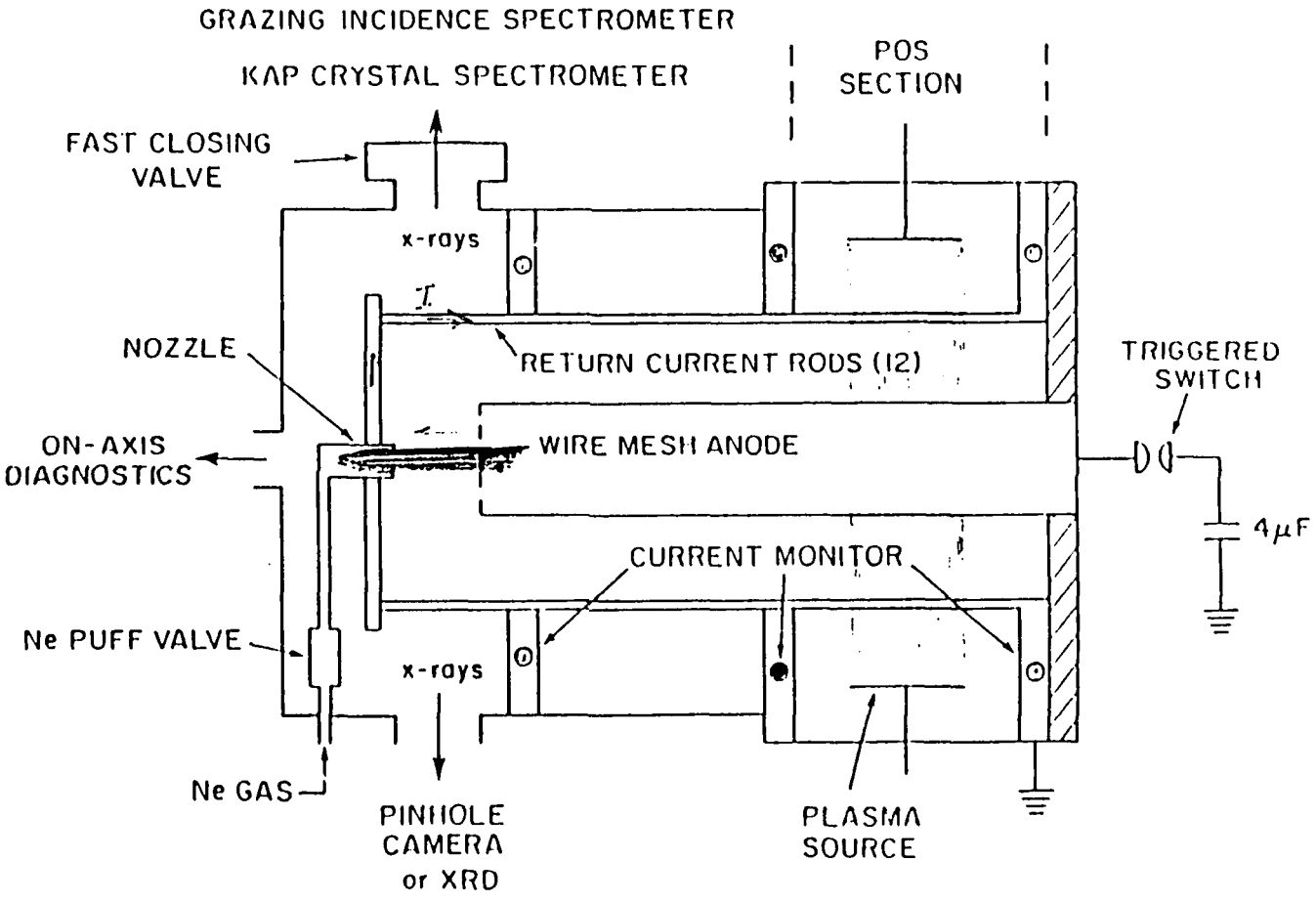

Figure 14.

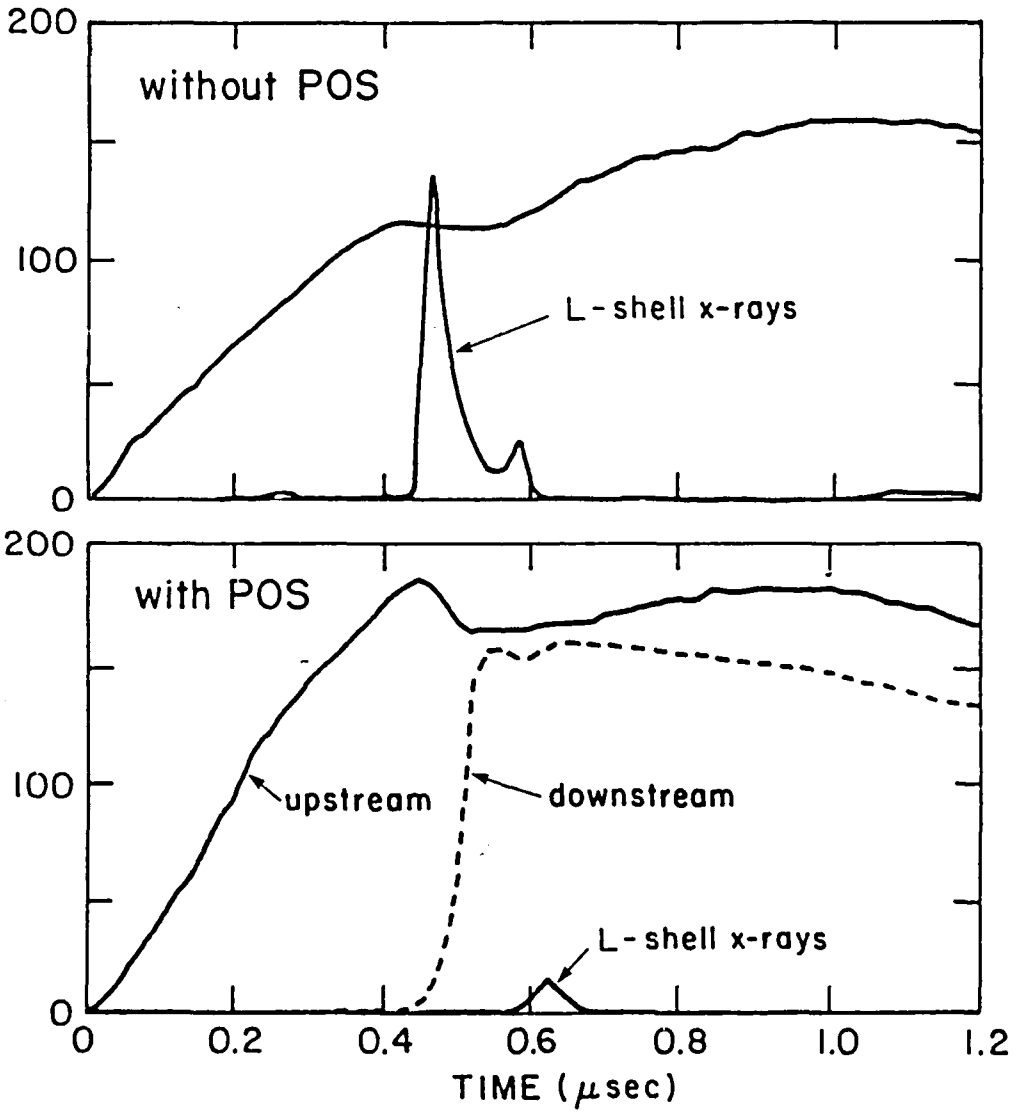
200
without POS
100
L-shell x-rays
0
200
with POS
100
upstream
downstream
L-shell x-rays
0
0
0.2
0.4
0.6
0.8
1.0
1.2
TIME (μsec)

Figure 15.

Level Diagram for Ne VIII and Ne IX

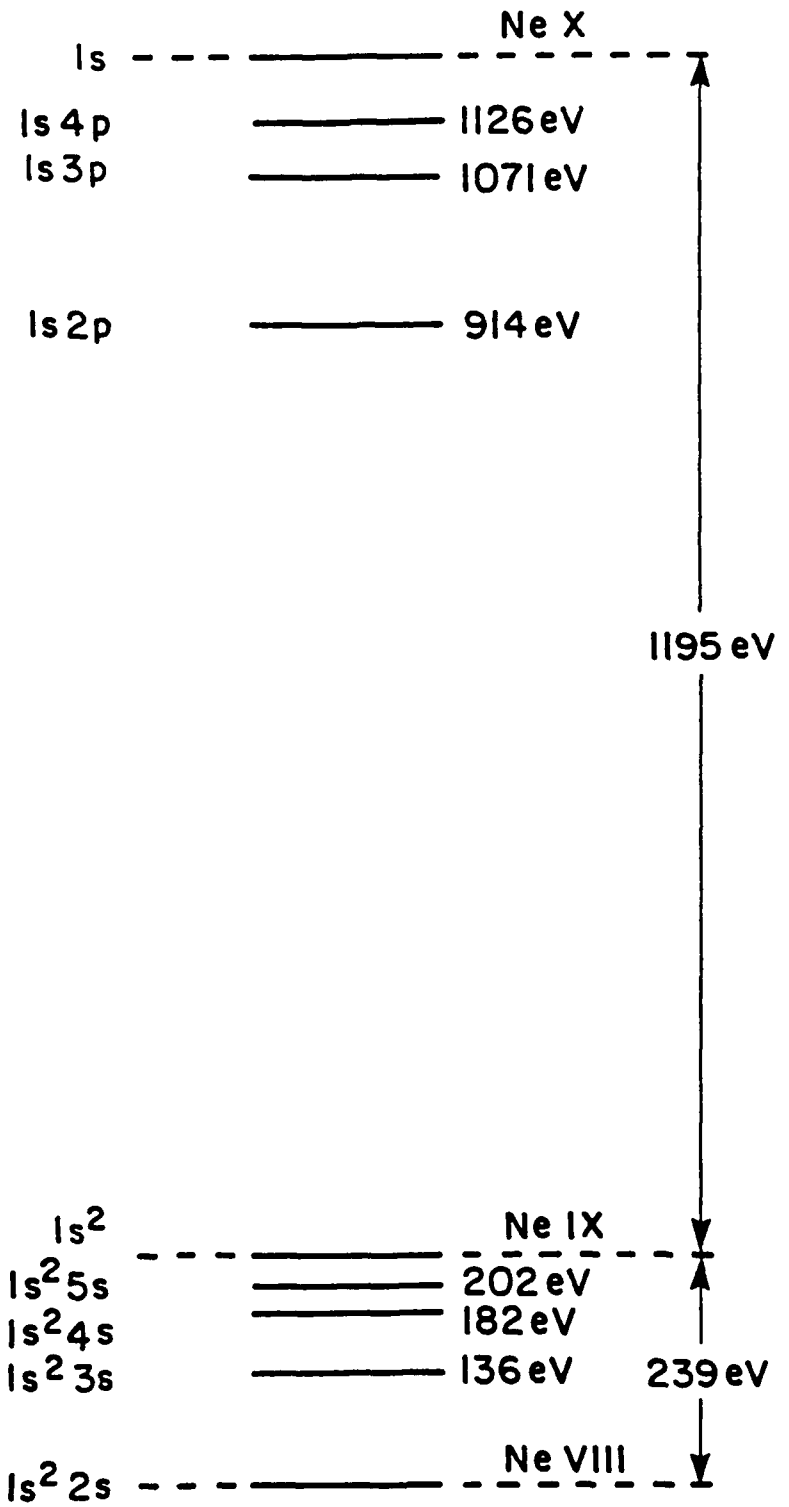

Figure 16.

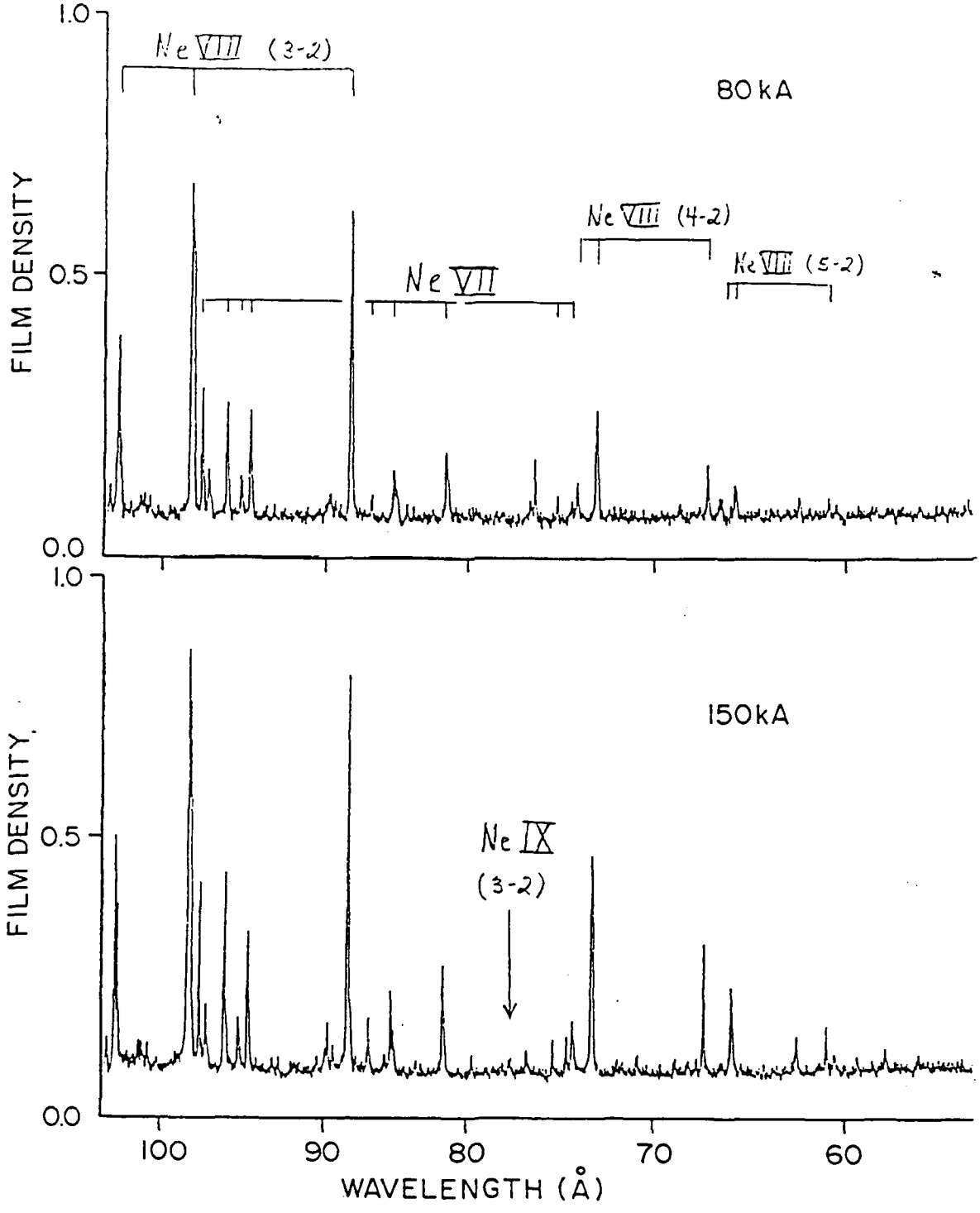
GRAZING INCIDENCE SPECTRA OF IMPLODED NEON
1.0
0.5
0.0
FILM DENSITY
Ne VIII (3-2)
80 kA
Ne VII
Ne VIII (4-2)
Ne VIII (5-2)
1.0
0.5
0.0
FILM DENSITY
150kA
Ne IX
(3-2)
100
90
80
70
60
WAVELENGTH (Å)

Figure 17.

BRANCHING-RATIO MEASUREMENT

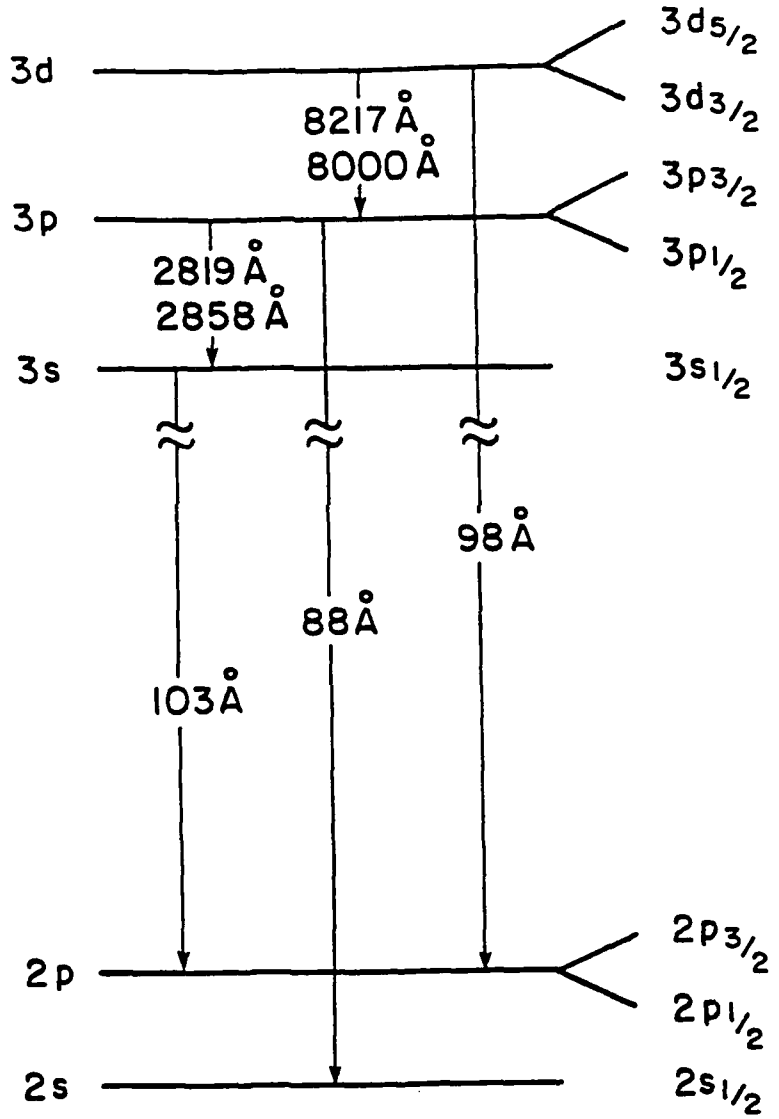

Ne VIII

Figure 18.

NaF CAPILLARY SOURCE FOR DOUBLE-EAGLE TO PRODUCE SEVERAL HUNDRED GW OF SODIUM PUMP RADIATION

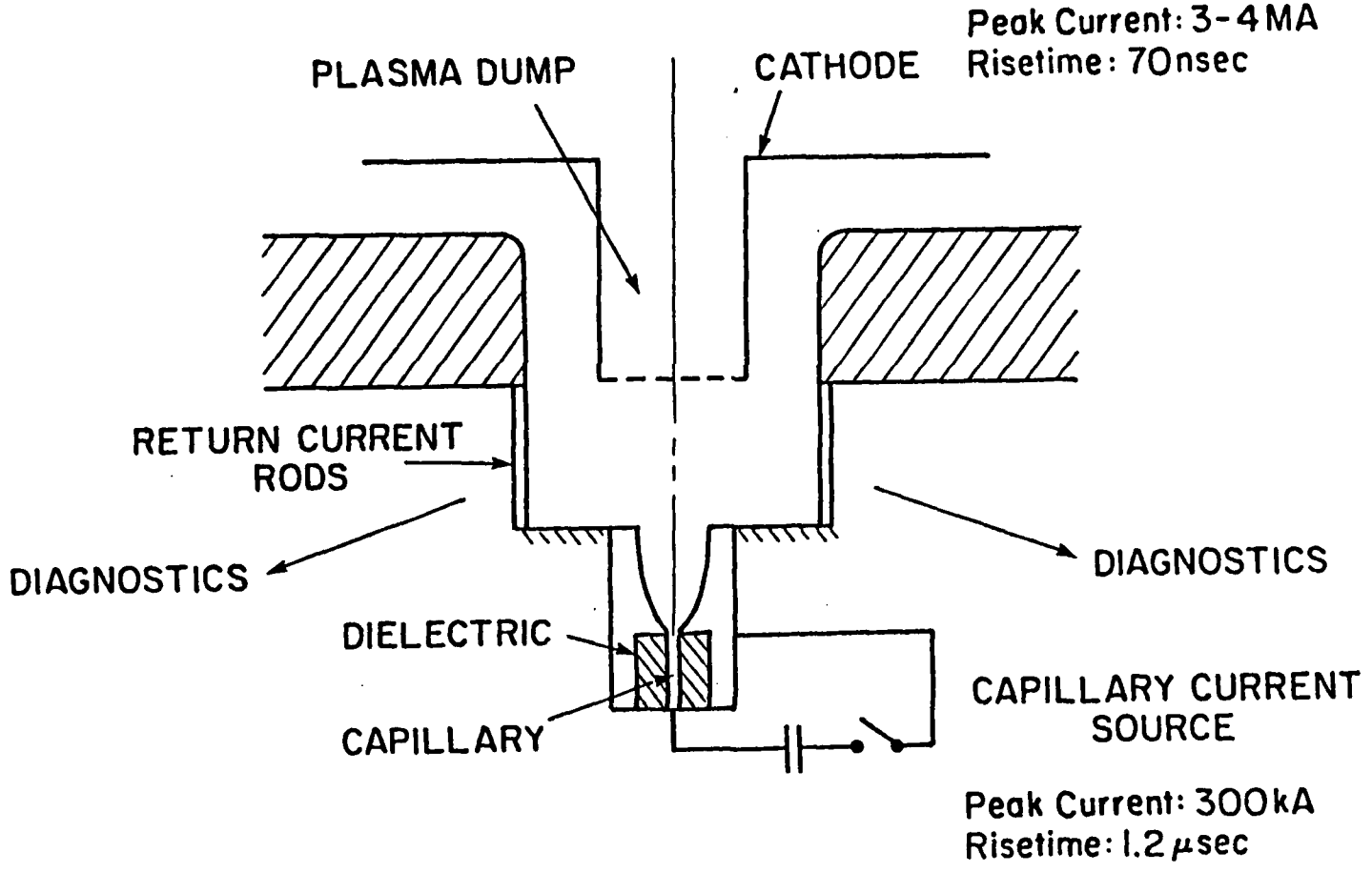

Figure 19.

Section II

MODELING OF AN AUGER-PUMPED NEON-NEON 514 Å LASER SUITABLE FOR THE NRL GAMBLE-II GENERATOR

J. P. Apruzese, A. Dasgupta, P. C. Kepple, and M. Buie

Radiation Hydrodynamics Branch

I. INTRODUCTION

The recent successful demonstrations of Auger-pumped lasers in the 1000 Å region[1-4] encourage efforts to scale such schemes to obtain shorter wavelength lasing. The original 1975 Auger- inversion proposal by McGuire[5] is an attractive possibility for such scaling and also appears well suited to the capabilities of the NRL Gamble-II generator. In his paper McGuire devoted most of his work to singly ionized (neon-like) sodium but also pointed out that neutral gaseous neon itself would be a promising Auger laser medium. In this chapter we first consider the basic mechanism, then describe the model which has been created to guide NRL's experiments. The final section presents some results and assesses their implications for experimental configurations. Requirements for model improvements are also discussed.

II. LASER MECHANISM

As explained in Ref. 5, photoionization of a K-shell (1s) electron in neutral neon leads to two processes occurring in the resultant Ne II ion. About 2% of the ions will stabilize via radiative decay to the Ne II ground state, emitting an 849 eV (14.6 Å) photon. The other 98% undergo Auger decay to various states of Ne III. The branching ratios of these decays are such as to set up population inversions among some of these states, as shown in Fig. 1. Transient (subnanosecond) population inversions can be achieved relative to the ground state configuration of Ne III; however, for a pulsed-power driven pump source with a radiation risetime of several nanoseconds no useful gain can be obtained in such transitions. Therefore the present analysis concentrates on the $1s^2 2s^o 2p^6\ {}^1S_o$ - $1s^2 2s 2p^5\ {}^1P_1$ 514 Å transition, which can sustain a steady state inversion due to the rapid emptying of the lower level as shown in Fig. 1. The energies given in Fig. 1 have been obtained from the data of Ref. 6; the radiative and Auger decay rates also shown have been calculated using the atomic structure code developed by Cowan.

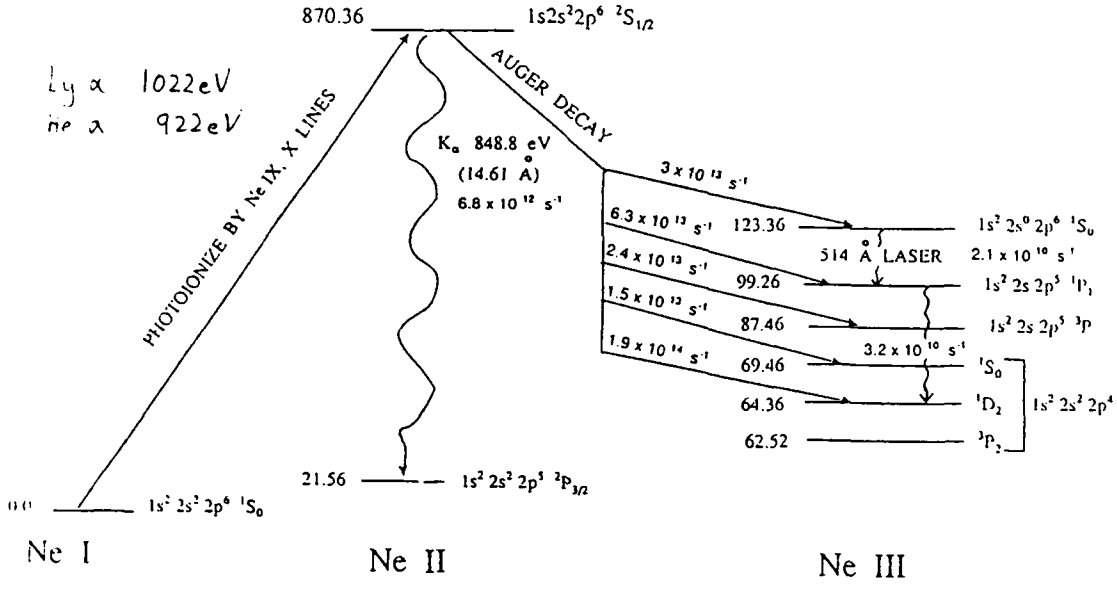

Fig. 1. Energy level diagram for Ne I - Ne III showing levels and processes relevant to the establishment of an Auger-pumped laser in Ne III.

III. MODEL FOR GAIN CALCULATIONS

The model consists of a fully time dependent solution of the coupled rate equations describing the evolution of the populations of the relevant atomic states in Ne I - Ne III. Processes which connect the levels in the calculation are: photoionization by an assumed time-varying pump radiation field, prompt collisional ionization by ejected photoelectrons, radiative and Auger decay, and electron collisional excitation and de-excitation among levels in Ne III which affect the gain coefficient. Cross sections for electron collisional ionization are taken from Ref. 7, photoionization cross sections from Ref. 8, applying the prescription of Ref. 9 to ionization stages above neutral. The bound-bound collision rates were obtained with distorted wave[11] and/or semiclassical[11] computations, as appropriate. The numerical integration of the rate equations was carried out using the algorithm of Young and Boris[12].

The neon lasant is assumed homogeneous. The ions are assumed to remain cold during the duration of the pump (15 ns), which is an order of magnitude shorter than the electron-ion thermal equilibration time. The electron energy distribution consists of freshly stripped photoelectrons and secondaries created in the resulting cascade ionization. The electron-electron thermal equilibration time is less than a nanosecond; however, the time to ionize a neutral neon atom is less than this equilibration time by nearly an order of magnitude. No attempt is made to obtain a fully self-consistent electron energy distribution. The rate equations account for the prompt collisional ionization by the ejected photoelectrons; thereafter the electrons are assumed to equilibrate to a temperature which is treated as a variable parameter. Additional ionizations caused by the thermal population are taken into account in the rate equations. Our principal objective in exercising this model is to investigate how the atomic populations and predicted gain depend upon the density of the neon lasant, and the spectral distribution and strength of the photoionizing pump flux.

IV. RESULTS

We begin by describing a baseline calculation which reflects the capabilities of the NRL Gamble II generator to realize such an Auger- pumped laser. Gamble II can produce a neon gas-puff Z pinch with currents of 1.0 - 1.5 MA which yields up to 7 kJ of neon K-shell radiation. This neon K-shell radiation consists primarily of 922 eV helium-alpha and 1022 eV Lyman-alpha photons, with some continuum up to ~ 2 keV. Note the neon Z pinch is the pump source. An additional cold neon cylinder a few centimeters from the pinch serves as the pumped lasant. The threshold for inner-shell photoionization of Ne I is 870 eV; therefore, the intense helium-α and Ly α photons from an adjacent Z pinch are attractive photoionizing pumps. All the calculations to be described assume a 15 ns full-width-at-half-maximum (FWHM) Gaussian pump. The spectral distribution of the pump is characterized by the energy contained in helium-α, Lyman-α and the continuum-which is assumed to be located at 2 keV. The baseline pump spectrum is 3 kJ at 922 eV, 3 kJ at 1022 eV, and 1 kJ at 2 keV.

Figure 2 displays the results of the baseline calculation as well as the effect of shifting pump energy from 922 to 1022 eV. When 2 of the 3 kJ of 922 eV He α pump energy are shifted to Ly α, a small decrease in predicted gain is noted. This is due primarily to the lower photoionization cross section at the higher photon energy. Note, however, that at the assumed neon-neon separation of 3 cm, gains in excess of 10 cm^{-1} at 514 Å are obtained in each case in the 514 Å Ne III potential steady-state laser. The assumed fill pressure of 100 torr is achievable in a 2 μm thick Kimfol gasbag[13]. When 2 kJ of pump energy is assumed shifted from Ly α to He α, not surprisingly, a similar increase in the predicted gain occurs (not shown).

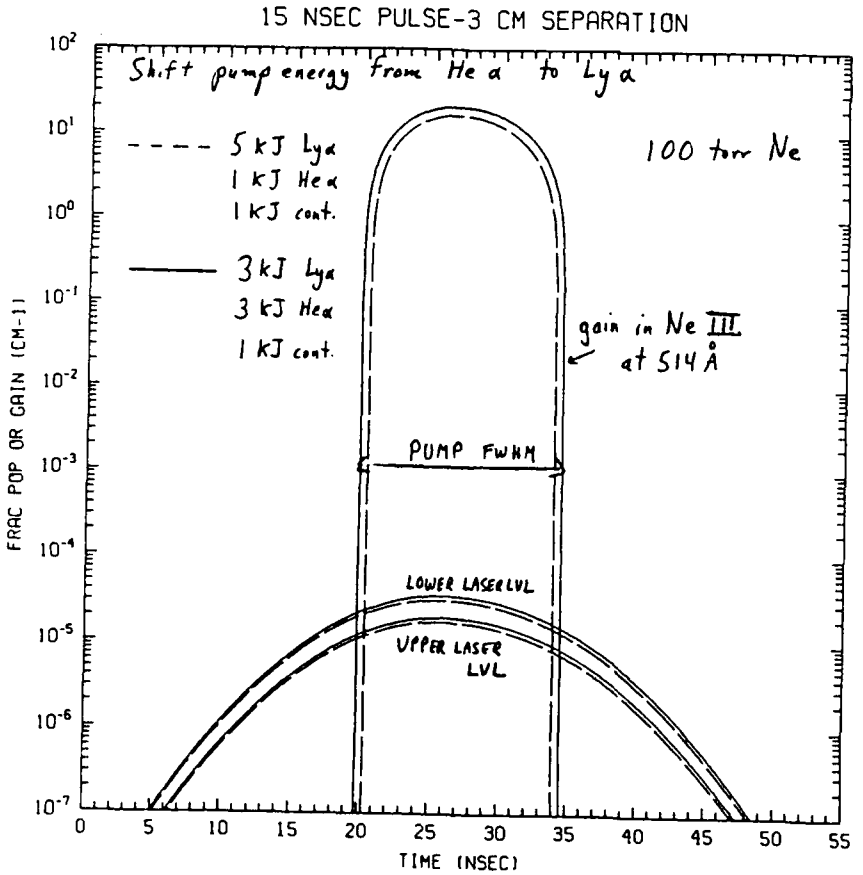

Fig. 2. Gain in the Ne III 514 Å laser transition, and population in the Ne III $1s^2 2s^0 2p^6\ ^1S_0$ upper laser level and Ne III $1s^2 2s 2p^5\ ^1P_1$ lower laser level are shown vs. time. The FWHM and assumed yields of the x-ray pump fluxes are indicated. Cold neon fill pressure is 100 torr.

The effect of lowering the neon fill pressure from 100 to 50 torr (atomic densities: 3.5×10^{18} cm^{-3} reduced to 1.8×10^{18} cm^{-3}) is shown in Fig. 3. The gain falls by 50% simply due to the reduced lasant ion density, but is still substantial (8 cm^{-1}). This need to reduce the lasant density may arise if unexpected radiative trapping effects turn out to reduce the gain. Finally, the effect of increasing the pump-lasant separation from 3 to 4 cm is illustrated in Fig. 4. The pump yields assumed in Fig. 4 are those of the baseline calculation. However, the increased separation reduces the flux at the cold neon. The reduction in flux is calculated using the exact expression for the reduction in the effective solid angle subtended by the pump Z pinch. The effect on gain is quite substantial; a factor of 4 reduction (20 cm^{-1} to 5 cm^{-1}). At separations greater than 5 cm, no gain is predicted.

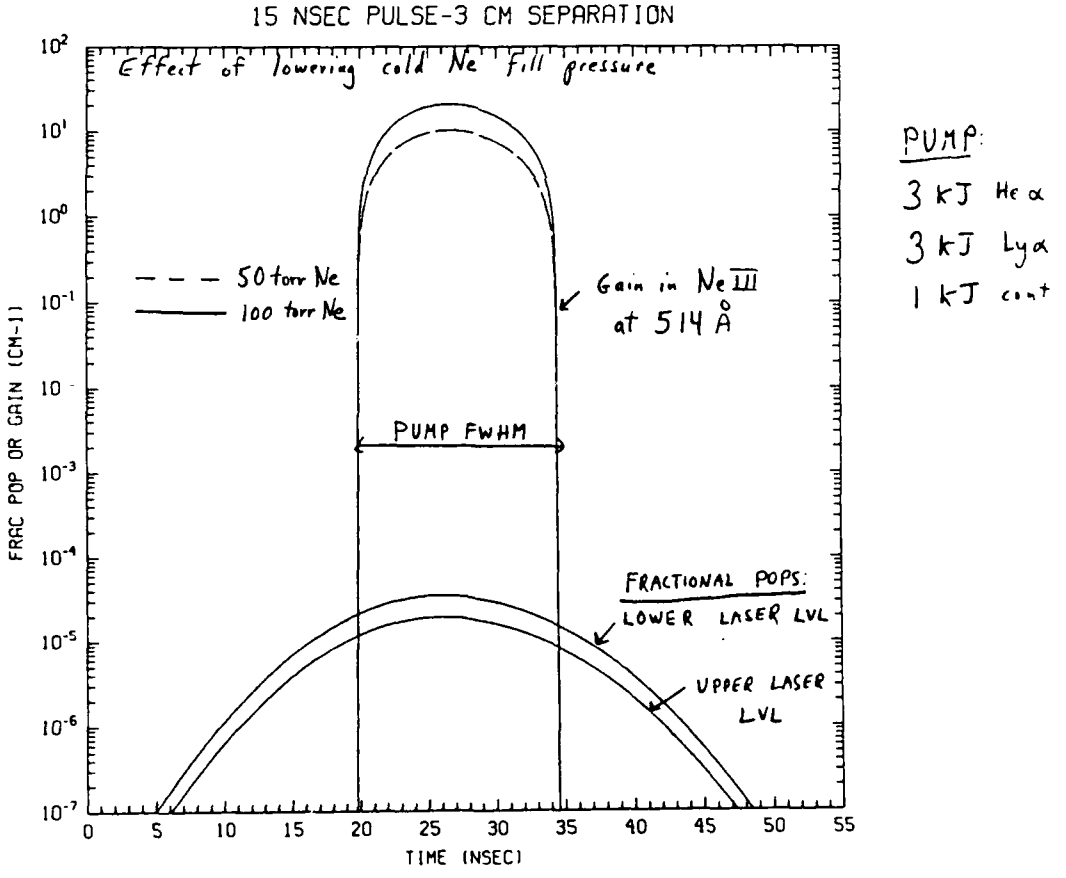

Fig. 3. As in Fig. 2, except that a calculation reducing the cold neon fill pressure from 100 to 50 torr is shown.

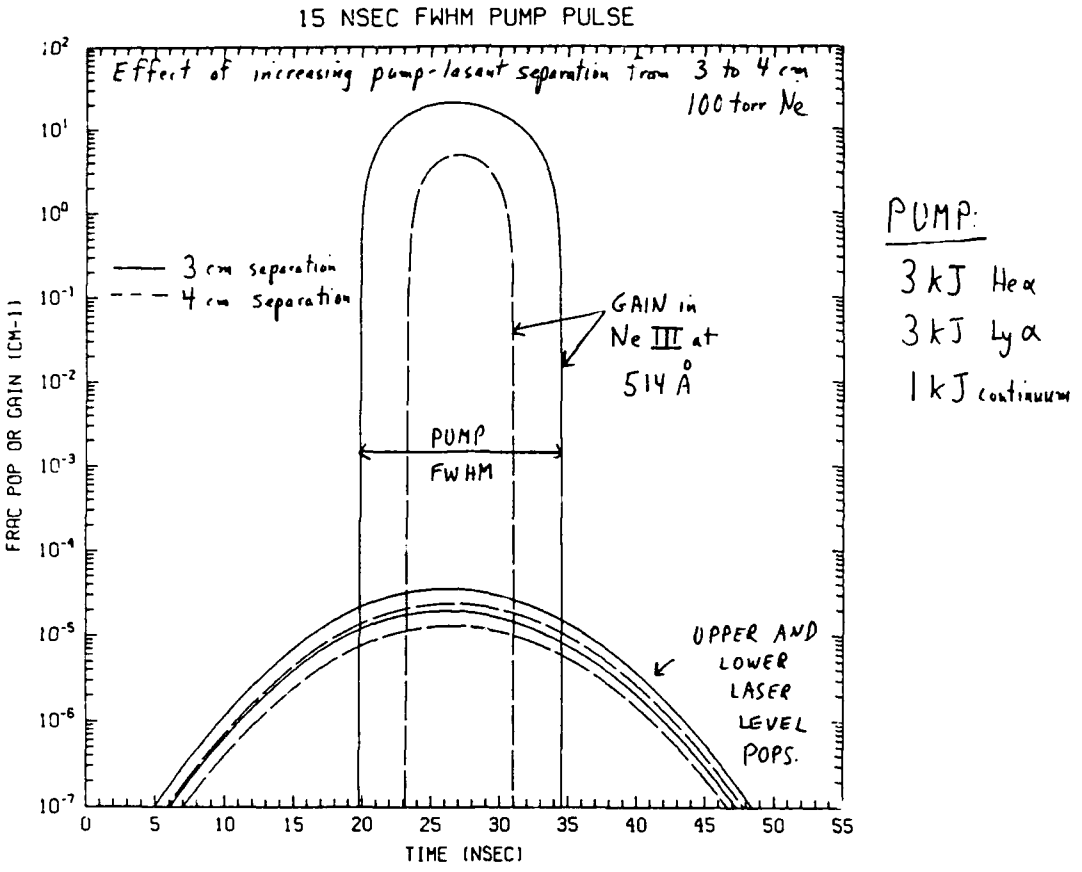

Fig. 4. As in Fig. 2, except that the neon-neon separation has been increased to 4 cm and is compared with the baseline 3 cm case.

IV. CONCLUSIONS AND FUTURE PROSPECTS

The basic results of the calculations presented above give some cause for optimism that NRL's Gamble-II generator may be able to pump an Auger-effect far- UV laser at 514 Å. With 7 kJ of neon K shell x-rays incident in 15 ns upon a separate cold neon cylindrical lasant, significant gain is calculated at neon-neon separations $\leq$ 4 cm. The model employed includes most of the physics which affects the evolution of the pumped neon and hence its gain. However, careful scrutiny of the results suggests that the radiative transfer of the important Ne III lines may have some effect on the gain by altering the populations through photon trapping. Future modeling efforts will be undertaken in close collaboration with Code 4770 to include such effects, based on possible future observations of self-absorption. Also, no recombination has been included in the present calculation, primarily due to the great uncertainty in the electron energy distribution. Inclusion of recombination is virtually certain to increase the predicted gain because Ne II and Ne III ions would be "recycled" to Ne I to undergo repeated pumping and Auger- decay lasing. We plan to include at least dielectronic recombination in the next round of model upgrades.

References

1. H. C. Kapteyn, R. W. Lee, and R. W. Falcone, Phys. Rev. Lett. 57, 2939 (1986).

2. G. Y. Yin, et al., Opt. Lett. 12, 331 (1987).

3. M. H. Sher, J. J. Macklin, J. F. Young, and S. E. Harris, Opt. Lett. 12, 891 (1987).

4. H. C. Kapteyn and R. W. Falcone, Phys. Rev. A 37, 2033 (1988).

5. E. J. McGuire, Phys. Rev. Lett. 35, 844 (1975).

6. D. L. Matthews, B. M. Johnson, and C. F. Moore, At. Data Nuc. Data Tables 38, 1 (1988).

7. W. Lotz, Ap. J. Suppl. Ser. 14, 207 (1967).

8. E. B. Saloman, J. H. Hubbell, and J. H. Scofield, At. Data Nuc. Data Tables 38, 1 (1988).

9. D. W. Missavage, S. T. Manson, and G. R. Daum, Phys. Rev. A 15, 1001 (1977).

10. J. Davis, P. C. Kepple, and M. Blaha, J. Quant. Spectrosc. Radiat. Transfer 16, 1043 (1976).

11. J. Davis, J. Quant. Spectrosc. Radiat. Transfer 14, 549 (1974).

12. T. R. Young and J. P. Boris, J. Phys. Chem. 81, 2424 (1977).

13. F. C. Young, Section I of this report.

Section III

COMPARISON OF COOLANTS FOR ACHIEVING SHORT-WAVELENGTH RECOMBINATION LASING

J. W. Thornhill, J. P. Apruzese, J. L. Giuliani,

and D. Roelant*

Radiation Hydrodynamics Branch

*Dept. of Nuclear Engineering, Univ. of Michigan,
Ann Arbor, Michigan, 48209.

Comparison of Coolants for Achieving Short-Wavelength Recombination Lasing

J. W. Thornhill, J. P. Apruzese, J. L. Giuliani, and D. Roelant[1]

Radiation Hydrodynamics Branch, Plasma Physics Division

Naval Research Laboratory, Washington D.C. 20375

I. Introduction

A major goal of current x-ray laser research is to shorten the lasing wavelength. One proposed application which would benefit from shorter wavelength x-ray lasers is that of holography. To this end, several approaches have been suggested. Perhaps the most promising scheme utilizes electron collisional excitation in nickel-like ions[1]. However, recombination pumping of hydrogenic aluminum[2], lithium-like chromium[3], or helium-like silicon[4] have also been proposed to bring the wavelength of x-ray lasers into the "water window", 23.3 - 43.7 A. Photons in this energy region are absorbed by the carbon K-edge at 43.7 A but are transparent to the oxygen K-edge at 23.3 A. If a laser holography system can be built to operate in this wavelength region it would be useful from a biological standpoint because of the inherent large contrast between water and protein[5]. It has recently been argued[6] that a laser operating near the long wavelength edge of the water window (44 - 45 A) is optimum for holography. The physics of plasma cooling developed in this paper apply to any short-wavelength recombination laser.

The purpose of this work is to build upon the the results of Ref. 4 and theoretically determine whether it is hydrodynamically possible to achieve the conditions necessary for producing significant gain in the Si XIII $3d^1$

1 Department of Nuclear Engineering, University of Michigan, Ann Arbor, Michigan 48109

- $2p^1$ line at 39.1 A. This work is performed in the context of a 1-D cylindrical geometry radiation hydrodynamics model. The model follows the evolution of a freely expanding cylindrical plasma, which consists of a primary coolant element that is seeded with silicon ions. The plasma is assumed compressed to a specified initial radius and the initial temperature and electron density are uniform throughout the plasma. As the plasma expands from its initial state we follow the temporal and spatial evolution and calculate the gain appropriate for the plasma conditions. To achieve significant gain, a coolant mixed with silicon must be capable of decreasing the plasma temperature by several hundred eV in a time span of tens of picoseconds. Two major ways of doing this are expansion and/or radiative cooling, but it most be done quickly, otherwise the atomic states will have time to equilibrate and there will be no inversion and gain. In this paper we compare the relative merits of cooling by both radiative and expansion mechanisms by examining the cooling and gain-producing capabilities of a variety of coolants (selenium, aluminum, carbon and hydrogen) seeded with silicon ions. This is an interesting comparison because the higher Z coolants are better radiators than the lower Z materials but they do not expand as quickly, due to their larger mass density. We also investigate the effects of varying the concentration of the silicon seed and the initial radius from which the plasma begins its expansion.

II. Model Description

The calculation proceeds in three stages. First, we follow the evolution of the expansion of the coolant from its inital state. In this stage we neglect the silicon when calculating the general hydrodynamic behavior of the expanding plasma. This is a reasonable assumption because in most cases

the concentration of silicon ions is less than 10 percent of the total ion density. Calculations in which this is not the case are commented on in later sections. The hydrodynamic model consists of continuity, momentum, and energy equations that are numerically solved in a Lagrangian reference frame with cylindrical geometry and axial symmetry. The fluid equations describing the plasma dynamics are:

Mass continuity,

$$\frac{dV}{dt} = \frac{V}{r}\frac{\delta}{\delta r}(ru) \tag{1}$$

Momentum,

$$\frac{du}{dt} = -V\frac{\delta P}{\delta r} - \frac{V}{r}\frac{\delta}{\delta r}(rQ) \tag{2}$$

and two equations describing the change in

Electron internal energy,

$$\frac{dE}{dt}e = -P_e\frac{dV}{dt} + \frac{V}{r}\frac{\delta}{\delta r}\left(rK_e\frac{\delta T}{\delta r}e\right) + R + 2\omega_c(T_i - T_e) \tag{3}$$

and Ion internal energy,

$$\frac{dE}{dt}i = -P_i\frac{dV}{dt} + \frac{V}{r}\frac{\delta}{\delta r}\left(rK_i\frac{\delta T}{\delta r}i\right) - VQ\frac{\delta u}{\delta r} - 2\omega_c(T_i - T_e) \tag{4}$$

In these equations V is the specific volume, u is the radial fluid velocity, P is the total particle pressure, P_e and P_i are electron and ion pressures, E_e and E_i are electron and ion internal energies, K_e and K_i are electron and ion thermal conductivities, T_e and T_i are the electron and ion temperatures, Q is the von Neumann artificial viscosity[7], R is the specific radiative loss

or gain term, and ω_c is the electron-ion collision term. The transport coefficients K_e, K_i, and ω_c are given by Braginskii[8].

These equations are put in closed form by using the ideal gas equation of state for the electrons and ions:

$$P_e = \frac{2V}{3} (E_e - E_z) \tag{5}$$

$$P_i = \frac{2V}{3} E_i \tag{6}$$

where E_z is the potential energy due to ionization and excitation of the atoms.

Several quantities in the above equations are obtained by solving ionization and radiation dynamics equations for the appropriate coolant. They are R, the radiative loss rate, E_z the ionization and excitation energy density, and Z the effective charge of the plasma. The ionization and radiation dynamics is treated self-consistently using a time-dependent version of the collisional-radiative (CR) radiation and atomic physics models developed at NRL (see the references listed in Ref. 9). Typically, all of the ground states and up to 40 excited levels are included in the atomic physics models for the various coolants. The exception is hydrogen for which we completely neglected the ionization dynamics since the ionization energy is such a small fraction of the initial internal energy (internal energy is definded to be the sum of thermal and ionization energies). We assume that the hydrogen plasma is completely stripped and that the radiation loss is only due to bremmstrahlung. These are good assumptions because the plasma temperatures of interest exceed 100 eV, virtually assuring that the hydrogen plasma will be completely ionized.

Radiation is coupled to the plasma formed from the coolant element through emission and absorption processes. Photoionization and photoexcitation directly affect the populations while inner-shell absorption

and radiative cooling produce indirect changes by altering the temperature T_e of the plasma. In order to self-consistently include these processes, the radiation field must be transported. This is accomplished by a probabalistic transport scheme in which angle and frequency averaged escape probabilities are calculated for each emission process[10,11]. Coupling of photons from cell to cell is described by differencing the escape probabilities across the cell boundaries. We typically transport about 50 lines for each coolant.

The second stage of the modeling involves calculating the evolution of the atomic states of silicon as they change when the silicon seed portion of the plasma is forced to follow the same hydrodynamic path as calculated for the coolant element. This is done by using atomic physics and radiation and ionization dynamics models for a silicon plasma. The level structure and number of lines transported is similar to that described above.

Once the hydrodynamic profiles and the time evolution of the ground states of hydrogenic and helium-like silicon are known the gain can be calulated using the detailed multilevel gain model described in Ref. 4. The only significant alteration we made to this model is that we replaced the original Sobelev escape probability[12] with the more accurate angle-averaged Sobelev escape probability for axially symetric plasmas[13]. This escape probability is essential for gain calculations because it allows for photon escape in frequency space due to large velocity gradients and curvature effects present in the plasma. The reduced opacity decreases the trapping of the lower level $1s^2$ - $1s2p\,^1P$ transition significantly compared to the case of no bulk Doppler effects in the radiation transport. It should be mentioned that Doppler and curvature effects were not accounted for in the first two stages of the calculation because it is computationally expensive and difficult to transport all the affected radiation. The consequences of this are discussed at the end of subsection A. of the results section.

III. Results

A. Comparison of the cooling capabilites of different atomic number elements.

In this section we contrast the cooling capabilites of selenium, aluminum, carbon and hydrogen plasmas seeded with silicon as they freely expand in cylindrical geometry from an initial radius of 5 μm. The coolant is seeded with silicon ions of density 10^{21} cm^{-3} and the density of coolant is such that the intial electron density is 10^{23} cm^{-3}. The plasma is initially in collisional-radiative-equilibrium at an electron temperature of 1000 eV, see Fig. 1. We know from Ref. 4 that conditions at the time of optimal gain are electron temperatures below 500 eV and electron densities near 10^{22} cm^{-3}. However, in order to produce significant gain the plasma must be ionized considerably more than the collision-radiative-equilibrium state at these same temperatures and densities. Therefore in order to assure that the plasma is initially over-ionized we choose an initial temperature of 1000 eV. Although this specific temperature is not critical, based upon the results of numerous simulations, it appears that the choice of initial electron temperature and density are near optimal for producing gain. Unless otherwise stated, the results displayed in this section as well as those that follow are for parameters, such as T_e and N_e, of the "optimal gain-producing zone" as a function of time. In general, these results are valid over a radial expanse of 3 to 10 μm.

Similar to Epstein[14], we find that rapid expansion is the most important mechanism for cooling small diameter, hot , expanding plasmas. This is illustrated in Figs. 2 and 3 where the electron temperature and density of

the same zone, one chosen near the edge of the plasma where gain occurs but not necessarily the optimal zone for producing gain, of the various coolants are displayed as a function of time. The fact that the temperature decreases more rapidly for the lower Z materials is an indication of the greater expansion cooling that occurs in the low Z plasmas. The larger expansion cooling is in agreement with the time asmptotic behavior of the velocity of the edge of the expanding plasma $V_{edge} \simeq \delta((1+Z)kT_e/M_i)^{1/2}$ [15], where Z is the initial effective charge, M_i is the ion mass, and δ is a geometric factor that depends on the final density profile of the expansion. With the exception of selenium, which had an initial effective charge of $\simeq 30$, the coolants were almost completely stripped. Because of the large electron temperatures involved, thermal conduction is very efficient and these plasmas remain nearly isothermal over considerable radial expanse, 10s of μms. Therefore the temperature histories of the optimal gain-producing zone for each of the coolants are nearly identical to those displayed in Fig. 2. This is not the case for the electron densities, as can be seen by comparing Fig. 3 with Fig. 4 where the electron densities of the optimal gain-producing zones are shown. To demonstrate that expansion is the dominant cooling mechanism, the ratio of the energy radiated from the zone to the total change in internal energy is plotted in Fig. 5. Here as expected the larger Z coolants radiate an appreciably greater fraction of energy in 50 ps than the lower Z elements, 24 percent for selenium versus 2 percent for carbon. However, the enhanced radiative cooling of the high atomic number materials is not sufficient to offset their lower rate of expansion cooling. When comparing the cooling capabilities of moderate Z coolants, such as aluminum and carbon, we find that they are nearly identical. This is because the smaller expansion cooling of aluminum is compensated by a larger radiative cooling rate, while just the opposite of this occurs in carbon. Of

course, in magnetically confined plasmas radiative cooling will dominate and has demonstrated its effectiveness in promoting recombination lasing[16].

Fig. 6 shows a plot of the velocity gradient of the optimal gain-producing zone as a function of time for the various coolants. In this work velocity gradient is defined to be (u/r + du/dr), where u is the radial fluid velocity and r is the radial position. The size of this velocity gradient, which is a measure of the degree of Doppler shift and curvature effects present in the plasma, is important for determining the gain in the $3d^1 - 2p^1$ line. Because opacity is inversely proportional to the size of the velocity gradient, more reduction in opacity of the $1s^2 - 1s2p^1P$ lower level to ground state transition occurs for the larger gradients, which results in larger gain. Since velocity gradients calculated in this work are an order of magnitude larger than those postulated in Ref. 4, in which there was significant reduction of opacity, one expects the trapping of the $1s^2 - 1s2p^1P$ line to be appreciably reduced. This is clearly illustrated by comparing the optimal gains calculatated with and without Sobelev escape probabilities, Figs. 7 and 8. The gain displayed in Fig. 8 is calculated using the "local approximation" [17] for radiation transport. It does not include Sobelev escape probabilities.

Fig. 7 reveals how the two-fold advantages of fast expansion, i.e., greater plasma cooling and reduced trapping of the resonance transition, combine to give the largest gain when the lowest atomic number coolant is employed.

It was stated earlier that because the silicon seed represents a small percentage of the total ion density it can be neglected in the first stage of the calculation. However, in the selenium case considered in this subsection, the silicon ion concentration is about 30% of the total ion density. In this instance, it is estimated, assuming expansion at the

adiabatic sound speed, the same initial conditions ($N_e = 10^{23}$ cm^{-3}, T_e = 1000 eV, and Si ion density = 10^{21} cm^{-3}), and that the selenium and silicon remain uniformily mixed, that the inclusion of silicon in the initial stage of the calculation would produce a 1% - 2% increase in expansion velocity. This would not substantially alter the expansion cooling. Also, based on the results displayed in Fig. 5, we estimate that there would only be about a 10% reduction in the radiation output. These two minor changes would tend to offset each other, thus, it appears that neglecting silicon in the first stage of the selenium calculation is a reasonable assumption.

We conservatively estimated the error introduced by neglecting Doppler and curvature effects in the first two stages of the calculation by performing optically thin first and second stage calculations under the same conditions as described above for the selenium, carbon, and hydrogen coolant elements. Because selenium radiates significantly more energy than hydrogen and carbon, it was the only coolant element that showed any substantial changes in temperature and density profiles calculated in the first stage. The optically thin selenium case showed that the optimal gain-producing zone radiated about 30% more energy than the original static opacity calculation. We found in all three cases that the hydrogenic and helium-like silicon ground state concentrations calculated in stage two were significantly different than the static opacity results. This is expected behavior because neglecting opacity reduces the population of the excited optically pumped states, reducing ionization from those levels, and lowering the overall ionization state of the plasma. The results of the optically thin calculations showed no change in gain from the original selenium calculation but a reduction in gain from 6.3 to 4.5 cm^{-1} for hydrogen and a reduction in gain from 4.0 to 2.5 cm^{-1} for carbon. Apparently, the selenium gain remains unchanged because the enhanced cooling of the optically thin calculation

offsets the lower silicon ionization level. Though a laboratory plasma's true evolution probably lies somewhere between the static opacity and optically thin calculations, it is still evident that the faster expansion inherent of the lower Z materials is a better cooling mechanism.

B. Variation of silicon concentration

We now contrast the effects that varying the concentration of silicon ions has upon influencing the optimal gain. Aluminum is chosen as the primary coolant. First, we ran one hydrodynamic simulation for pure aluminum to obtain density and temperature profiles and then we re-ran the calculation over the same hydrodynamic path using different concentrations of silicon ions, 20, 40 , 70 and 100 percent. Because aluminum and silicon are next to each other in the periodic table, their hydrodynamic behavior should be similar. Therefore, even though the percentage of silicon is no longer a small percentage of the total ion density of the plasma, the results are still valid. Other than varying the amount of silicon seed, the simulations were performed starting with the same initial conditions as outlined earlier in section A, i.e., T_e = 1000 eV, $N_e = 10^{23}$ cm^{-3} and r_o = 5 μm.

The time profile of electron temperature is the same as that shown in Figs. 2 for the aluminum coolant. The evolution of electron density and the gain of the optimal gain producing zone for each of the different concentrations of silicon ions are shown Figs. 9 and 10, respectively. The interesting result of this comparison is that the concentration of silicon ions does not dramatically alter the achievable gain under the assumed initial conditions. If the plasma were completely optically thin, then the gain should increase linearly with ion concentration because of the

increased populations of the excited lasing states. Conversely, opacity increases with ion concentration and eventually reduces gain. Under static conditions in which there are no Doppler or curvature effects, opacity acts to limit gain to the extent that significant gain is not achievable for silicon ion concentrations in excess of 4×10^{19} cm^{-3} [4]. Although there is clearly an optimal gain-producing silicon ion concentration somewhere between 40% and 100%, what these calculations demonstrate is that the reduction in opacity due to Doppler and curvature effects is such that the the plasmas are in a buffered regime where any attempt to increase gain by going to larger silicon ion concentrations is somewhat negated by a corresponding increase in opacity.

The results presented in the next section show that expansion cooling, Doppler and curvature effects, and consequently gain are all diminished as the initial radius is increased. This prompts the speculation that at larger initial radius, opacity effects would dominate and the gain would fall for the larger silicon ion concentrations. Likewise, at very small initial radii, the plasmas are so optically thin that one expects enhanced gain with increasing silicon ion concentrations.

C. Variation of initial radius

In this subsection we examine the role that variations in the initial radius play in affecting the optimal gain. The simulations are run according to the initial conditions, T_e = 1000 eV, $N_e = 10^{23}$ cm^{-3}, and in this case, carbon is choosen as the primary coolant that is seeded with silicon ions of concentration 10^{21} cm^{-3}. The intial radius is varied from 5 μm to 15 μm. Again, the plasma is allowed to freely expand and the results for the optimal gain-producing zone are shown.

The change in electron temperature and density with time are shown in Figs. 11 and 12, respectively. Although, the comparison of electron density between the 10 and 15 μm plasma is ambiguous because the optimal gain-producing zone of the 15 μm plasma is closer to edge of the expanding plasma than for the 10 μm plasma, both of these figures demonstrate that plasmas with smaller initial radius cool more rapidly as they expand. This result is not surprising because it is basically a consequence of the first law of thermodynamics, $dE/dt = - PdV/dt$, which can be re-written to show that the internal energy of the expanding plasma decreases in time according to $(r_o/(r_o+ct))^{4/3}$, where c is the expansion velocity, r_o is the inital radius, and t is time. This relation assumes that the expansion velocity is nearly the same for all three initial radii and that the expansion is approximately adiabatic. The optimal gain for these three inital radial positions is plotted in Fig. 13.

Reduced trapping of the $1s^2$ - $1s2p^1P$ transition is also partially responsible for producing larger gain at smaller initial raii. This behavior is reflected in Fig. 14, where we see that the largest velocity gradients correspond to smaller initial radii.

IV. Discussion and Conclusions

We have investigated with detailed models whether it is possible to achieve the conditions necessary for producing recombination pumped lasing in the $3d^1$ - $2p^1$ line of Si XIII. We assumed that a laser had initially heated and/or compressed the plasma, which consisted of a coolant element seeded with silicon ions, to an inital state of T_e = 1000 eV, $N_e = 10^{23}$ cm^{-3}, and inital radius of 5 to 15 μm. We calculated gain achieved while the plasma recombines during free expansion from its initial state. The plasma

cools both by expansion and radiation. Although, we did not attempt to find conditions which optimized gain we did achieve significant gain under these initial conditions. There are two major conclusions that can be drawn from this work. First, based on our comparison of the cooling abilities of hydrogen, carbon, aluminum and selenium, we found it is better to use a low atomic number material as a coolant. This is because their larger expansion cooling rate offsets any radiative cooling advantage that is gained by using a high Z coolant, assuming the same initial r_o, T_e, N_e and concentration of silicon ions. Secondly, the escape of photons in frequency space as a result of curvature and large velocity gradients is crucial for reducing trapping of the lower level to ground state transition and thereby increasing gain. If we had not included this essential radiation transport physics in our model, we would not have calculated any significant gain. Using the faster expanding low Z materials as coolants is one way of achieving larger velocity gradients, while curvature effects as well as cooling rates both increase if the inital radius of the plasma is reduced. The usefulness of radiative cooling, however, in magnetically confined plasmas has been demonstrated experimentally[16]. For such a scheme, high atomic number radiative coolants may well be valuable.

References

[1] S. Maxon, et al., Phys. Rev. Lett. 63, 236 (1989).

[2] A. K. Dave', and G. J. Pert, J. Phys. B 17, 4953 (1984).

[3] B. L. Whitten, J. K. Nash, A.L. Osterheld, and M. Chen, Proc. 6th APS Topical Conf. Atomic Processes in Plasmas, (Santa Fe, NM), paper 4B2 (1987).

[4] J. P. Apruzese, P. C. Kepple, J. Davis, and J. Pender, IEEE Trans. Plasma Sci. 16, 529 (1988).

[5] J. E. Trebes, J. Phys. (Paris) 47, C6-309 (1986).

[6] R. A. London, M. D. Rosen, and J. E. Trebes, Appl. Opt. 28, 3397 (1989).

[7] J. von Neumann and D. Richtmyer, J. Appl. Phys. 21, 232, (1950).

[8] S. I. Braginskii, "Transport Processes in a Plasma," in Reviews of Plasma Physics Vol. 1, ed. M. A. Leontovich, Consultants Bureau New York, (1965).

[9] D. Duston, R. W. Clark, J. Davis, and J. P. Apruzese, Phys. Rev. A 27, 1441 (1983).

[10] J. P. Apruzese, J. Davis, D. Duston, and R. W. Clark, Phys. Rev. A 29, 246 (1984).

[11] J. P. Apruzese, J. Davis, D. Duston, and K. G. Whitney, J. Quant. Spectrosc. Rad. Trans. 23, 479 (1980).

[12] V. V. Sobolev, Sov. Astron. 1, 678 (1957).

[13] A. I. Shestakov and D. C. Eder, Lawrence Livermore National Laboratory

Report No. UCRL-100485, (1989).

[14] R. Epstein, Phys. Fluids B 1, 214 (1989).

[15] G. J. Pert, J. Phys. B 9, 3301 (1976).

[16] S. Suckewer, C. H. Skinner, H. Milchberg, C. Keane, and D. Voorhees, Phys. Rev. Lett. 55, 1753 (1986).

[17] D. E. Osterbrock, Astrophys. J., 135, 195 (1962).

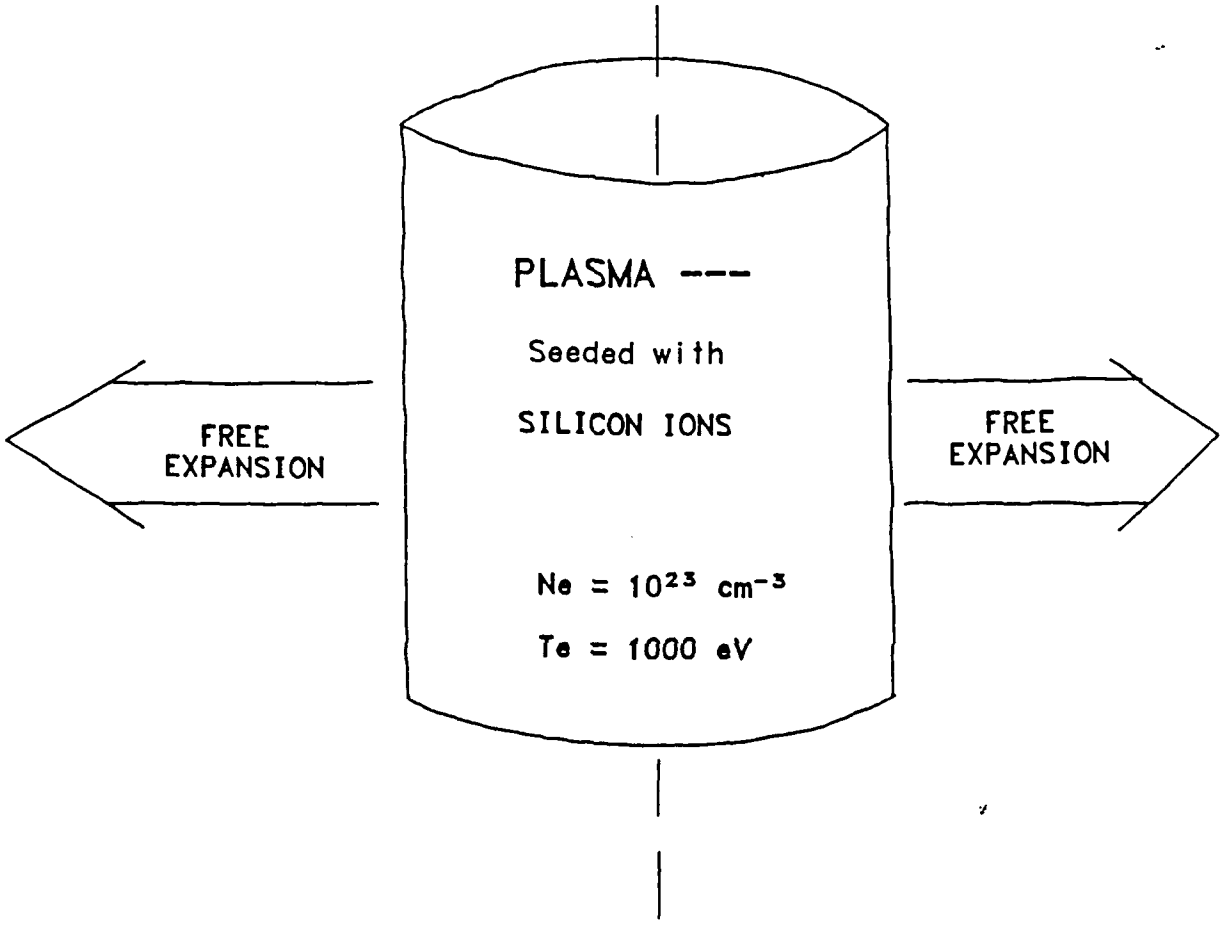

Figure 1. Initial plasma conditions for the calculations described in the text. Subsequent free expansion is assumed.

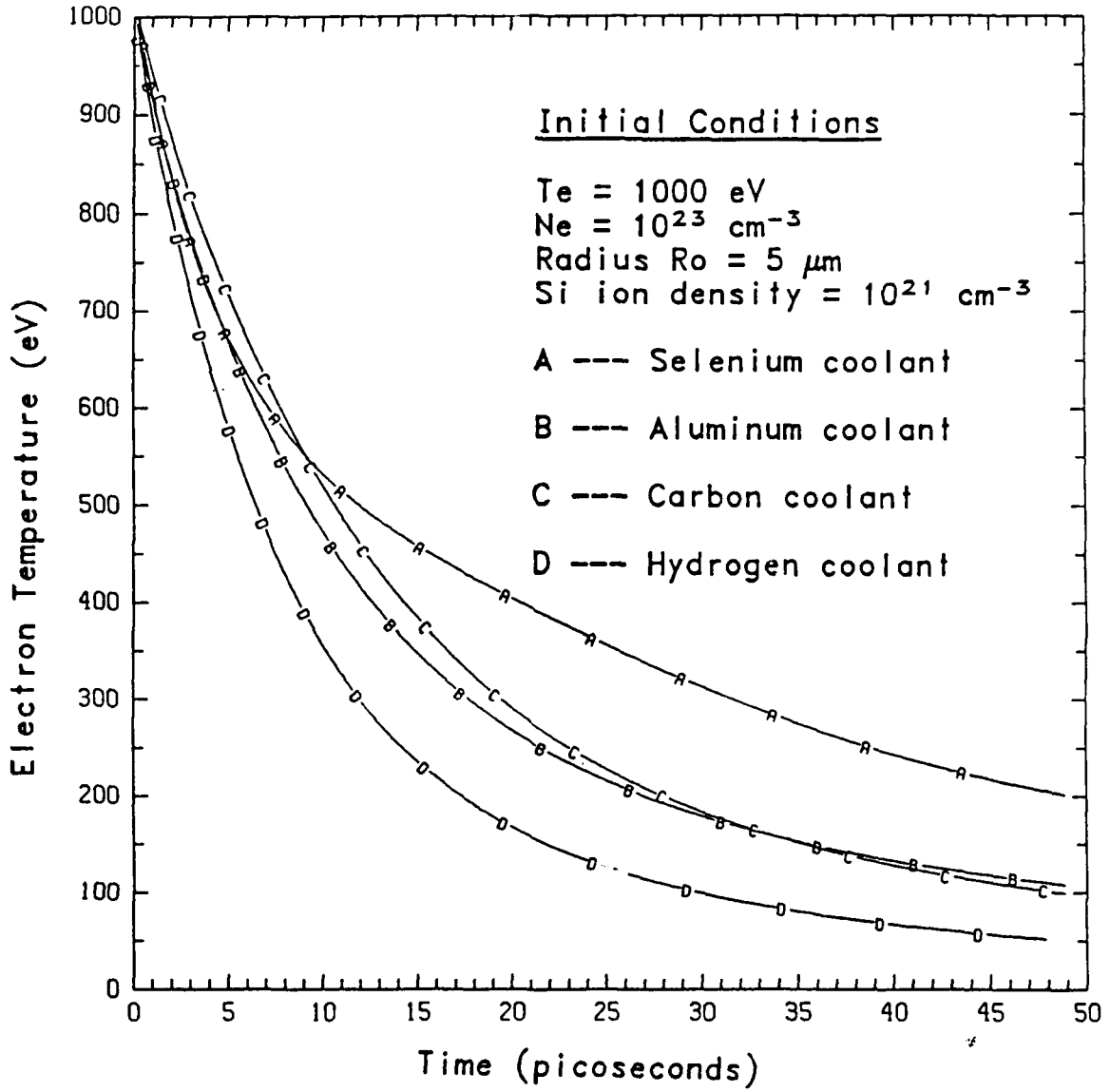

Figure 2. Time evolution of electron temperature for an identical zone located near the edge of the expanding plasma where lasing occurs for the selenium, aluminum, carbon, and hydrogen coolants.

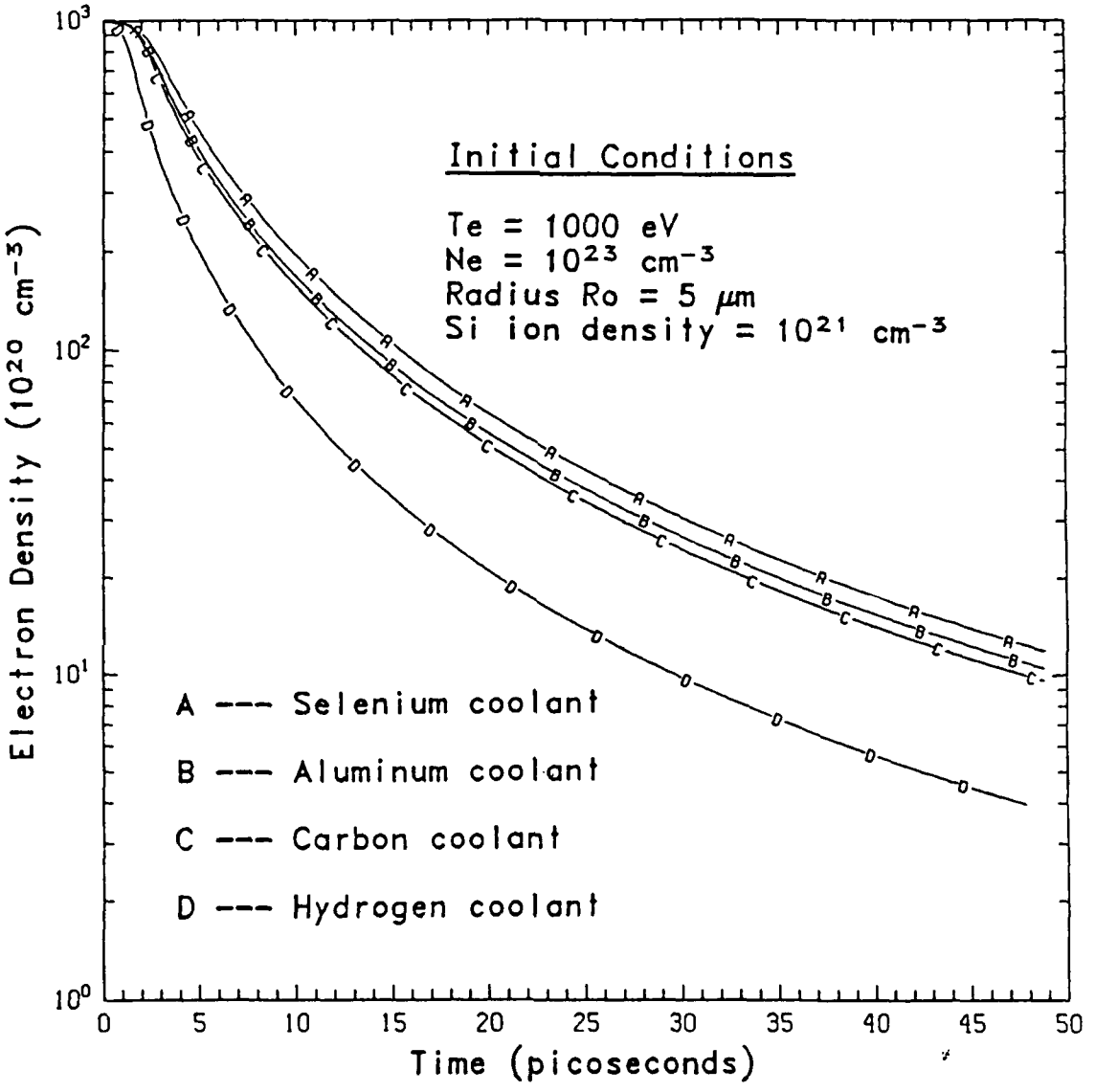

Figure 3. Time evolution of electron density for an identical zone located near the edge of the expanding plasma where lasing occurs for the selenium, aluminum, carbon, and hydrogen coolant elements.

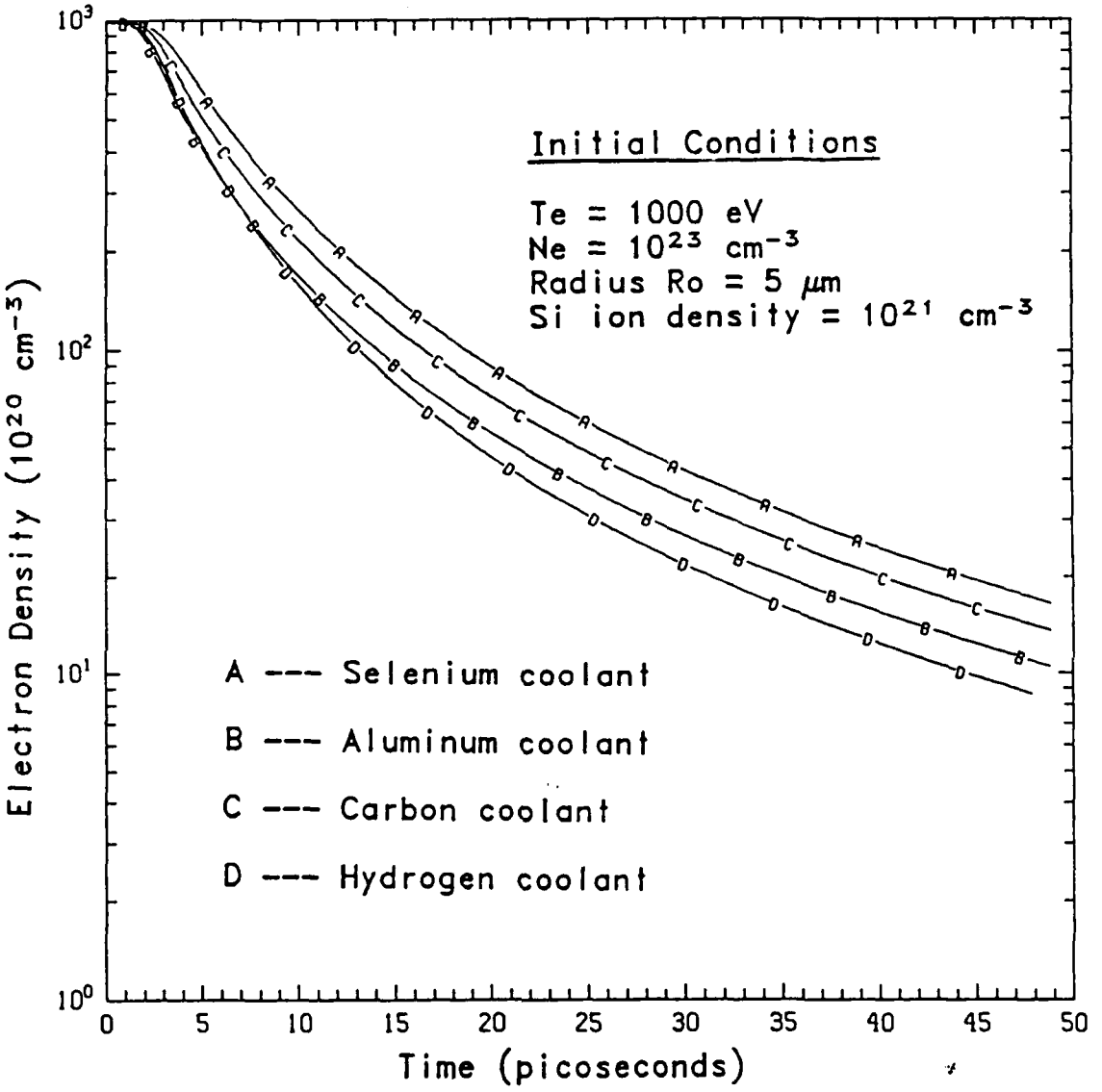

Figure 4. Time evolution of electron density for the optimal gain-producing zone for selenium, aluminum, carbon and hydrogen coolants.

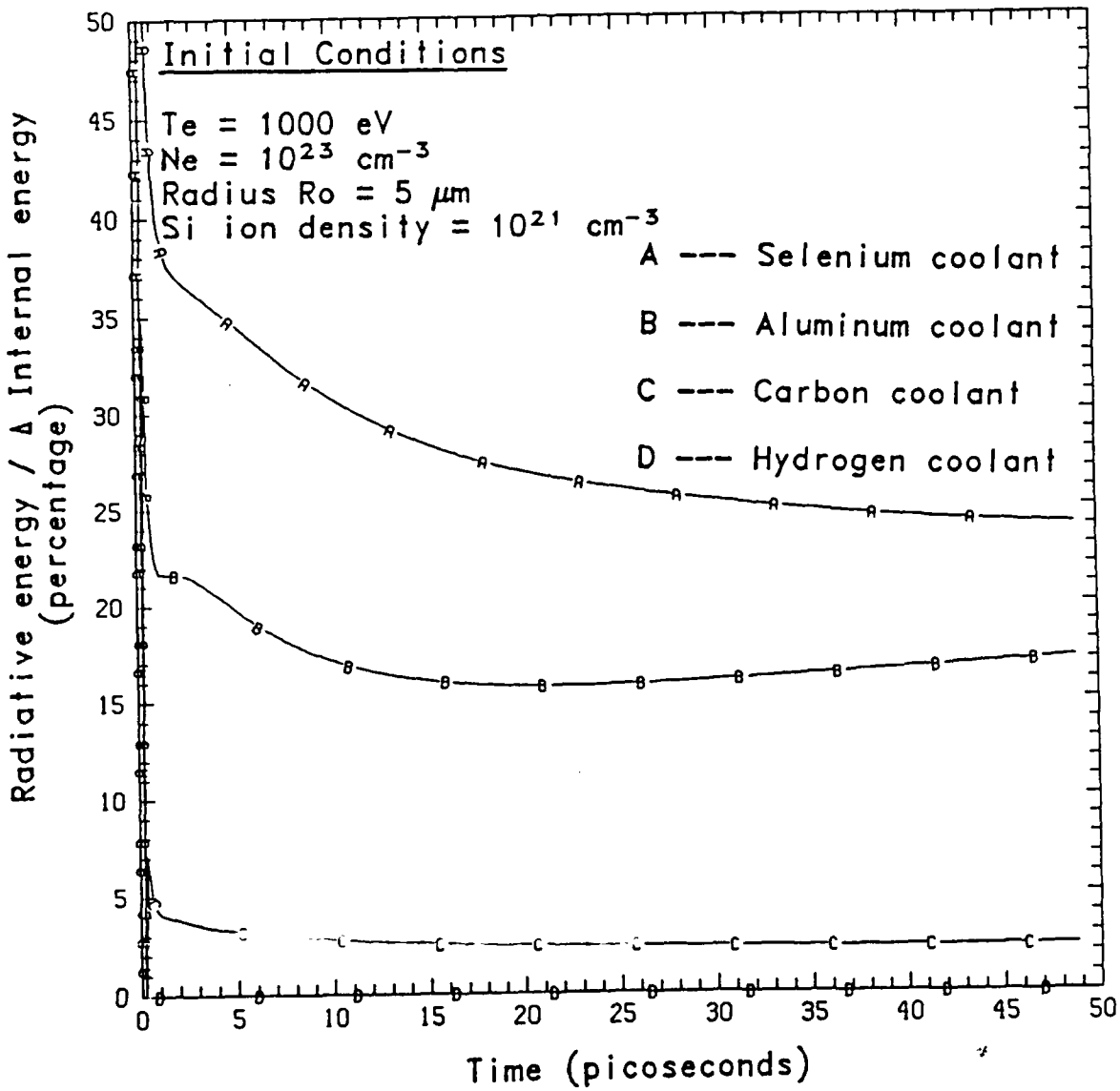

Figure 5. Time evolution of the radiative energy lost from the optimal gain-producing zone as a percentage of the total change in zonal internal energy. Results are shown for selenium, aluminum, carbon and hydrogen coolant elements.

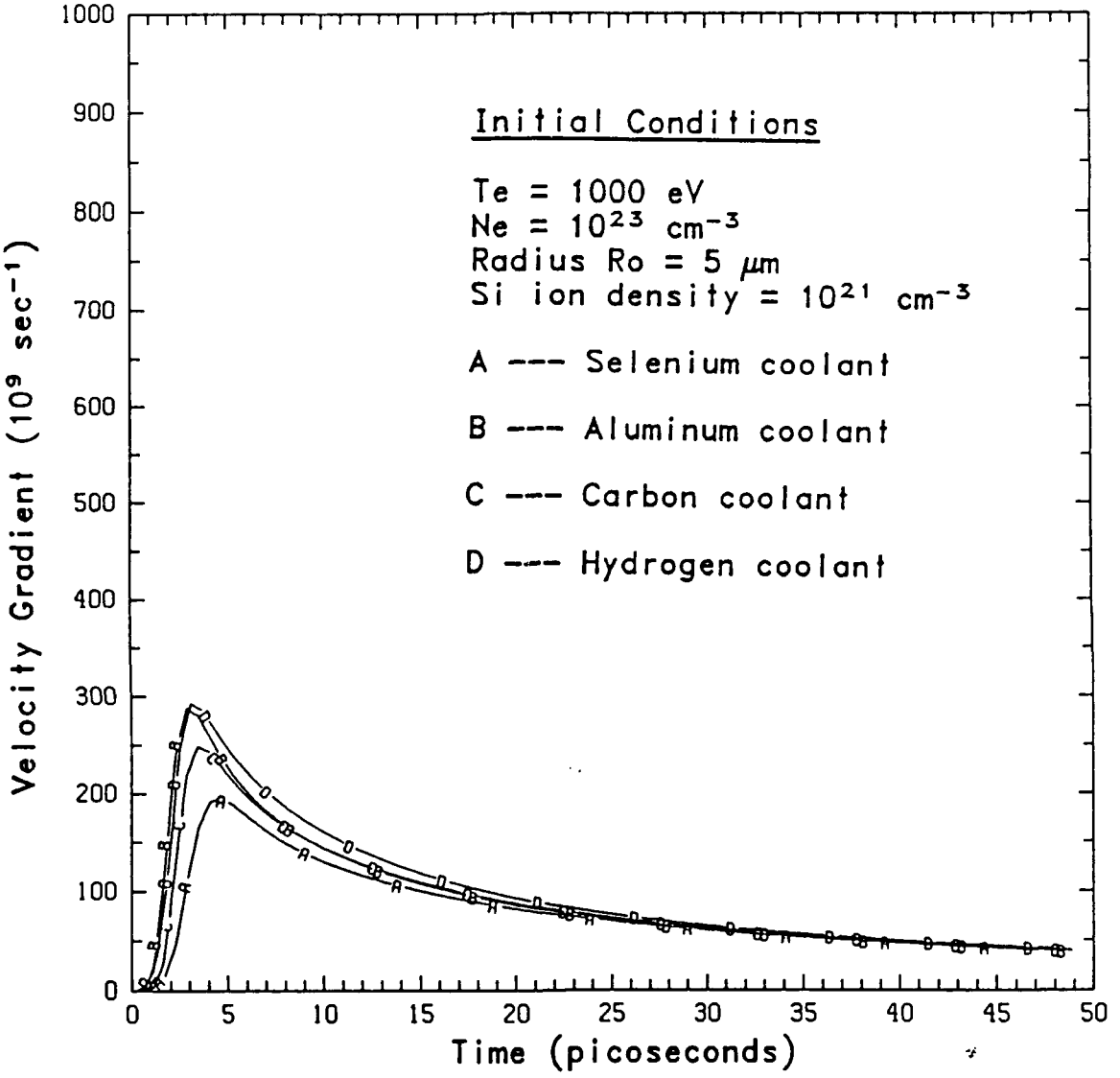

Figure 6. Time evolution of the velocity gradient for the optimal gain-producing zone for selenium, aluminum, carbon and hydrogen coolant elements.

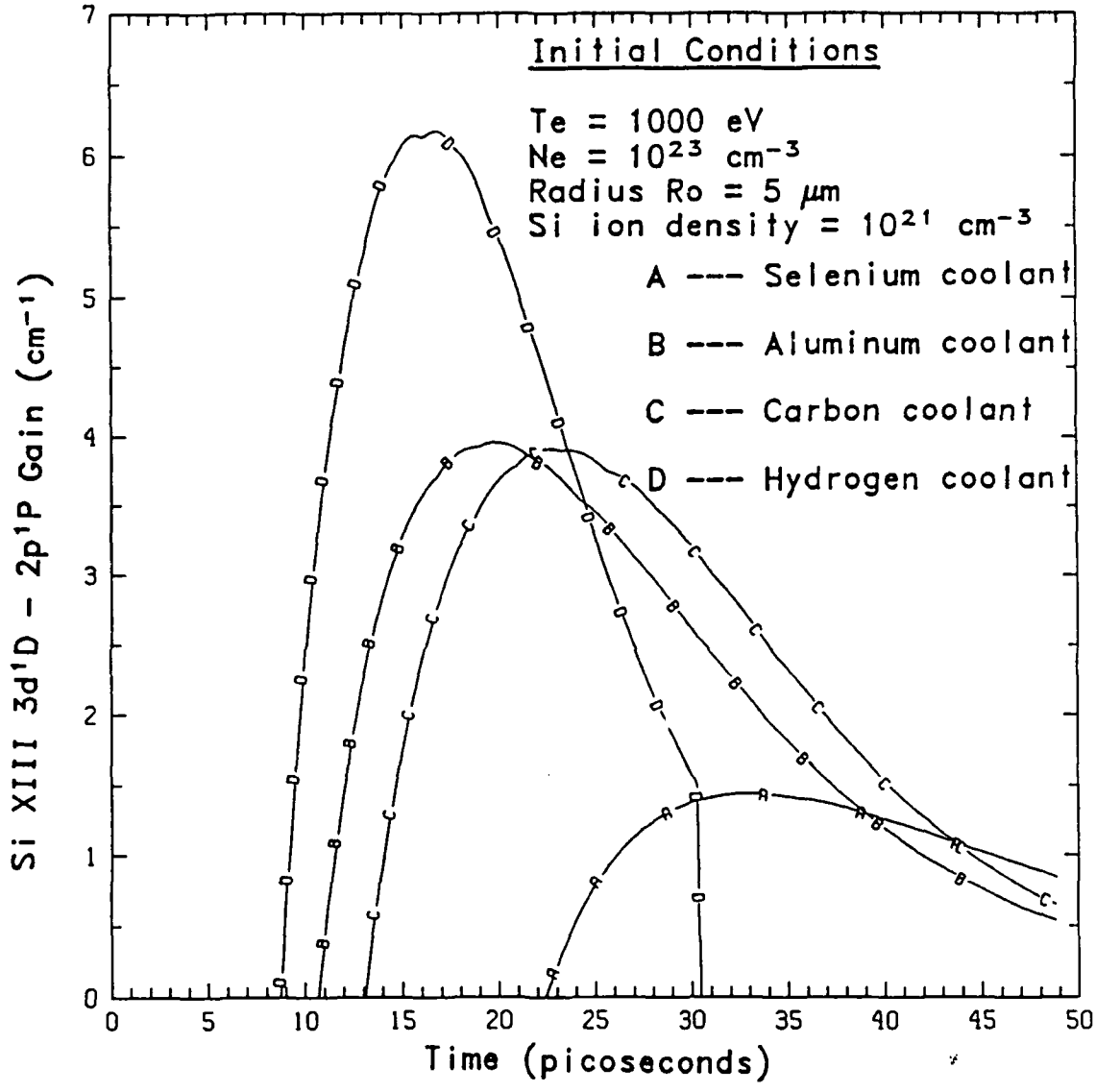

Figure 7. Time evolution of Si XIII $3d^1$ - $2p^1$ gain. Results are for the optimal gain-producing zone for selenium, aluminum, carbon and hydrogen coolant elements.

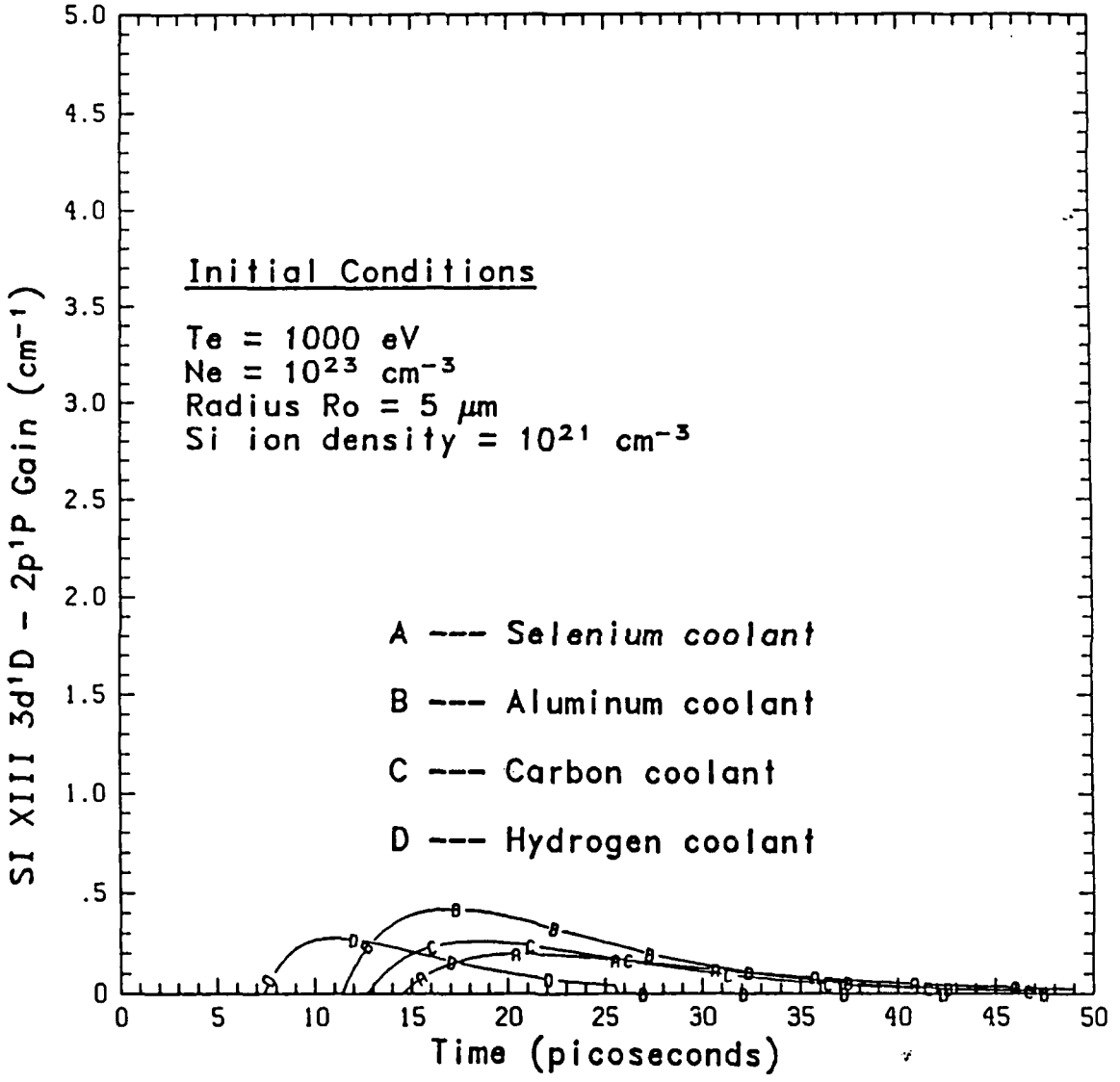

Figure 8. Time evolution of Si XIII $3d^1$ - $2p^1$ gain calculated without taking into account reduction in opacity due to Doppler shift and curvature effects. Results are shown for the optimal gain-producing zone for selenium, aluminum, carbon and hydrogen coolant elements.

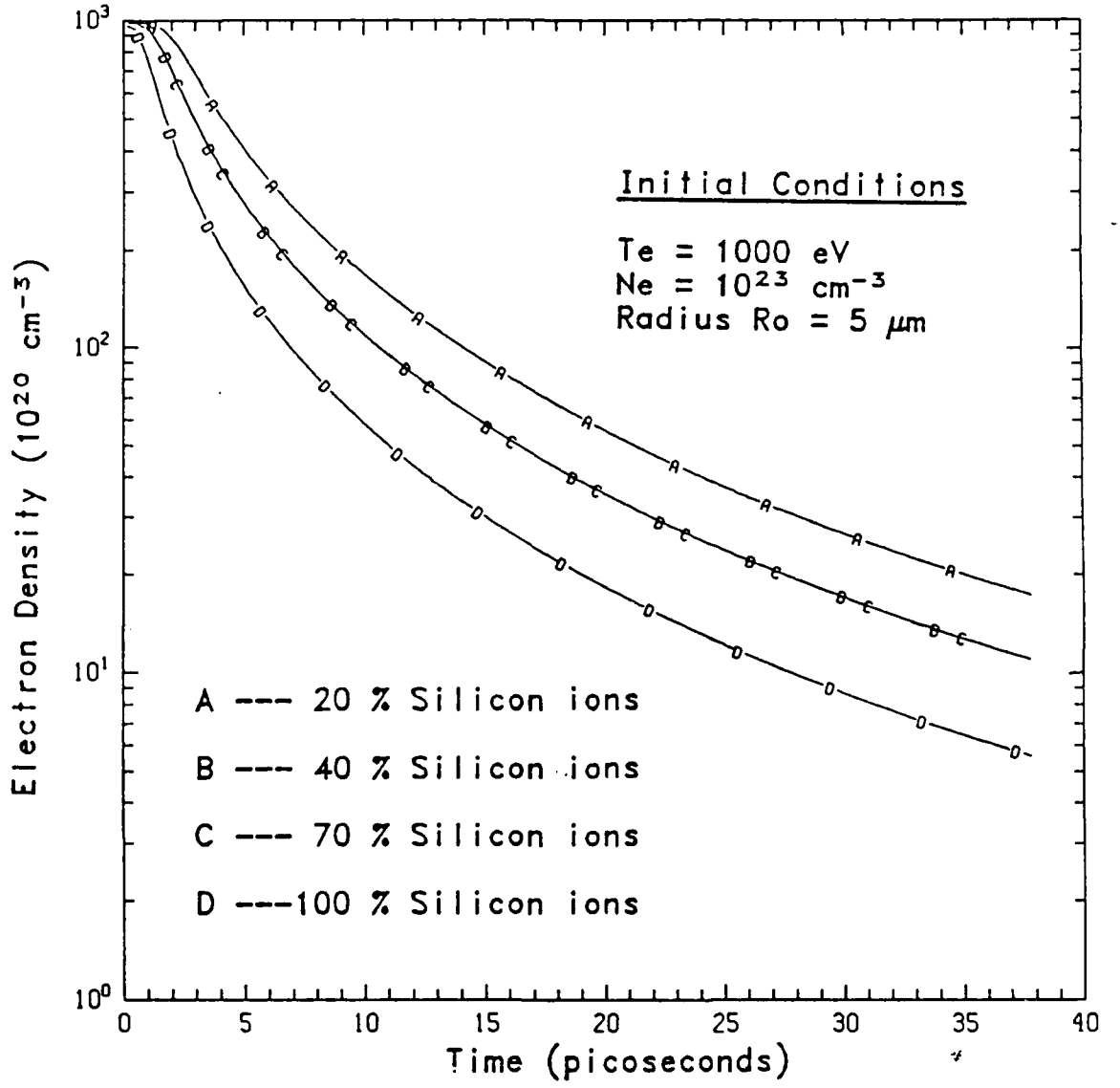

Figure 9. Time evolution of electron density of the optimal gain-producing zone for different concentrations of silicon ions. Aluminum is the coolant element.

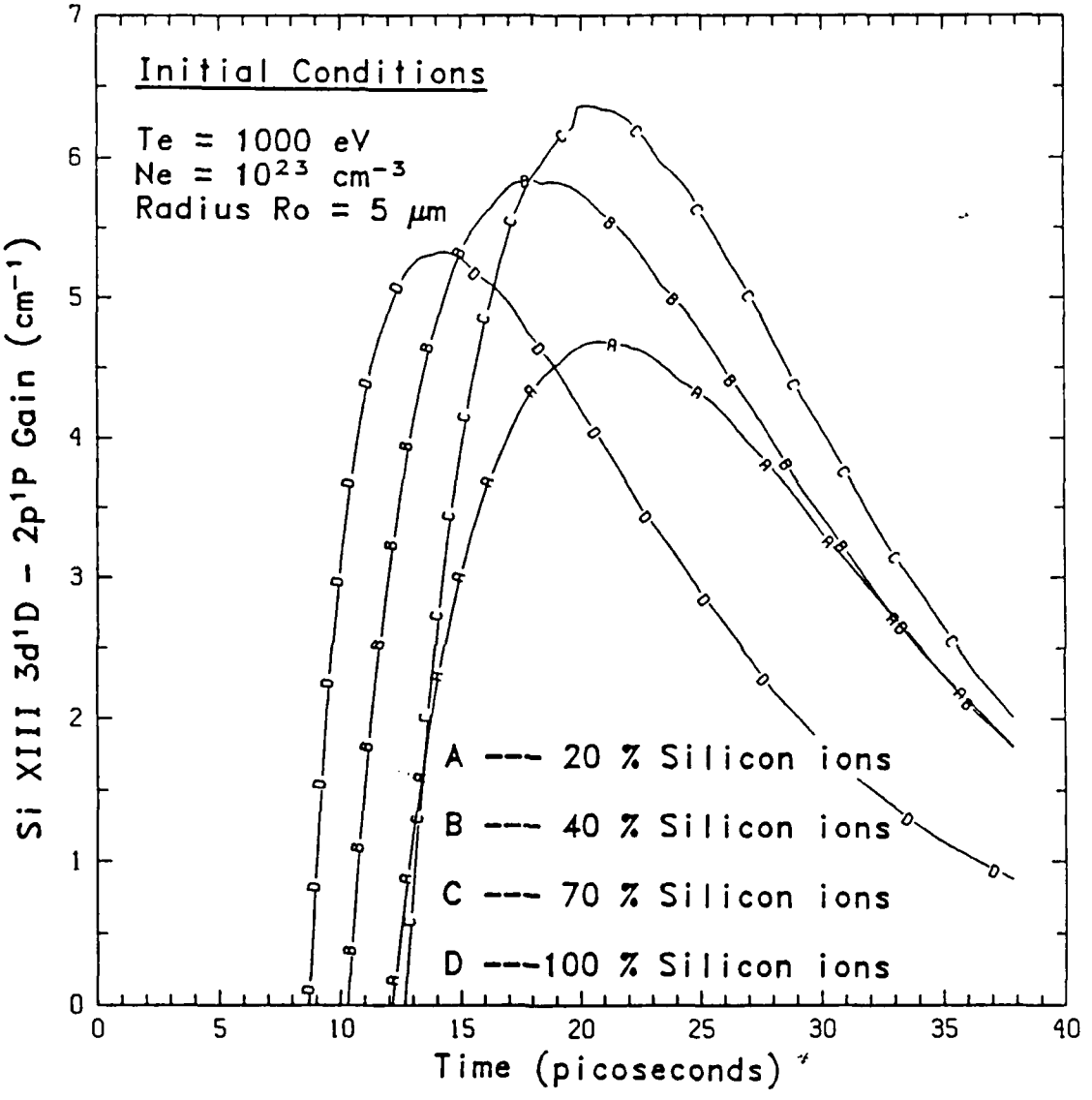

Figure 10. Time evolution of Si XIII $3d^1$ - $2p^1$ gain calculated for the optimal gain-producing zone for different concentrations of silicon ions. Aluminum is the coolant element.

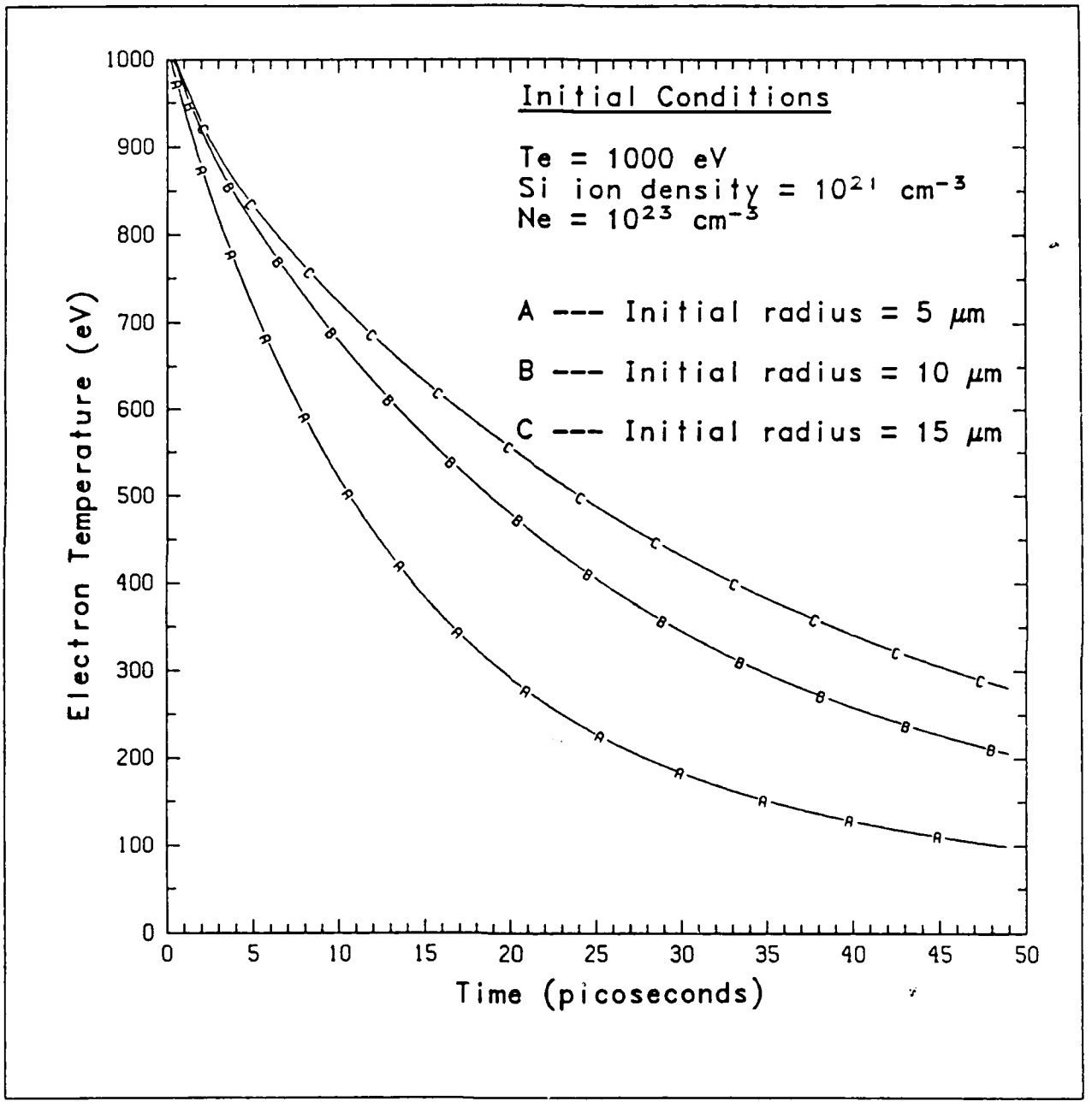

Figure 11. Time evolution of the electron temperature for the optimal gain-producing zone for different initial radii plasmas. Carbon is the coolant element.

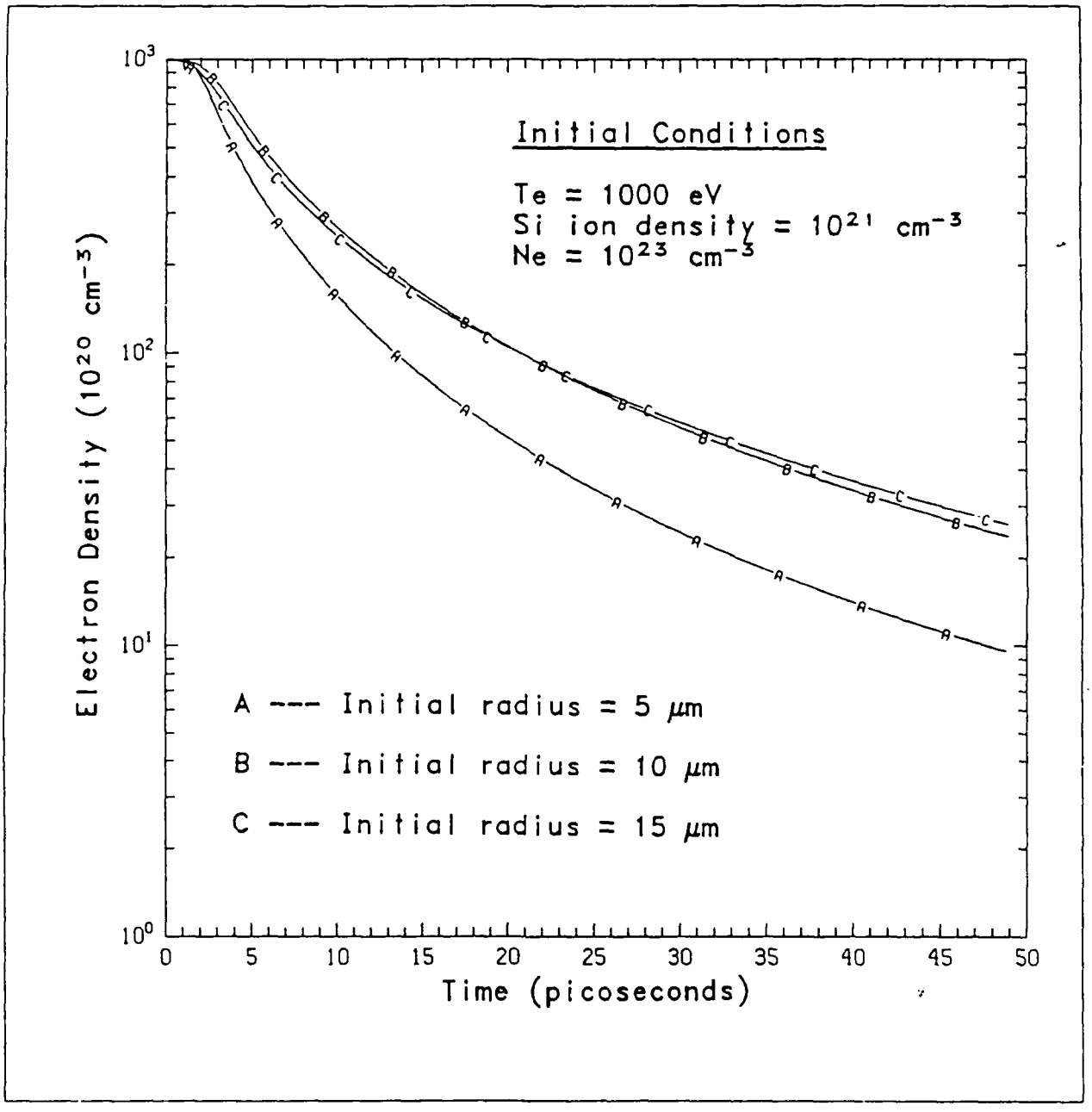

Figure 12. Time evolution of the electron density for the optimal gain-producing zone for different initial radii plasmas. Carbon is the coolant element.

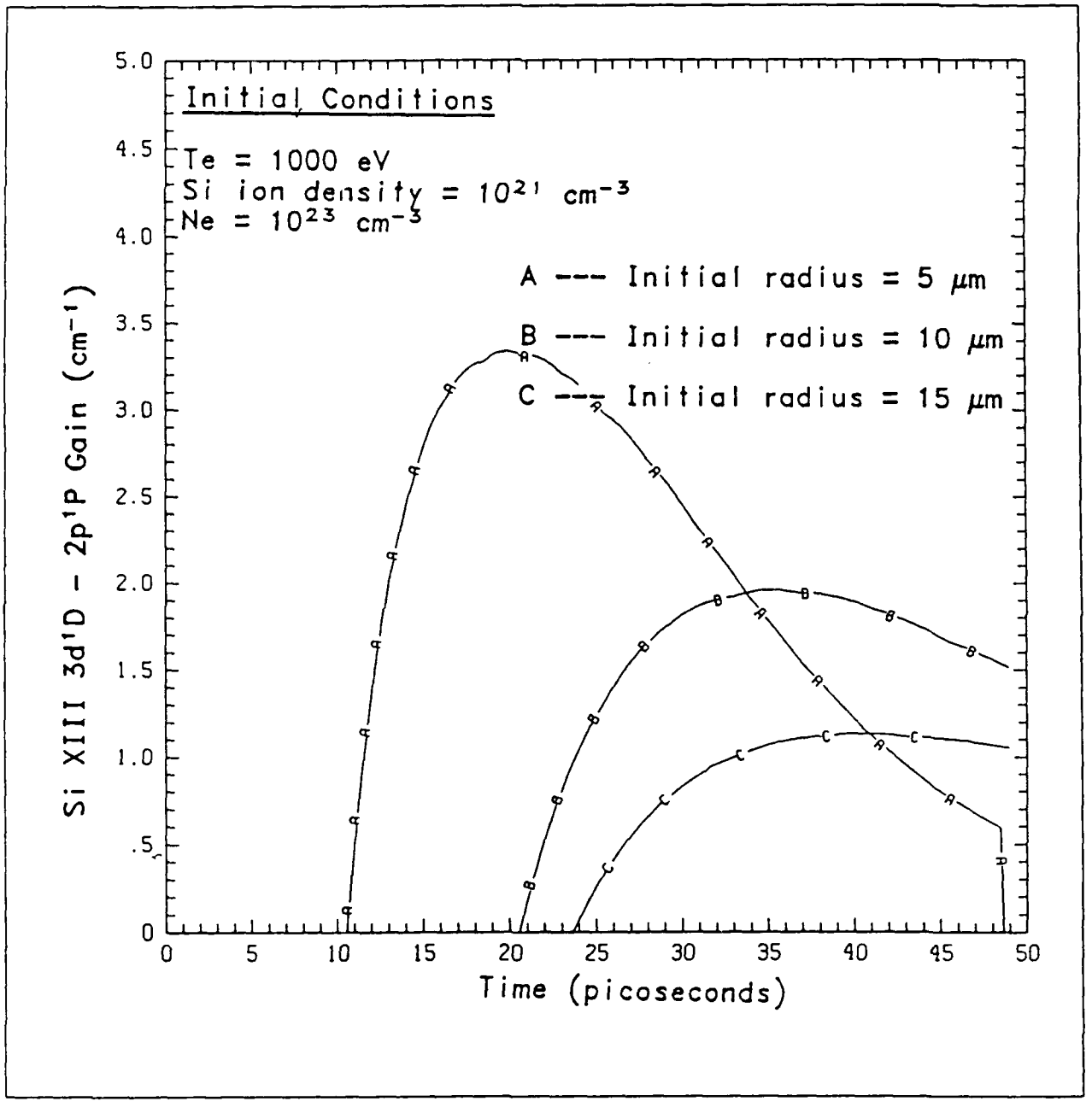

Figure 13. Time evolution of Si XIII $3d^1 - 2p^1$ gain calculated for the optimal gain-producing zone for different initial radii plasmas. Carbon is the coolant element.

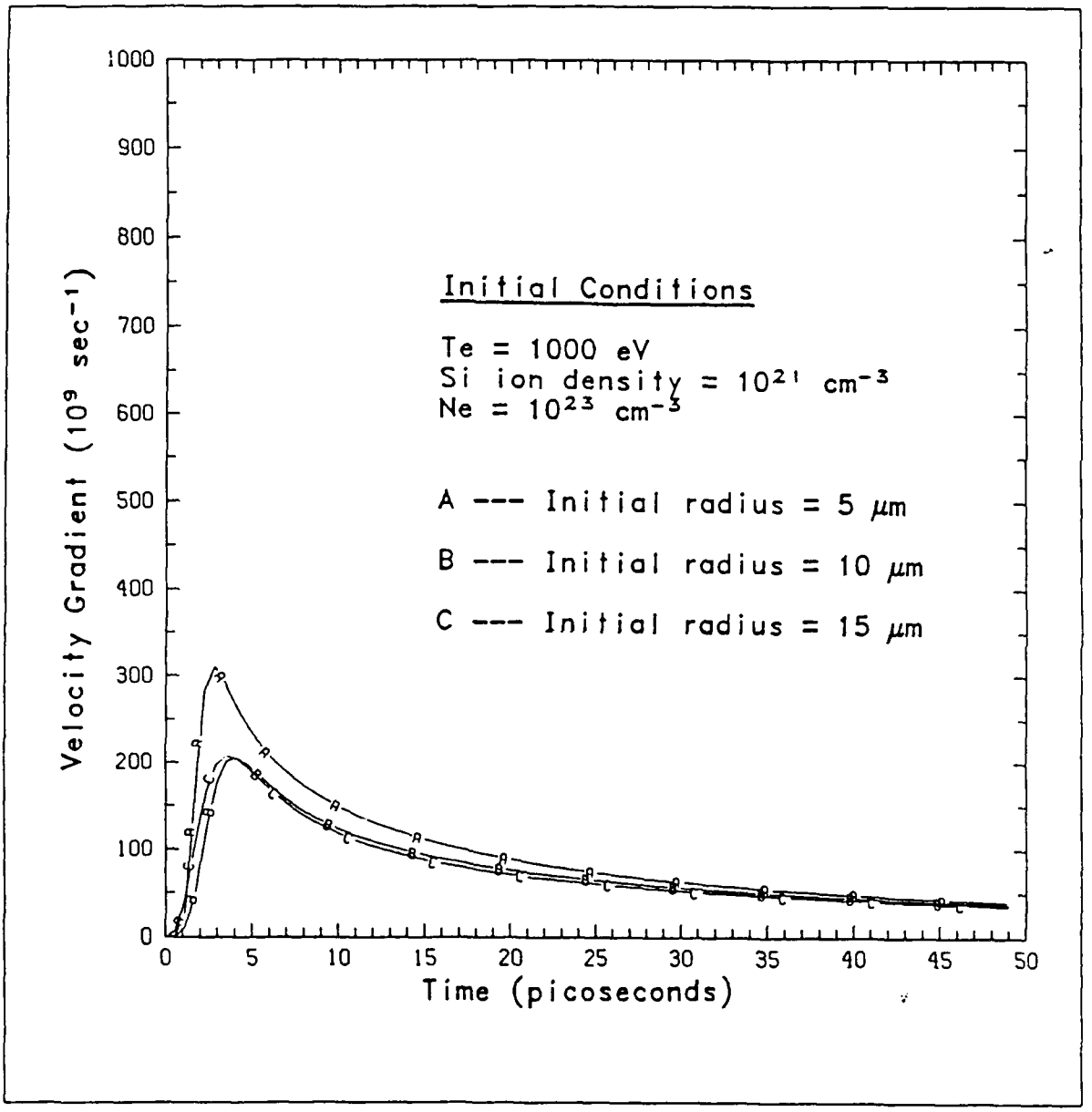

Figure 14. Time evolution of the velocity gradient of the optimal gain-producing zone for different initial radii plasmas. Carbon is the collant element.

Section IV

ABSOLUTE INTENSITY OF A SODIUMLIKE RESONANCE LINE FOR TEMPERATURE DIAGNOSIS OF NEONLIKE X-RAY LASER PLASMAS

M. C. Coulter*, J. P. Apruzese, and K. G. Whitney

Radiation Hydrodynamics Branch

* Berkeley Research Associates, Inc.
Springfield, Va.

I. Introduction

Beginning with the initial experiments at Lawrence Livermore National Laboratory, USA, using selenium and yttrium [1,2], a total of nine neonlike ions [1-7] ranging in atomic number from 28 to 42 have exhibited lasing in laboratory plasmas created by line focused high intensity lasers. Much effort has been expended, with considerable success [1-3,8-11], in experimental diagnosis and modeling of these plasmas. For instance, the plasma density and x-ray laser pulsewidth and timing are now directly measurable [1,11]. However, an accurate determination of the plasma temperature remains elusive [8]. Temperature is one of the most critical, if not the most critical, of plasma properties governing the x-ray laser kinetics. The rate of ionization and the relative importance of collisional excitation and recombination pumping are primarily determined by the temperature. The collisionally excited J=0 lasing transition, at first thought to be missing in selenium [1,2], has more recently been measured to show amplification in selenium and other elements [3-7], but is still generally weaker than predicted. In principle, a pure recombination neonlike laser is possible [10] although the presence of J=0 amplification indicates significant collisional excitation pumping in existing lasers. A review of the present status of the J=0 anomaly is given in Ref. 8. As pointed out in Ref. 8, the present techniques for measuring the plasma temperature are not in agreement either among themselves or with the most sophisticated simulations available. Experimental temperature measurement techniques which have been employed include stimulated Raman scattering [1,8,11], spectral measurements of line ratios [1,4,5,11], and the slope of the free-bound continuum using microdot spectroscopy [9].

In this paper we describe calculations that were carried out for a selenium (Z=34) plasma. They suggest an additional and potentially important temperature diagnostic: the absolute intensities of sodiumlike resonance lines. The wavelengths of these lines, given in highly accurate measurements in Ref. 12, generally lie near those of various neonlike laser lines and are frequently detected on the on- as well as the off-axis spectra obtained in the lasing experiments.

II. Description of the Model

In the present work we calculate intensity profiles for one particular resonance line: the $3p^2P_{3/2}$ to $3s^2S_{1/2}$ transition of sodium-like selenium at 201 Å, which lies near the neonlike lasing lines at 206 and 209 Å. The overall atomic model used in these calculations has been described in Ref. 13. It consists of a complete, hydrogenic set of excited states in each ionization stage. Excited state energies are thus discriminated only by their n quantum numbers. The degeneracy factors for these states, however, depend on the ionization stage in which they are located. In other words, in each ionization stage, each set of states with a given principal quantum number of the excited electron have been gathered together, for purposes of carrying out the ionization calculations, to form one state, whose degeneracy varies from one ionization stage to another. The model also contains one important exception to this procedure. Since we are particularly interested in a diagnostic based on one of the sodiumlike $\Delta n=0$ transitions, a detailed description of the 3p and 3d multiplet structure in sodiumlike Se XXIV is given. Thus, the atomic model describes all collisional and radiative couplings between the following seven excited levels: $(Ne)3p^2P_{1/2}$, $(Ne)3p^2P_{3/2}$, $(Ne)3d^2D_{3/2}$, $(Ne)3d^2D_{5/2}$, the consolidated n=4, the consolidated n=5, and the consolidated n=6 levels. Techniques used to obtain the atomic rate coefficients are summarized in Ref. 14.

The atomic processes populating and depopulating the levels are: collisional ionization, collisional and radiative recombination, collisional excitation a deexcitation, dielectronic recombination, and spontaneous radiative decay and photoexcitation. High lying n states are consolidated further into one excited state so that each ionization stage contains only four excited states and yet represents all of the important atomic structure in the ionization stage. The rate coefficients describing the coupling to these states are appropriately averaged and summed.

From the above selenium structure a one-dimensional (1D) collisional-radiative-equilibrium (CRE) rate equation calculation was carried out in cylindrical geometry for a homogeneous plasma of constant ion density and uniform electron temperature. An iterative technique [15] was used to obtain

self-consistency between the fractional level populations and the photoexcitation, collisional, and downward radiative rates.

Radiation transport couplings are generally calculated using a single average ray [16]. For a cylindrical geometry this average photon path can be specified by two angles: one for the radial direction and one for the longitudinal direction. In determining these angles, it has been assumed that the plasma length is much larger than the radius. Opacity effects on line intensity are accounted for by using a detailed frequency grid from 40 to 70 eV which spans the $3p\ ^2P_{3/2}$ to $3s\ ^2S_{1/2}$ transition at 201 Å [12], or 61.68 eV. Radiation is transported at each grid point. Outside of this region, individual lines are transported probabilistically as in Ref. 16.

The absolute intensity of the 201 Å line and fractional populations are calculated for a longitudinally uniform cylindrical plasma viewed radially. Two different plasma radii are considered: 0.01 and 0.1 cm. The 0.01 cm case is close to the thickness achieved in actual linear plasmas. The 0.1 cm calculations illustrate the effect of increased optical depth, which is relevant to axial spectrographs whose view of the plasma includes cm-scale optical paths. In both cases, the electron temperature was varied from 100 to 880 eV, while ion density was varied from 10^{19} to 10^{21} cm^{-3}. The intrinsic line profiles were assumed to be Voigt functions whose width was self-consistently computed from the lifetimes of the levels inclusive of collisional and radiative processes.

III. Results and Interpretation

By determining which blackbody curve the peak in the emitted flux in the 201 Å line lies on, a brightness temperature for our model plasma can be determined. As the calculated flux approaches the physical blackbody limit, the brightness temperature will approach the actual plasma temperature. Usually the largest brightness temperature will be at line center. If, however, there is a significant amount of reabsorption at line center, the wings of the line may yield a higher equivalent blackbody temperature. Outside of the temperature or density region where the sodium-like ground state is no longer highly populated or strongly coupled to the 3p state, the brightness temperature will fall below the plasma temperature. Figures 1 and 2 quantify this behavior. They contain plots of the brightness temperature reached at line center by the 201 Å line as a function of ion density and electron temperature for the two radii. Note,

these contour plots determine the relationship between the equivalent blackbody temperature of the 201 Å line and the actual plasma temperature when the plasma is viewed radially. Another important diagnostic feature of this line is its width. Figures 3 and 4 show the calculated full width at half maximum (FWHM) of the 201 Å line as a function of temperature and density. The radially measured line width and brightness temperature may be used in conjunction with the measured density and Figs. 1-4 to estimate or set limits to the plasma electron temperature. The physics underlying these variations is now considered.

The principal factors determining the closeness of the line brightness temperature to the electron temperature of the plasma are the density and line optical depth. The density determines the degree to which the level populations approach the Saha-Boltzmann ratio required for true blackbody emission. The radiative transition probability for the 201 Å line is 1.8×10^{10} sec^{-1}. The collisional de-excitation rate coefficient varies from 4×10^{-9} cm^3 sec^{-1} at 100 eV to 1.8×10^{-9} cm^3 sec^{-1} at 800 eV. The excitation rate coefficient is 4.4×10^{-9} at 100 eV and 3.3×10^{-9} at 800 eV in the same units. If the usual requirement for LTE populations that the collisional rates exceed the radiative coupling by an order of magnitude is imposed, an electron density of $\sim(10)1.8 \times 10^{10}/1.8 \times 10^{-9}$ $\sim 10^{20}$ is required, in agreement with Ref.17. Therefore, the electron densities of 3×10^{20} prevailing during neonlike selenium laser pulses [11] are more than sufficient to impose LTE populations on these sodiumlike levels. Clearly, the only factors which may prevent full blackbody emission from being achieved are lack of optical depth in the line and/or a cool outer boundary layer which dominates the line source function. The optical depth depends on the density, fractional sodiumlike population, and path length. In these calculations the line center absorption coefficient typically varied between 10 and 2000 cm^{-1}. Figs. 3 and 4 reflect the combined effects of both Doppler and opacity broadening on the line width. Therefore, viewed axially for paths of about 1 cm, the line should nearly always reach the blackbody limit.

Figures 5 and 6 show the neonlike fractional population for 0.01 and 0.1 cm radii, respectively. At least 50% of the plasma is in the neonlike stage for temperatures ranging from around 250 to around 650 eV and for ion densities ranging from about 2×10^{19} to more than 10^{21} cm^{-3}. From around 200 to 300 eV, about 50% of the plasma is in the sodiumlike ionization stage, shown in Figures 7 and 8. This is the region where the actual plasma temperature is closest to

the equivalent blackbody temperature (Figs. 1 and 2). If the plasma is viewed axially along with the gain lines instead of radially, the optical path will increase. As a consequence, one would expect the relationship between the two temperatures to be even stronger. The present calculations are meant to be suggestive. Full two-dimensional calculations of the axial radiation emission will reveal the possible effects of boundary layers as well as the increased optical depth.

IV. Concluding Remarks

When a selenium x-ray laser plasma is viewed radially, there is a definite relationship between the actual plasma temperature and the brightness temperature for the $3p\ ^2P_{3/2}$ to $3s\ ^2S_{1/2}$ transition of sodiumlike Se at 201 Å. By viewing the plasma axially, this relationship should become stronger, making the absolute intensity of the sodiumlike resonance lines a potentially useful tool in diagnosing the temperatures reached by neonlike laser plasmas.

Simple arguments based upon the collisional and radiative rates as well as detailed numerical calculations show that the upper and lower levels of the $3s\ ^2S_{1/2}$ - $3p\ ^2P_{3/2}$ sodiumlike selenium line will be populated in the Saha-Boltzmann ratio for electron densities exceeding 10^{20} cm^{-3}. The brightness temperature of the line is an indicator of the actual plasma temperature if the path along which the line is viewed is optically thick.

We conclude with a comment on the Z scaling of this diagnostic. Applying hydrogenic scalings to the sodiumlike stage (collision rates scale as Z^{-3}, radiative as Z^4), one expects that the electron density required for Saha-Boltzmann populations will scale approximately as Z^7. However, higher density plasmas are necessary to obtain x-ray lasing at shorter wavelengths and higher atomic number, as discussed in detail in Refs. 18 and 19. Therefore, the usefulness of this diagnostic will persist for higher atomic number plasmas.

Acknowledgments

We are grateful to P. K. Kepple for calculations of some of the atomic rates.

References

1. M. D. Rosen, et al.: Phys. Rev. Lett. **54**, 106 (1985).
2. D. L. Matthews, et al.: Phys. Rev. Lett. **54**, 110 (1985).
3. B. J. MacGowan, et al.: J. Appl. Phys. **61**, 5243 (1987).
4. T. N. Lee, E. A. McLean, and R. C. Elton: Phys. Rev. Lett. **59**, 1185 (1987).
5. B. Yaakobi, et al.: Proc SPIE, editor C. Randol Jones, **875**, 9 (1988).
6. T. N. Lee, E. A. McLean, J. A. Stamper, H. R. Griem, and C. K. Manka: Bull. Am. Phys. Soc. **33**, 1920 (188).
7. C. Keane, et al.: Bull. Am. Phys. Soc. **33**, 2041 (1988).
8. B. L. Whitten, et al.: Proceedings of the International Conference on Lasers, Lake Tahoe, Nevada, edited by R. C. Sze and F. J. Duarte (STS, Mclean, VA, 1989), p. 90.
9. B. K. F. Young, R. E. Stewart, C. J. Cerjan, G. Charatis, and Gar. W. Busch: Phys. Rev. Lett. **61**, 2851 (1988).
10. J. P. Apruzese, J. Davis, M. Blaha, P. C. Kepple, and V. L. Jacobs: Phys. Rev. Lett. **55**, 1877 (1985).
11. M. D. Rosen, et al.: Phys. Rev. Lett. **59**, 2283 (1987).
12. J. Reader, et al.: J. Opt. Soc. Am. B **4**, 1821 (1987).
13. K. G. Whitney and M. C. Coulter: IEEE Trans. on Plasma Sci. **16**, 552 (1988).
14. D. Duston, R. W. Clark, J. Davis, and J. P. Apruzese: Phys. Rev. A **27**, 1441 (1983).
15. J. P. Apruzese, J. Davis, D. Duston, and R. W. Clark: Phys. Rev. A **29**, 246 (1984).
16. J. P. Apruzese: J. Quant. Spectrosc. Radiat. Transfer **25**, 419 (1981).
17. W. H. Goldstein and R. S. Walling: Phys. Rev. A **36**, 3482 (1987).
18. J. P. Apruzese, J. Davis, P. C. Kepple, and M. Blaha, J. Phys. (Paris) Colloque C6, **47**, 15 (1986).
19. M. D. Rosen, R. A. London, and P. L. Hagelstein, Phys. Fluids **31**, 666 (1988).

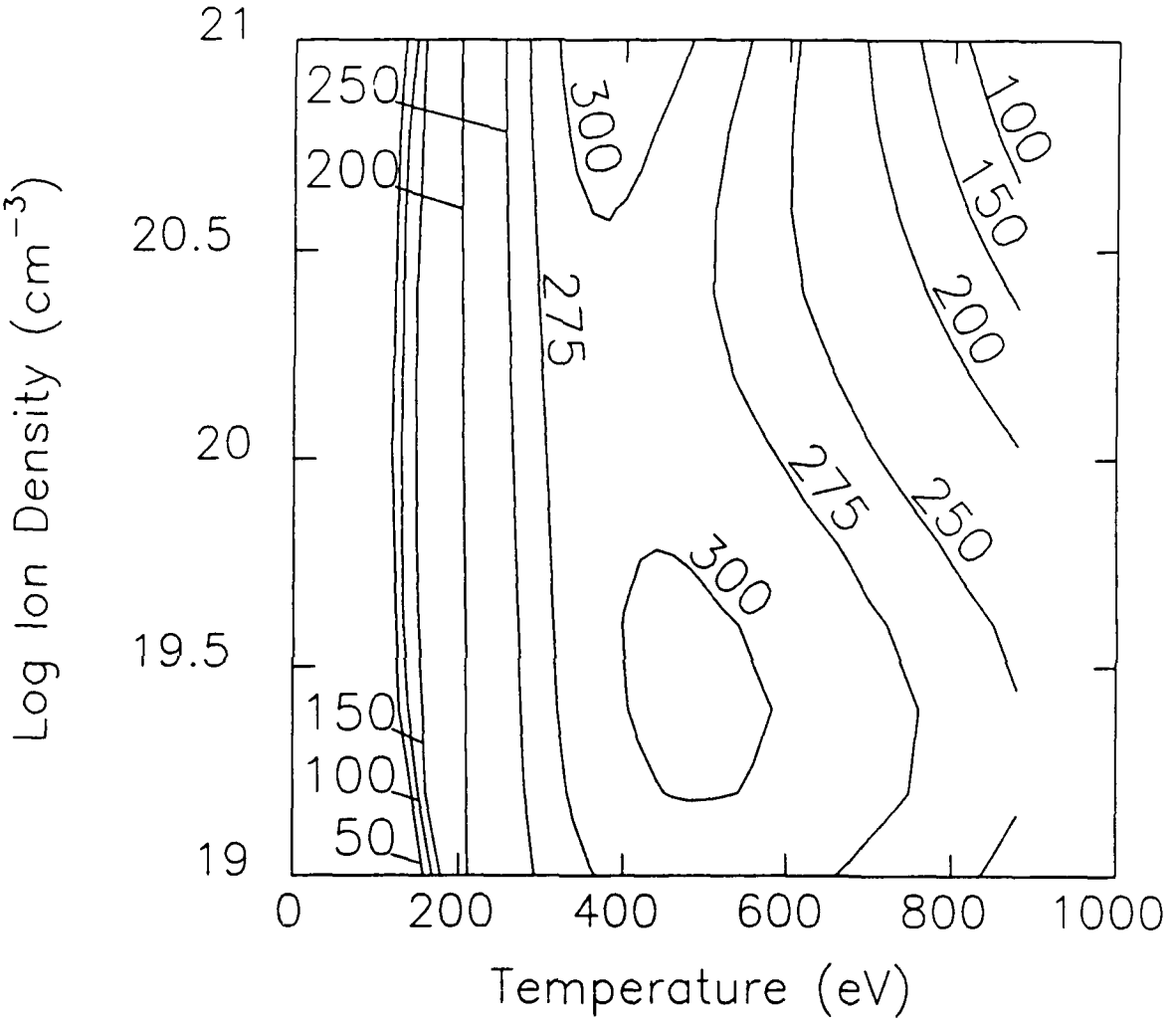

Fig. 1. Brightness temperature of the Se 201 Å sodiumlike line at line center as a function of the ion density and the electron temperature for a plasma radius of 0.01 cm.

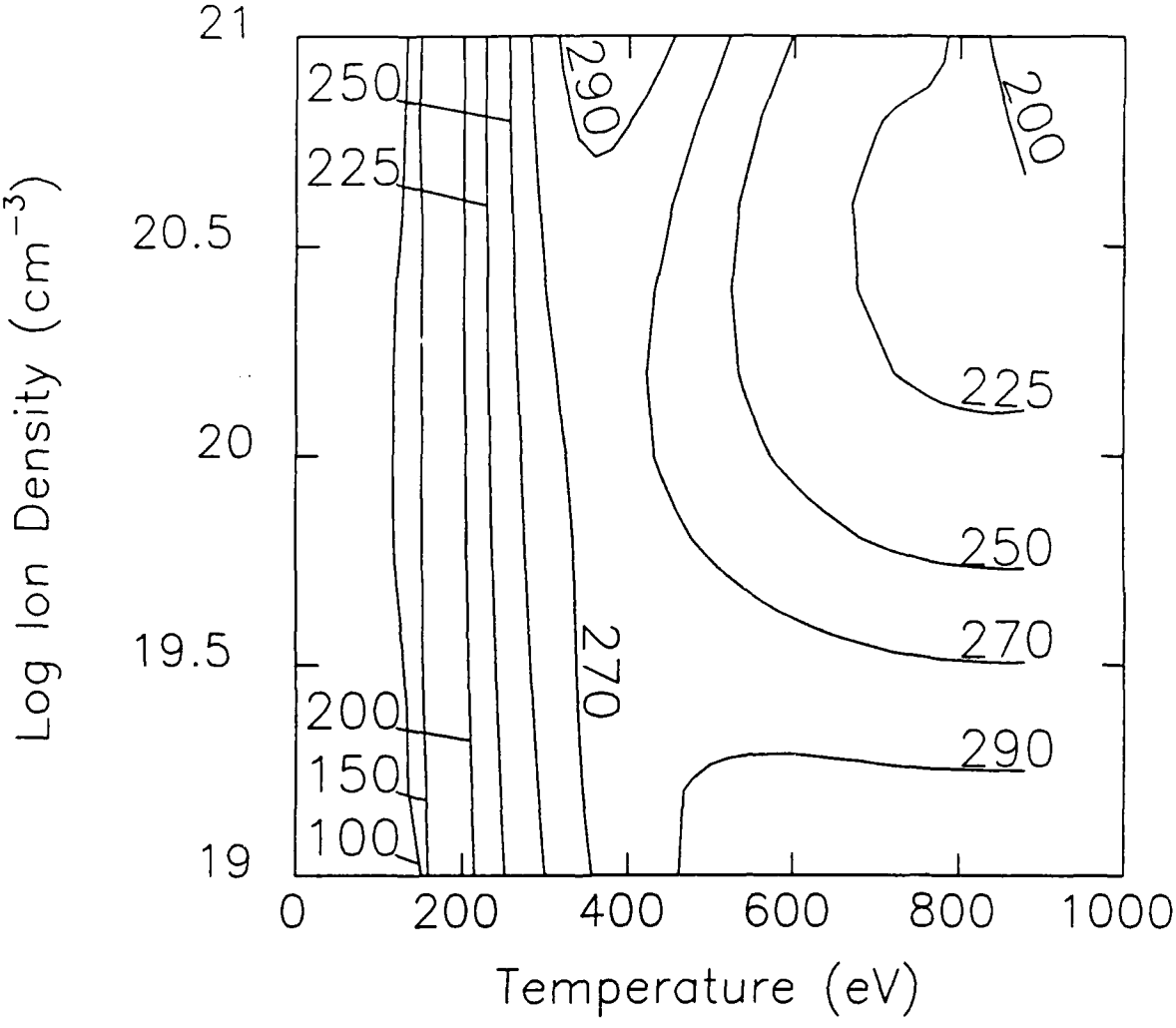

Fig. 2. Same as Figure 1 except for a plasma radius of 0.1 cm.

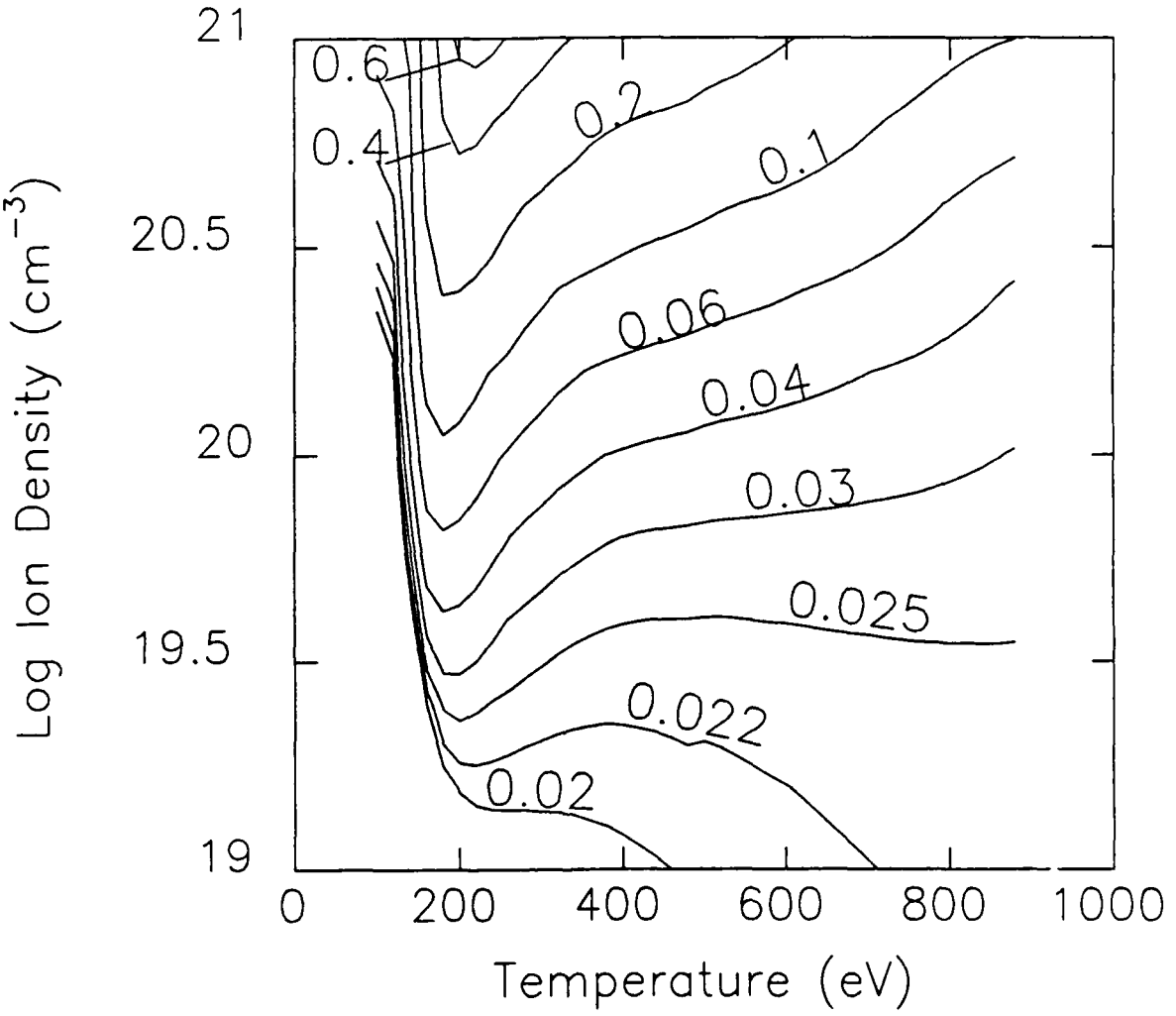

Fig. 3. Full width at half maximum (in eV) for the 201 Å line emission as a function of the ion density and the electron temperature for a plasma radius of 0.01 cm.

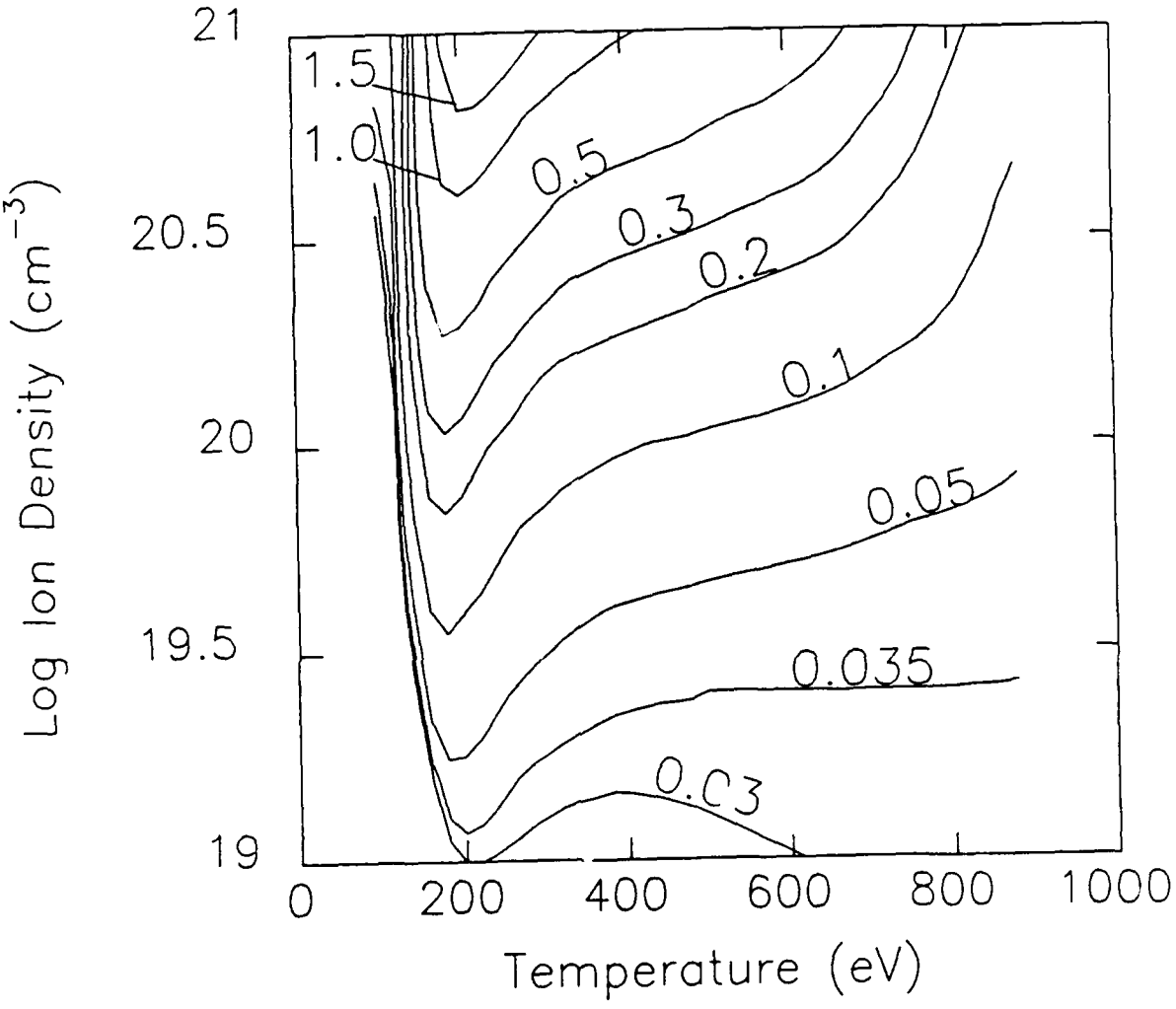

Fig. 4. Same as Figure 3 except for a plasma radius of 0.1 cm.

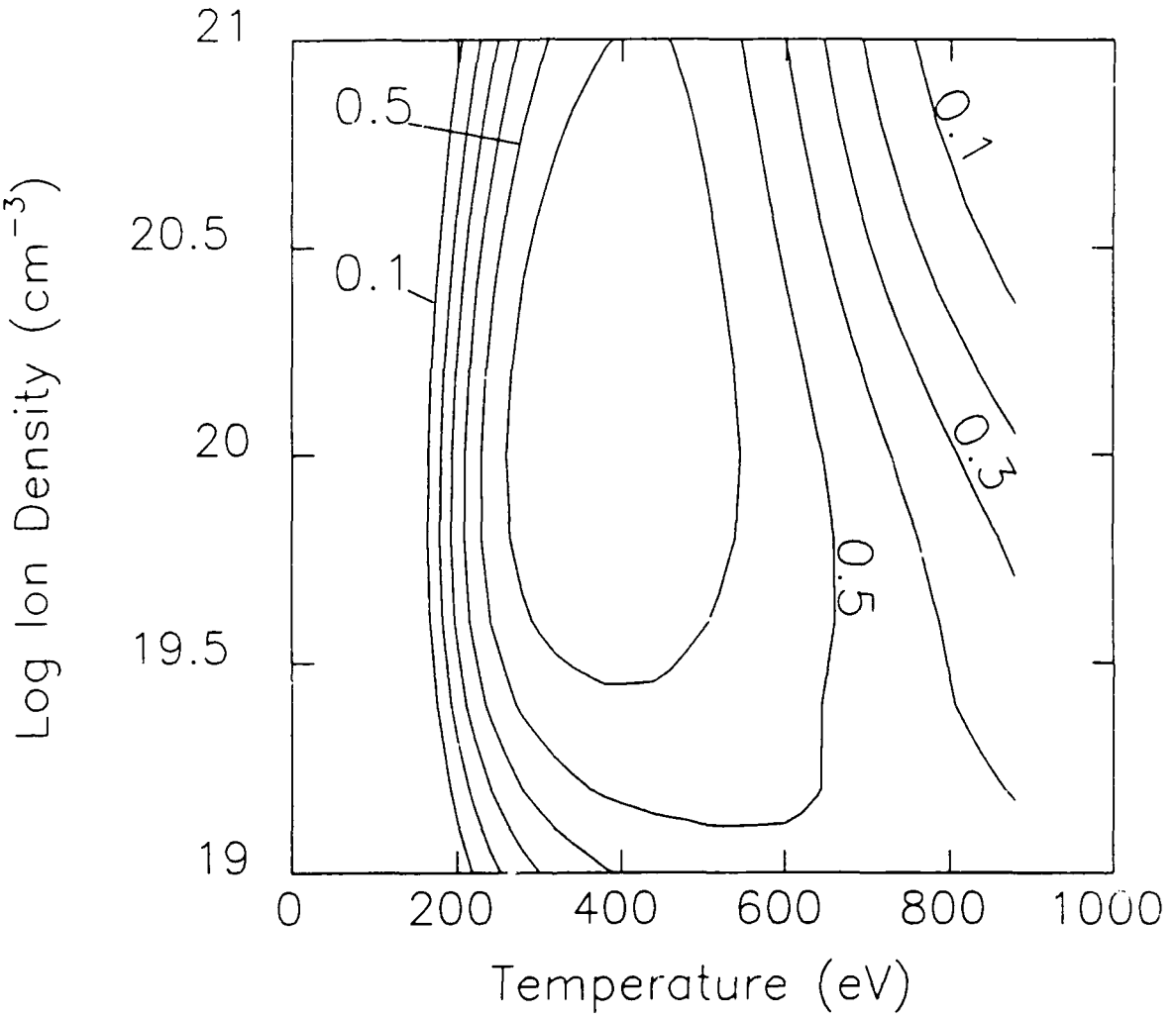

Fig. 5. Neonlike Se fraction as a function of the ion density and the electron temperature for a plasma radius of 0.01 cm. Interval between contours is 0.1.

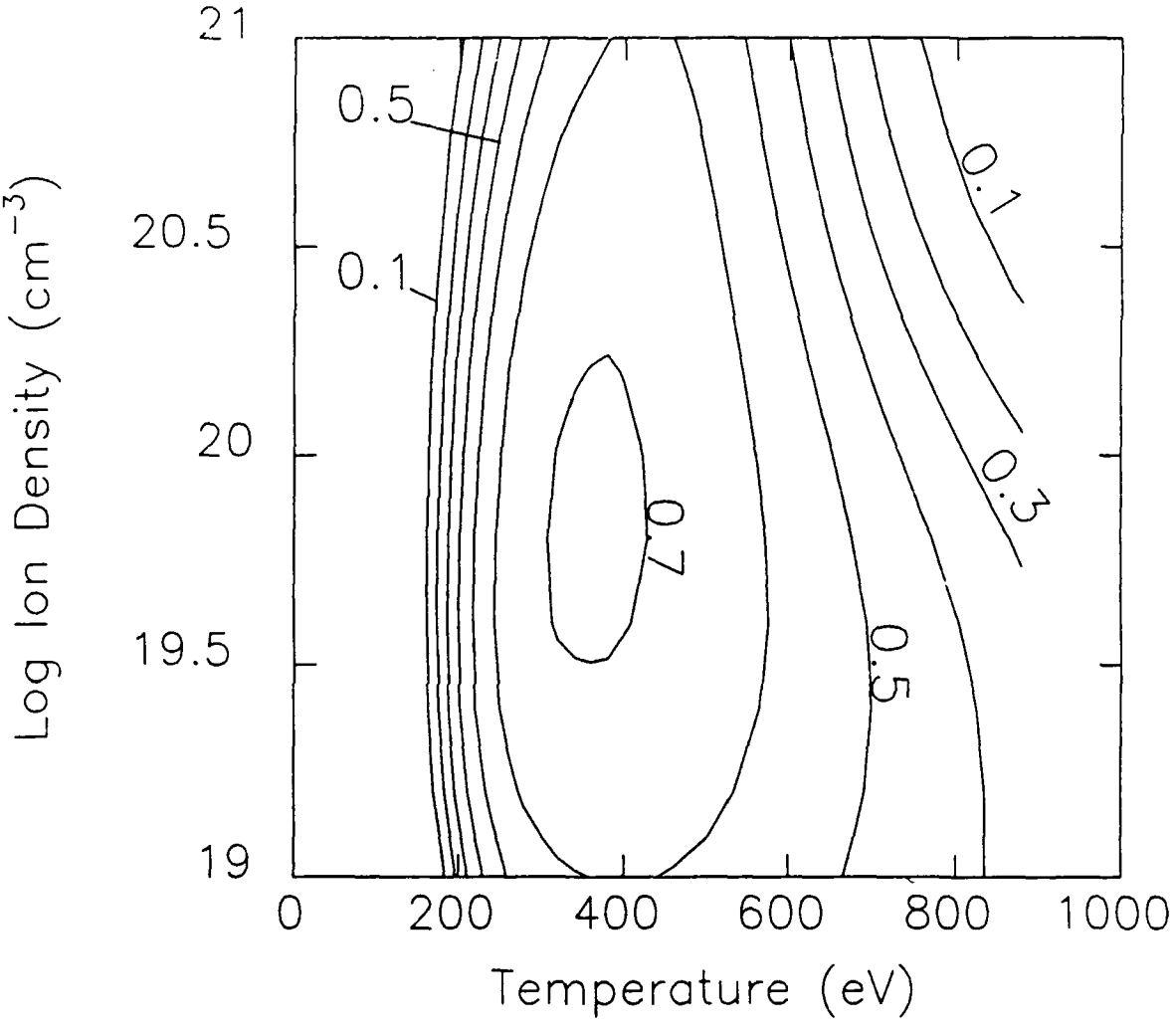

Fig. 6. Same as Figure 5 except for a plasma radius of 0.1 cm.

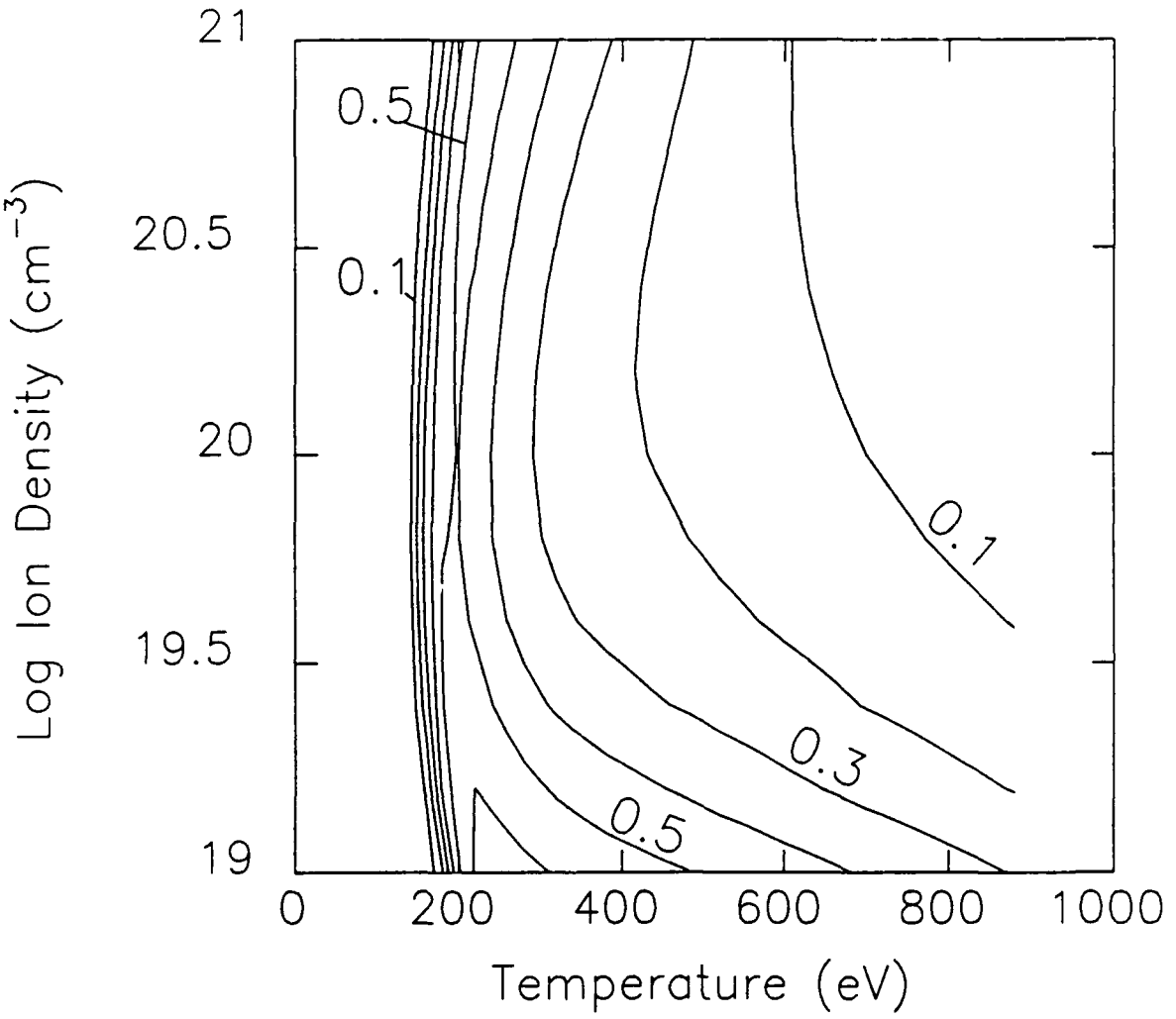

Fig. 7. Sodiumlike Se fraction as a function of the ion density and the electron temperature for a plasma radius of 0.01 cm. Interval between contours is 0.1.

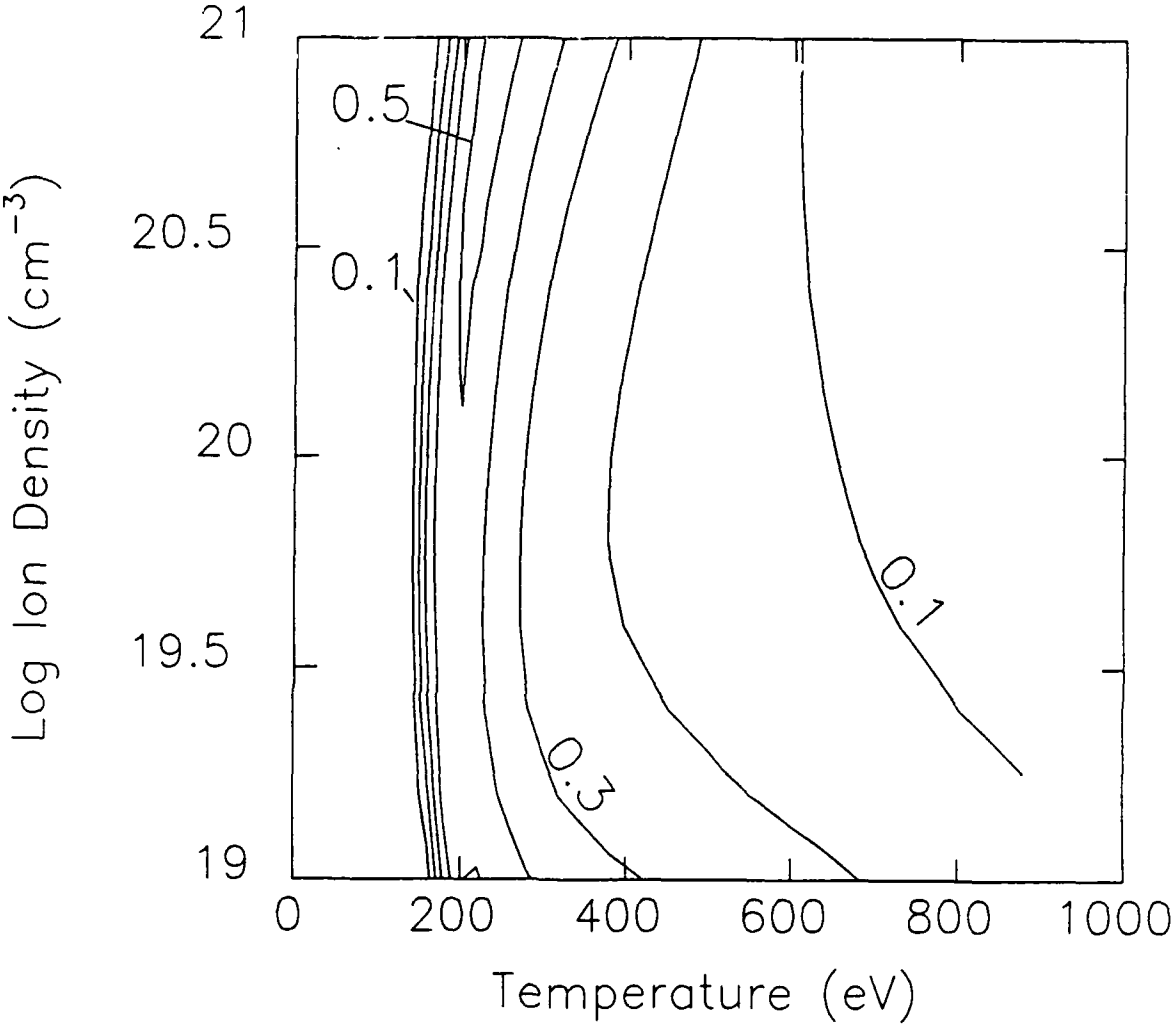

Fig. 8. Same as Figure 7 except for a plasma radius of 0.1 cm.